NTNU – Trondheim
Norwegian University of
Science and Technology

Shaly Sand Petrophysics and its Impact on Full Field Reservoir Simulation

Anders Opsal Mæland

Petroleum Geoscience and Engineering
Submission date: June 2014
Supervisor: Jon Kleppe, IPT
Co-supervisor: Yngve Bolstad Johansen, Det norske oljeselskap

Norwegian University of Science and Technology
Department of Petroleum Engineering and Applied Geophysics

Preface

This Master thesis is a result of work done on real data provided by Det norske oljeselskap. The purpose is to investigate differences between two petrophysical approaches, and at the same time creating a basis for the writing of a best practice within the company. As a student without company deadlines, meetings or a general social life, the opportunity to investigate this opened up. Suddenly the issue could be explored in a way based more on systematic work than gut feeling, intuition and general petrophysical experience.

Acknowledgements

First of all, I would like to thank my supervisor at Det norske oljeselskap, Yngve Bolstad Johansen, for re-introducing me to petrophysics and providing the topic for this thesis. He has been excellent in his support, patiently answering the same questions over and over again. After this spring, I think he will think twice before tempting new students with topics for their master thesis.

I also want to thank Lodve Hugo Olsborg for help in multiple sessions, for listening and showing me how to build models in Petrel.

A big thank you also goes to Geir Frode Kvilaas and Kjell Christoffersen for assistance on the reservoir simulation part and providing input for the base case simulations.

At the end I want to thank my supervisor at NTNU , Prof. Jon Kleppe. His experience together with guidance and availability has been much appreciated.

Sammendrag (Norsk)

Petrofysikk kan gi svar på mange av spørsmålene man stiller seg når et felt skal utvikles. Hvordan er egenskapene til reservoaret, og hvor mye olje finnes det egentlig? Etter at brønner er boret og logget starter denne evalueringen. Skifer er en bergart som vil påvirke både målingene i borehullet og egenskapene til reservoaret, slik som porøsitet og permeabilitet. Man må generelt sett eksuldere porøsiteten fra skifer og non-net når man bygger geomodeller. Det finnes flere metoder for å gjøre dette, men hvilken er best? Denne oppgaven tar sikte på å undersøke to metoder som brukes til å korrigere målt porøsitet. Den ene er effektiv porøsitet, der porøsiteten i skiferen trekkes fra porøsiteten i sandsteinen. Den andre er å justere ned den totale porøsiteten tilsvarende volumet skifer i den aktuelle sonen.

For å sammenligne disse to metodene har begge blitt brukt som input til Ivar Aasen geomodellen i Nordsjøen. I tilleg til å undersøke hvor stor forskjell det egentlig er mellom metodene, har de blitt testet i forhold til usikkerhet i skifervolum. Metoden har gått ut på å tolke alle brønnene på Ivar Aasen, bygge unike geomodeller og kjøre simuleringer på modellene. Resultatene viser at det er stor forskjell på om man bruker total eller effektiv porøsitet som basis for tolkning og simuleringer. De har ganske lik sensitivitet i forhold til skifervolum, men det kan synes at total porøsitet kanskje er en anelse bedre enn effektiv porøsitet.

Abstract

Analyzing logs in shaly formations to make accurate petrophysical models is a challenging task. As clay minerals in shale add electrical conductivity to the formation, water saturation tends to be overestimated using conventional clean sand approaches.

A standard resolution density log, used to determine porosity, has about a 0.4 meters measurement interval. If thin shales of smaller scale than 0.4 meters are present, they will be measured together with nearby clean sands and the section will seem to have poorer reservoir quality than it actually does. The fact is, dependent on the amount and distribution of shale, the sands can have excellent porosity and permeability contributing to the oil production. To correct for the shale in the formation, two approaches are commonly applied. The total sand porosity is either multiplied with the fraction of sand, or the total porosity is converted into effective porosity by simply subtracting the volume of shale porosity.

In this Thesis a total porosity model with Waxman & Smits shaly sand equation have been compared with an effective porosity model with the Poupon & Leveaux Indonesia equation. To investigate the full effect of this choice, a comparison of the full field reservoir simulations was made.

In laboratories, core-samples are dried before total porosity is measured. After that, air is flowed through some of the samples and a pressure drop is recorded. The calculated permeability is then logarithmically correlated to the porosity. This means that a small difference in porosity input will have a large effect on permeability. Other factors, such as water saturation in the geomodel grid, are calculated based on porosity and permeability. Further out in the workflow, relative permeability is again dependent on the water saturation and it is affecting the flow rate of the different fluids. By using data from the two Ivar Aasen field models, all these effects are investigated to quantify the full differences and see what effect the two petrophysical models has on the prognosis of production and estimation of volumes.

In addition, both methods were tested for their sensitivity to uncertainties in volume of shale. The simulation results proved significant differences between the models, both in terms of volumes and production rates. This indicates that no matter which model is chosen, effort should be made to limit this uncertainty as much as possible. The models have proved to have approximately the same sensitivity to the volume of shale, with the total porosity model behaving slightly better in this study. The effect of sealing faults and variations in vertical transmissibility was also investigated, showing a different response based on the chosen model. As we can see the choice of petrophysical model has a much larger impact than faults or transmissibility settings.

Contents

Preface i

Acknowledgements i

Sammendrag (Norsk) ii

Abstract iii

1 Introduction 1

2 Background 3
2.1 Porosity . . . 3
2.1.1 Porosity from core analysis . . . 4
2.1.2 Porosity from log analysis . . . 6
2.1.3 Errors in determining porosity . . . 8
2.2 Shale . . . 9
2.2.1 Volume shale from log measurements . . . 9
2.2.2 The distribution of shale . . . 11
2.3 Pore space . . . 13
2.4 Effective porosity . . . 14
2.5 The Net-to-Gross Ratio . . . 16
2.5.1 Fractional Net to Gross at petrophysical log scale . . . 18
2.5.2 Thomas and Stieber method . . . 20
2.5.3 Logging in a laminated sand/shale formation . . . 21
2.6 Permeability . . . 24
2.6.1 Permeability from core analysis . . . 24
2.6.2 Permeability from log analysis . . . 24
2.7 Water saturation equations . . . 25
2.7.1 Archies Equation . . . 25
2.7.2 Indonesia Equation . . . 26
2.7.3 Waxman & Smits Equation . . . 27

3 Methodology 29
3.1 Input to geomodel . . . 30
3.1.1 Sensitivity of the porosity models . . . 31
3.2 Field overview . . . 34
3.3 Shale volume . . . 35
3.4 Porosity and Water Saturation . . . 39
3.5 Permeability . . . 41
3.6 Cut off's & editing . . . 41
3.7 Case overview . . . 42
3.8 Upscaling of well logs . . . 46
3.9 Creating the 3D model . . . 47

3.10 Simulation model 48
3.11 Production constraints and limits 49
3.12 Model differences 49
3.13 Log/Core comparison 54

4 Results **55**
4.1 Simulation results 55
4.2 Sensitivity to volume shale 60
4.3 Sensitivity to reservoir engineering editing 62
4.3.1 Vertical Transmissibility changes 62
4.3.2 Sealing faults 63

5 Discussion **67**

6 Conclusion **70**

A Simulation results **75**

B Base case Property Histograms **83**
B.1 Porosity 83
B.2 Permeability 85
B.3 Water saturation 87

C Log/Core comparison **89**

List of Figures

1 Porosity vs. bulk volume . . . 3
2 Boyles law porosimeter . . . 6
3 NMR, T2 Distribution curve . . . 8
4 Empirical shale volume correlations . . . 10
5 Neutron/Density crossplot . . . 11
6 Shale distribution modes . . . 11
7 Thin section from Ivar Aasen . . . 12
8 Pore model with log and core responses . . . 13
9 Net to Gross definitions . . . 16
10 Net to Gross cross section . . . 17
11 3D resistivity butterfly plot . . . 19
12 Image log from 16/1-16A . . . 20
13 Thomas-Stieber diagram . . . 21
14 Effect of bulk measurements . . . 22
15 Core photos from well 16/1-11 . . . 23
16 Log resolution, CNL . . . 23
17 Shaly sand water saturation equation flowchart . . . 25
18 Waxman & Smits . . . 27
19 Waxman & Smits pore model . . . 28
20 Methodology flowchart . . . 30
21 Arithmetic volume shale uncertainty . . . 32
22 Arithmetic ϕ_{shale} uncertainty . . . 33
23 Arithmetic volume shale and ϕ_{shale} uncertainty . . . 34
24 Map of Ivar Aasen . . . 35
25 Neutron Density crossplot from 16/1-9 . . . 36
26 GR shale input, 16/1-9 . . . 36
27 Neutron/Density shale input, 16/1-9 . . . 37
28 Volume Shale from 16/1-11 . . . 38
29 Porosity calculation inputs, 16/1-11 . . . 39
30 Water saturation calculation inputs, 16/1-11 . . . 40
31 Porosity - Permeability regression . . . 41
32 Model input: LO, BC, HI cases. 16/1-9 . . . 43
33 Model input: LO, BC, HI cases. 16/1-11 . . . 44
34 Waxman & Smits and Indonesia pore model comparison . . . 45
35 Upscaling well logs . . . 46
36 Normalised water saturation vs. J-function . . . 47
37 Petrophysical modelling . . . 48
38 Simulation model . . . 48
39 Log comparison, 16/1-9 . . . 50
40 Log comparison, 16/1-14 . . . 51
41 Water saturation comparison . . . 52
42 Relative permeability curve . . . 53
43 Log/Core comparison . . . 54
44 Base case: Oil production rate and Cumulative oil production . . . 55
45 Base case: Field oil in place . . . 57
46 Volume-adjusted case: Oil production rates and cumulative oil production . . . 58
47 Volume-adjusted case: Cumulative oil production vs. Cumulative water injected 59

48 Volume shale cases: Cumulative oil production . . . 60
49 Standard deviation: Volume shale . . . 61
50 Vertical transmissibility cases: Cumulative oil production . . . 62
51 Standard deviation: Vertical transmissibility . . . 63
52 Fault case streamlines . . . 64
53 Sealing fault cases: Cumulative oil production . . . 65
54 Standard deviation: Sealing faults . . . 65
55 Base case: Gas production rate and Cumulative oil production . . . 75
56 Base case: Water production rate . . . 76
57 Base case: Field Water-oil ratio . . . 77
58 Base case: Average reservoir pressure . . . 78
59 Base case: Field Gas-Oil ratio . . . 79
60 Base case: Field water injection rate and cumulative injection . . . 80
61 Base case: GOR, gas production rate and downhole pressure in DOP02 . . . 81
62 Shale uncertainty study: Field oil in place . . . 82
63 Porosity, PHIT . . . 83
64 Porosity, PHIE . . . 84
65 Porosity difference, PHIT-PHIE . . . 84
66 Permeability, PHIT . . . 85
67 Permeability, PHIE . . . 86
68 Permeability difference, PHIT-PHIE . . . 86
69 Water saturation, PHIT . . . 87
70 Water saturation, PHIE . . . 88
71 Water saturation, PHIT-PHIE . . . 88
72 Log - Core comparison, 16/1-9 . . . 89
73 Log - Core comparison, 16/1-11 . . . 90
74 Log - Core comparison, 16/1-16 . . . 91

List of Tables

1 Atomic formulae of Pure Clay Minerals [17] . . . 9
2 Petrophysical Model inputs . . . 31
3 Table of porosity inputs for Thomas & Stieber . . . 40
4 Initial oil in place comparison . . . 61
5 Cumulative oil production comparison . . . 66

1 Introduction

In 1942, G.E. Archie of Shell made electrical measurements on cores filled with brine in an attempt to relate resistivity to permeability. Instead his work resulted in a generalized relationship of a formation factor as a function of porosity. He also noticed from the recent work of M.C. Leverett that a relationship between water saturation and relative resistivity existed. Together this made the basis for the Archie equation, still used to determine water saturation in clean sands today.

As the understanding of shale, clay minerals and bound water became better, the industry tried to incorporate this in the predictions of hydrocarbon production. In 1946, equipped with slide rules, the physical chemist Monroe Waxman started his work on what would become a fundamental basis for well log interpretation in shaly sands. Most of the shaly sand equations still in use today, including the Waxman & Smits equation, were published as early as the 1960s and 1970s. Today, advanced reservoir simulators have dramatically improved the calculation capacities since the theories were developed. However, the problems shale introduce still remains a challenge for engineers and petrophysicists.

There are numerous reasons for this. First, log readings have a finite resolution, often too coarse to detect the thinnest shale laminations. Shale also has different distribution modes, all with different impact on permeability and porosity readings. As shale is deposited at different geological times, sometimes even after an existing pore network, variations in mineral composition and shale properties can vary along the wellpath. The presence of shale has a large impact on reserves and complicates the determination of porosity and saturation in net sands. Net sand is defined as the part of the reservoir, which either contains hydrocarbons or potentially could contain hydrocarbons if located sufficiently high above the free water level. This also yields for laminated sands of scale less than the bulk log measurements. The sand properties are fundamental input to reservoir simulators, and it adds uncertainty the prediction of field performance.

The early approach in the industry was based on total porosity from the logs, and this property was assigned to every interval determined as net reservoir in the simulator. Since then, the total porosity model from the early days have transformed into two different models, both adjusting sand properties for shale. One method is to convert the measured total porosity into effective porosity by subtracting the porosity within the shale. The other, is to adjust the porosity by a factor related to the fraction of shale within the specific interval.

This study will apply and compare the total porosity and effective porosity approaches. The total porosity approach is combined with a fractional net to gross curve and the Waxman & Smits [23] water saturation equation. The effective porosity approach is used together with the Poupon & Leveaux, Indonesia equation [18] for water saturation calculations. Both methods have been applied to the simulation model of Ivar Aasen, a field development in the North Sea. In order to decide which approach best reflect reality, the porosity and permeability logs were also compared with the available core data.

The choice of method will have effects on multiple reservoir parameters either correlated to or directly dependent on porosity. This study will demonstrate the difference between the two models from the steps of log interpretation to reservoir simulation. Sensitivity to the volume of shale, which normally is one of the most uncertain parameters, was also investigated to screen for differences in the behavior of the two models. As most shale indicators provide an upper limit, shale volume determination will vary from petrophysicist to petrophysicist based

on their assumptions and the data available to them. Oil companies usually have individual best practices concerning the use of effective and total porosity, but there is a gap in the knowledge of how this choice exactly will affect a full scale field simulation study. The first question is if there is a large enough difference between the methods for the petrophysicist to worry, and secondly how the models react when uncertainty is introduced to the shale volume. All eight appraisal wells at Ivar Aasen have been included in this study. Each case got all the logs interpreted differently, and unique geomodels was built. Simulations with the real field constrains was run, and in the end, the results compared.

2 Background

As an introduction to the theory applied in the study, this section will review and summarize some of the literature on shaly sand petrophysics.

2.1 Porosity

Porosity in itself is a simple principle. It is the fraction of the bulk volume that is not matrix. This fraction can be filled with fluids. The pore volume to bulk volume defines total porosity with the following equation:

$$\phi_T = \frac{V_p}{V_b} = \frac{V_p}{V_p + V_g} \tag{1}$$

in which the bulk volume (V_b) is the sum of the pore volume (V_p) and grain volume (V_g). In other words, it is an intrinsic property of the reservoir rock that indicates its storage capacity. Figure 1 shows a view of porosity where we start on approximately 10 μm-scale and zoom back out to a 1 m-scale for the bulk volume. The total porosity will oscillate depending on bulk volume investigated, but the general perception when we talk about porosity is on the scale between the red lines.

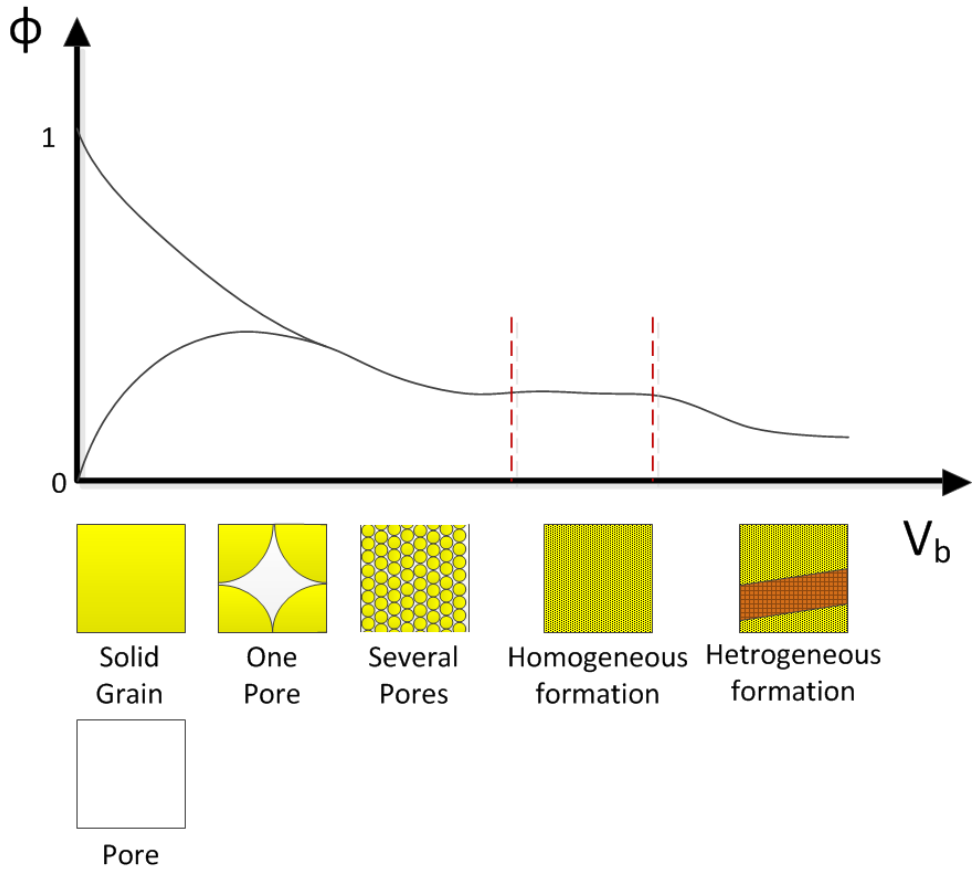

Figure 1: *Porosity as a function of increasing bulk volume, V_b*

Porosity may be determined from either core or log analysis. There are several differences between the two. First, logs measure properties in-situ, the core analysis does not. When a rock is exposed to confining pressure as it is buried, porosity is the first thing that will suffer. One parameter calculated from SCAL analysis is therefore a geomechanical correction factor to convert porosity measured in laboratories to equivalent porosity with a net confining pressure (NCP) of the reservoir. Another difference between logs and cores is the resolution. A standard porosity log has a vertical resolution of 0.4 m, and will give an average porosity of this interval. They will however typically provide continuous measurements every 6 in or so. The cores are discrete measurements, limited to the cored length and plugs drilled from the core, usually in the horizontal direction. A core plug used to calculate porosity is usually 1.5 x 2 inches large.

With the techniques used to determine porosity on logs and cores, it is hard enough to get the total porosity right. There are several methods of drying cores and measure porosity, as well as different ways of obtaining porosity from log analysis. In order to use the logs as reliable input for the geomodels, they must match the cores that are assumed to reflect the reality. That means for every depth, the porosity values determined by indirect log measurements should be about the same as measured at the cores. It is therefore important to understand the processes and methods involved when obtaining the porosity estimates. Are we really comparing apples to apples?

2.1.1 Porosity from core analysis

Before any routine core analysis can be made, the cores must be cleaned of hydrocarbons and salt. It is important to use cleaning and drying methods that do not alter the pore geometry, as this will affect the later measurements. Temperature control is a keyword in shaly sand reservoirs, as irreversible removal of crystal lattice water can occur. The principal methods of high temperature core cleaning in the laboratories are [17]:

1. Dean-Stark extraction
2. Soxhlet extraction
3. $C0_2$-Toulene, huff and puff extraction
4. Retort Distillation

It is also possible to flow solvent through the samples at low temperatures by applying a low pressure. Low flow rates are used to minimize the chance of damaging the plugs by mobilizing fines. Alternating periods of injecting solvent allows periods of soaking and flushing that are continued until the samples are clean.

After the sample has been cleaned, the solvent must be removed. The standard procedure of drying a cleaned sample is to first replace the solvent with nitrogen before placing them in a convection or vacuum oven at 80 °C for 16 to 24 hours [17], or ambient at 60 °C for $>$ 48 hours.

In shaly sands in the subsurface, clay minerals are always wet. The clay particle surface is covered with one or two layers of polar water molecules and small pores will hold water by capillary forces. In smectites, interlayer water and any exchange cation water will start evaporating at 83 °C. This water is part of the total pore volume and will leave the sample together with with the surface water of adhesion and pore water at around 110 °C. If brine is added back to the sample, the water will re-hydrate their respective places. If temperatures exceed 200 °C, an

irreversible process of transforming the clay minerals to ceramic begins. At this point, hydroxyl water that are part of the minerals and grain volume starts evaporating.

Another heat induced change to clay minerals is the gradual transformation of smectite to illite. At 95 °C, the K^+ ion has enough energy to replace the hydrated Na ion together with the water molecules. The waters released during this process result in overpressuring and induced stress that harm fibrous illite. If illite is harmed, the permeability measurements will be done on damaged cores, and the results underestimated.

If illite is present, a method of Critical Point Drying can be applied. The idea is to never let a liquid-gas phase to form that can break the fibrous clay mineral structure by capillary force actions. The liquids in the sample is displaced by liquid CO_2 and the pressure is increased until it is above its critical point. Then temperature is increased above the gas zone before pressure is reduced turning the CO_2 into gas phase. The CO_2 is then flushed using nitrogen. This is a gentle, but expensive and time consuming procedure and should therefore only be applied when necessary.

Both the oven drying and the critical point drying will result in a porosity measurement very close to total porosity on the core plugs. How close to the total porosity will of course depend on how complex the clay structure is. Example, lots of smectite would increase the amount of water left in clays, thus the porosity also would be a bit further away from true total porosity.

It is also possible to dry the cores while trying to retain the clay-bound water, a process called humidity controlled drying. The samples are dried under constant relative humidity conditions at low temperatures. This drying method will give effective porosity measurements, however it is a difficult process and the objective is seldom achieved.

After the cores has been cleaned, determining porosity from plugs consist of measuring two out of the three parameters in equation 1; pore volume, grain volume or bulk volume.

Figure 2 shows one way to determine the pore or grain volume by a gas expansion method, referred to as Boyle's law porosimeter. The dried sample is placed in one of two cells with known volume. The cell is closed and pressurized. Then a connection between the two is opened and the new pressure is recorded. This method measure the volume of connected pores, since helium cannot enter the closed pores. If for some reason the core is not entirely dried, and some water, hydrocarbon or salt are left in the pores, the helium cannot enter these pores. In that case, total porosity will be underestimated and grain densities calculated too low. These are inherent uncertainties the petrophysicist need to be aware of.

Another way to determine the pore volume is to saturate a dry sample with a fluid with known density. The increase in weight from before to after is directly related to the pore volume of the connected pores. Use of the Boyle's law porosimeter is the standard in the industry. For most companies, core porosity after stress correction is considered to be the reference measurements.

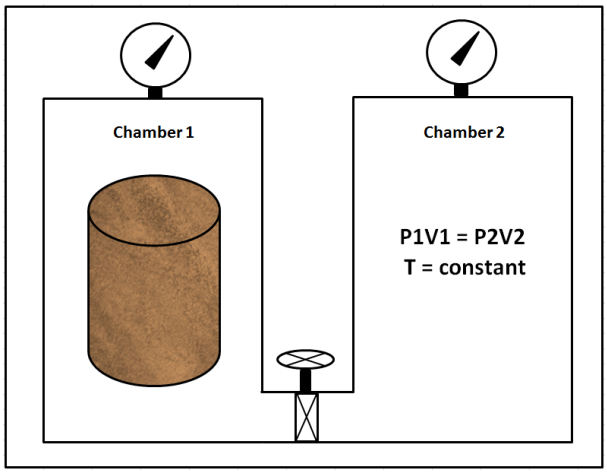

Figure 2: *Boyles law porosimeter. After the valve is opened, helium enters from one container to the other, filling the pores of the sample*

2.1.2 Porosity from log analysis

Density log The most used method to determine porosity is use of the density log. The density measurement is basically a measurement where a chemical radioactive source emits X-rays through a collimated window out into the formation. Receiving photomultipliers measure the intensity and the number of returning gamma rays. From this the formation density can be inferred. Electron density is proportional with mass density and hence an estimate of formation density can be obtained. The density log is used to calculate porosity, evaluate complex lithologies, detect gas and more.

The formation bulk density (ρ_b) is related to the fluid density (ρ_{fl})and formation matrix density (ρ_{ma}) as:

$$\rho_b = \rho_{ma}(1-\phi) + \rho_{fl}\phi = \rho_{ma} - \phi(\rho_{ma} - \rho_{fl}) \tag{2}$$

When solved for porosity, it gives the following relation between the density log and porosity:

$$\phi_D = \frac{\rho_{ma} - \rho_b}{\rho_{ma} - \rho_{fl}} \tag{3}$$

Neutron log The neutron log uses high energy neutrons that collide with the formation before captured at sensors. The receiving sensors measure the number of returning neutrons, but they only sense and count neutrons that have lost most of their energy (Thermal neutrons). The hydrogen atom has about the same mass as a neutron, thus a lot of energy is transferred from the neutron as they collide. Hydrogen is mostly concentrated in the liquids; hence the measurement is highly sensitive to the porosity of the formation. The downside to the neutron log is that there are numerous environmental corrections that must be applied.

Sonic log The sonic logs measure acoustic parameters of the formation. The tool transmits sound waves and record the time it takes the waves to travel a given distance.

The porosity is calculated by Wyllies equation, which uses the velocities for the matrix and the fluids and combines the two into the tool response. The proposal from Wyllie was that the interval transit time (Δt) can be represented as the sum of the transit time in the matrix (Δt_{ma}) and the liquid (Δt_f).

$$\Delta t = (1 - \phi)\, \Delta t_{ma} + \phi \Delta t_f \tag{4}$$

Re arranging into sonic derived porosity:

$$\phi_s = \frac{\Delta t - \Delta t_{ma}}{\Delta t_f - \Delta t_{ma}} \tag{5}$$

The tool response is however not necessarily a volume-weighted average of the porosity, so corrections may be applied.

NMR (Nuclear Magnetic Resonance) is a total porosity measurement that measures, like density and other methods, porosity in μ-pores of shale to larger pores in sand [14]. The tool works by introducing a static magnetic field that aligns the protons (or hydrogen) in the fluid. A series of magnetic pulses thereafter create electromagnetic echoes that decay in strength. If inverse laplace transformed, the exponential decay say something about the amount of porosity in large vs. small pores in a so-called T2 distribution shown in figure 3. The protons in clay-bound and capillary-bound water will relax faster than the protons located in the larger pores. To create cut-offs in relaxation times, core samples are saturated with brine in the laboratory, and scanned prior to and after centrifugation. The difference in the T_2 distribution curves then creates the values to determine the producible fluid volumes. The NMR log gives us information about fluid amounts, fluid types and their distribution among different pore sizes. A part of the free fluid volume might be oil or gas with lower hydrogen index. When the free fluid volume is corrected for this, the NMR porosity should be very similar to the density derived total porosity.

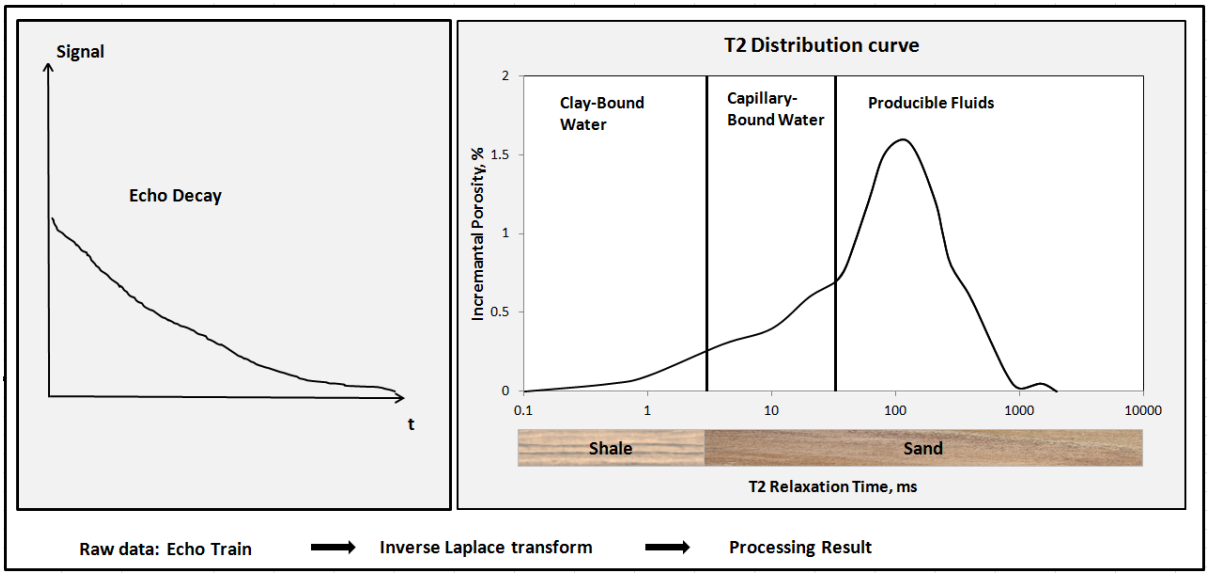

Figure 3: *NMR (Nuclear Magnetic Resonance). Example of a partitioned T2 curve obtained from deconvolution of the T2 spin echo trains*

2.1.3 Errors in determining porosity

The measurement of porosity on cores is a direct measurement, while porosity from logs is an indirect measurement. With the indirect measurements, some potential sources of error will follow [17]. First, the evaluation of the density log often assume grain densities of 2.65 or 2.71 g/cm^3. If possible, grain densities from cores should always be used when calculating the porosity from the density log. Another error is the assumption that the neutron log measure hydrogen content in the pores. This is not true in formations containing clay minerals, as hydrogen exist in the clay structure. The fluids are also assumed to be either water or oil, with similar hydrogen index. If gas is present, the neutron-derived porosity will be to low if this assumption is applied.

The sonic log assumes a constant travel time for the matrix, and that this travel time is known. If clay minerals are present, their distribution (section 2.2.2) will have an impact on the travel times. The matrix travel time will be a function of mineralogy, lithology and stress. If vugs are present, they can create serious errors in the sonic derived porosity.

When comparing the porosity from cores to logs, other errors appear. Because both methods investigate different volumes of rock, it is going to be differences in the measurements. Another source of differences is a depth-shift of the logs to the cores. This shift does not have to be constant, as logs experience stick-slip effects, especially with the tools using pads such as the density log.

The porosity calculated from the density log depend on the choice of fluid density as ρ_{fl} is in the denominator of equation 3. This density will vary with fluid type and salinity. The saturation in the flushed zone is used to calculate an average fluid density used in the porosity calculations.

The assumption that core analysis is correct is also dangerous. As a comment in L.P. Dakes book about reservoir engineering states: *"The only definite thing we know about core is that it is not in the reservoir any more"* [13]. Handling the cores correct is essential, and incomplete cleaning of the cores will result in calculating too low grain densities and too high porosities.

2.2 Shale

Shale is a collective term, defined and used slightly different among the disciplines. For a geologist, shale can be defined as a fine-grained, sedimentary clastic rock with a grain size below 0.031 mm and with $> 35\%$ clay minerals and silt grains. From a geomechanic point of view, shale would be a rock where the clay minerals contribute significantly to load bearing parts of the formation. For a reservoir engineer, shale can generally be characterized as low permeability formations, with little regard to the mineral composition. This is especially true for the formations referred to as shale in relation to shale-gas and shale-oil developments.

Back to the more geological definition of shale, the clay minerals are the single most important component. They have a plate like structure of alternating silica tetrahedras and alumina octahedras with slightly different chemical compositions differentiating the minerals [5]. The basic groups of clay minerals, based on their crystal structure are listed in table 1.

Table 1: *Atomic formulae of Pure Clay Minerals [17]*

Clay Mineral	**Atomic Formulae**
Kaolinite	$Al_2O_3 2SiO_2 2H_2O$
Illite	$KAl_2(OH)_2AlSi(O,OH)_{10}$
Smectite	$(NaMgCa)Al_2O_3 5SiO_2 nH_2O$
Chlorite	$(MgFe)_3Al(AlSiO_3)O_{10}(OH)_5$

Other characteristics of true shale include fissility, the ability to split into thin layers. Since logs don't show the degree of fissility in the subsurface, it is not included in the petrophysical definition of shale.

Shales are mainly deposited in places as river floodplains, lakes, deltas, basin slopes and in deep marine environments. It is differentiated between authigenic and detrital types of shale. The detrital shale is deposited as part of the rock matrix and the authigenic refers to clays that has grown after the matrix was deposited, either as pore-filling, pore-lining or pore-bridging. Diagnetically fromed clay, such as illite, may be recycled back after erosion into new sediments as a detrial component [5].

Increasing shale content has an impact on the neutron porosity and result in a larger separation between the neutron/density curves. This happens as hydrogen is a prominent member of the clay minerals. Shale typically shows high gamma-ray responses and low resistivity ($< 10\ \Omega m$].

2.2.1 Volume shale from log measurements

Gamma Ray The volume of shale in a formation will affect almost all the logs [10]. The most common curves used to estimate shale volume is the GR and neutron-density. As a shale indicator, one value for clean sand and one value for shale are determined, and the volume of shale is distributed between the endpoints.

A linear relationship can be assumed, but is often found to be too pessimistic and overestimate the volume of shale in the formation. For the gamma ray, the linear equation can be written as:

$$V_{sh,gr} = \frac{GR_{log} - GR_{sand}}{GR_{shale} - GR_{sand}} \tag{6}$$

and in figure 4 some non-linear relationships summarized by Bassiouni [1] show that true V_{sh} is usually less then linear V_{sh}. The wide spread between the curves illustrates the uncertainty related to determining V_{sh} from the logs.

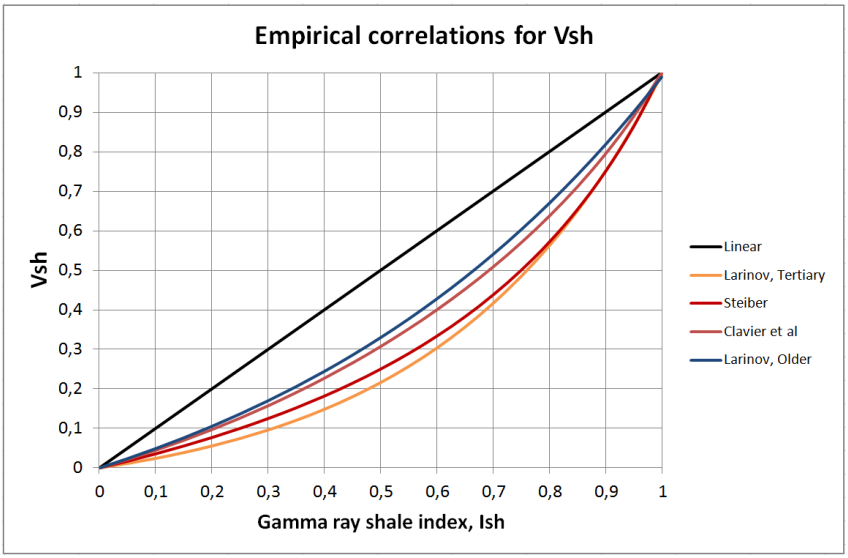

Figure 4: *Empirical correlations relating shale content, V_{sh} to gamma ray shale index, I_{sh}. The linear relationship is shown in black, with other correlations predicting less shale.*

Neutron-Density The combination of density and neutron responses can also be used to estimate volume shale, and is often more accurate than V_{sh} from single log measurements [17]. Both the measurements are affected by porosity, hydrocarbon density and lithology, which include both clay and nonclay minerals [6]. If we know two of these parameters, it can be solved for the other two, meaning we can get estimates for both volume shale and porosity in oil/water filled sand. A triangle is made between a 100% sand matrix point, a 100% shale point and a theoretical 100% porosity point. Responses for clean sand will plot along the clean sand line, and shift towards the shale-point as the volume of shale increases. This happens because of the additional hydrogen in the form of hydroxyls in the shale makes the neutron log read higher values than the density log. Formations containing gas will plot in the upper left corner.

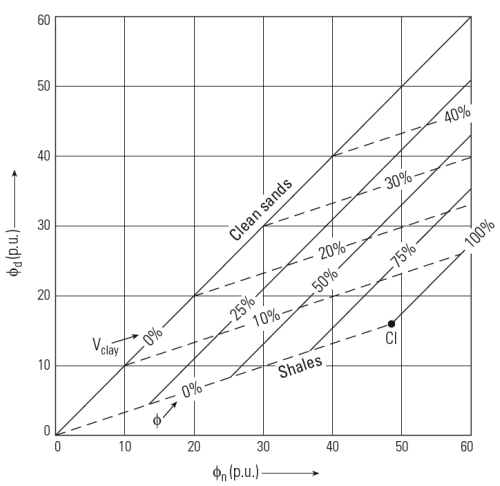

(a) Neutron / Density crossplot. From Ellis & Singer [6]

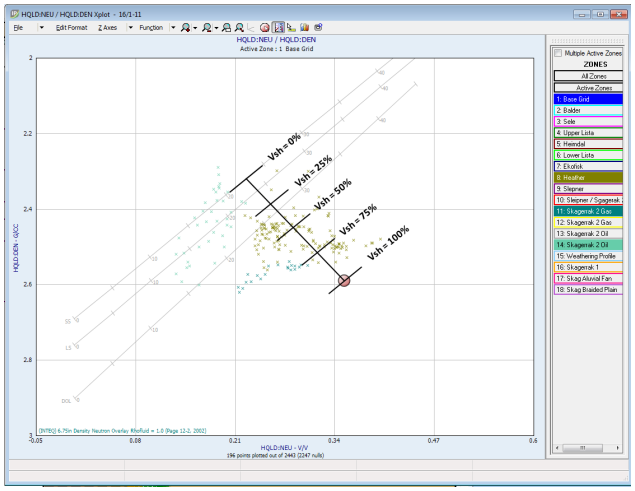

(b) Neutron-Density Xplot from 16/1-11

Figure 5: *Neutron-Density X-plot's used to determine volume shale. A linear relationship is established between the clean formation and the shale point. Different lithology lines exits based on their clean responses.*

2.2.2 The distribution of shale

Shale can be distributed across a reservoir sand body as a combination of three different modes: laminar, structural or dispersed shown in figure 6. The distribution is closely related to how the shale was deposited and will have great influence on the determination and effect of volume shale (V_{sh}). A volume of shale in laminar mode may prove helpful in reducing water coning, while the same amount of shale in dispersed mode may influence permeability significantly and reduce production.

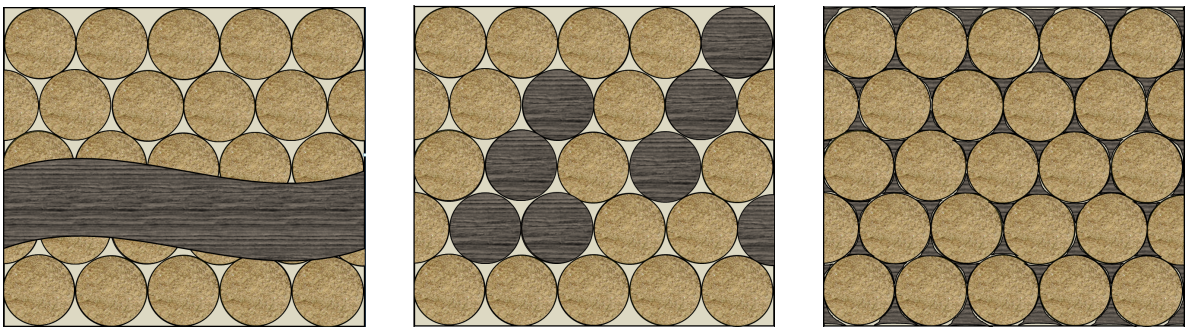

(a) Laminar (b) Structural (c) Dispersed

Figure 6: *Shale distribution modes. The distribution is of considerable importance as the bulk volume of shale is determined and its use in various equations and models.*

One difference between grains of sand (quartz) and shale is that shale has its own porosity. The pores can either be filled with bound water, or some organic content as kerogen or vitrinite making them a potential source of hydrocarbons.

In the laminar case, shale is distributed as layers. In a given bulk volume of sand grains, some have to be removed to make space for the shale. The porosity in this case will be on the form:

$$\phi_T = \phi_{clean\,sand} - V_{sh,\,lam} \cdot \phi_{clean\,sand} + V_{sh,\,lam} \cdot \phi_{sh} \tag{7}$$

$$\phi_E = \phi_T - V_{sh} \cdot \phi_{sh} \tag{8}$$

In the structural case, shale is present as grains within the sand. Since shale has its own porosity, the total porosity in this case increases compared to clean sand.

$$\phi_T = \phi_{clean\,sand} + V_{sh,\,str} \cdot \phi_{sh} \tag{9}$$

$$\phi_E = \phi_T - V_{sh} \cdot \phi_{sh} \tag{10}$$

Dispersed shale is a term for shale distributed inside the pores of the sand. The clay minerals can be precipitated from moving pore fluids, or be a result of sand and silt grains transforming into clay minerals. Since the pore volume and pore throats are reduced as a result of this, the permeability in the formation will be reduced. The porosity will follow the equations:

$$\phi_T = \phi_{clean\,sand} - V_{sh,\,disp} + V_{sh} \cdot \phi_{sh} \tag{11}$$

$$\phi_E = \phi_T - V_{sh} \cdot \phi_{sh} \tag{12}$$

Limiting our self to this simple definition of shale distribution found in the literature can cause errors to be made when evaluating a shaly formation. Figure 7 shows one of the thin sections from Ivar Aasen, and we see that the distribution of shale is not as simple as in figure 6.

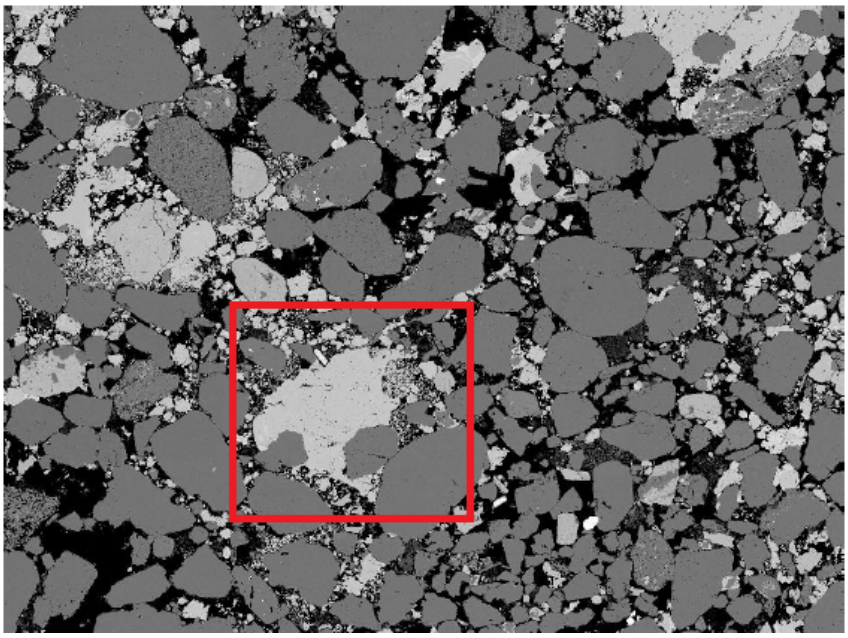

Figure 7: *Shale distributed in a way that would appear as Laminar. Thin section from Ivar Aasen.*

We notice how the grain shapes and sizes vary. During one of the process where structural shale is produced, feldspatic grains are chemically altered into clay minerals in a diagenetic process [17]. The original grain shape and size can be preserved, or shale can be squeezed into the adjacent pore throats. If the original feldspar grain was larger than the average grain, we now have a situation where the structural shale occupies some of the potential pore space. If we revisit equation 7, we see that the situation this represent is the laminar case. Thus, if we have structural shale grains larger than the average grain size; they will appear as laminated shale by means of equation 7. Many large shale clasts, as in the red square of figure 7, will lead to a situation where $V_{sh,lam}$ is overestimated.

2.3 Pore space

The response of the traditional porosity logs is based on readings from different parts of the pore space in a shaly sand. Figure 8 show the differences between what the different logs measure and how cores are dried for porosity measurements.

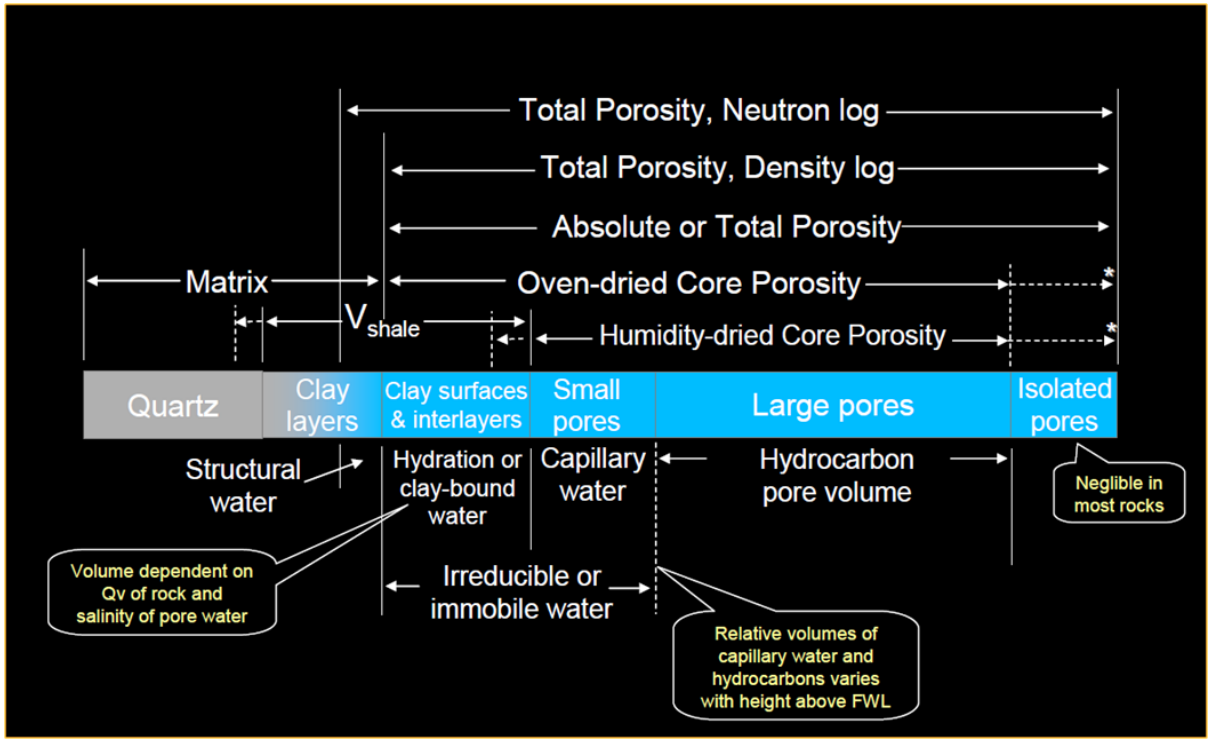

Figure 8: *Pore model with log and core responses. Based on Eslinger, ch9 [5]*

Quarts Quarts is the main matrix mineral and is very common in sedimentary rocks. Sand is defined to have grain sizes ranging from 2 mm down to 0.0625 mm and silt from 0.0039 mm to 0.0625 mm.

Clay layers The individual clay particles consist of layers of two building blocks, the Silica Tetrahedron and the Alumina Octahedron. Depending on different interlayer materials such as water and exchange ions, potassium or magnesium they make up the main different clay mineral groups: Kaolinite, Chlorite, Illite and Smectite

Interlayer Water Smectite has a molecular structure where two water molecules and one exchange ion are separating the silica tetrahedrons and alumina octahedrons. The water molecules can be expelled from the mineral structure either by heating or compaction, but the exchange ion stays in place. This leads to a situation where water can again be added to the interlayers and the smectite will swell. This water will act as bound water.

Bound Water In a shaly sand, some water will exist as clay bound water. Because of the structure of the clay minerals, which is the largest source of charge effects, they will most of the time have a negative charged surface. The formation water is salty, and have anions (for example Cl^-, negatively charged) and cations (for example Na^+, positively charged) in solution. Because water is a dipole molecule, the positive oxygen side will be attracted to the cation, and the positive hydrogen side will be attracted to the clay mineral. The cations, or exchange ions, can conduct current along the surface of the clay minerals much easier than trough the pore water. This leads to an extra conductive path relative to the concentration of exchange cations.

The bound water occurs in different ways as (Petroskills [17]):

1. Water on the surface due to adhension, typically a mono-layer
2. Water that hydrates the exchange cations
3. Water that is in the interlayers of the clay minerals (smectites)
4. Water that is in micro-pores due to capillary forces

Small pores In addition to the water associated with the exchange ions, some water molecules are by themselves bond to the charged mineral surface by van der Waal forces. This can be classified as capillary bound water, and these water molecules are much less mobile than the rest of the free water molecules in the pores.

Large pores Free water is water located in the pore space at saturations above the critical water saturation. It has relative permeability above 0 and will flow easier as the water saturation increases. Hydrocarbons sometimes make up a fraction of the pore space. Some will be produced, while some will be left behind as residual oil saturation.

2.4 Effective porosity

The porosity concept gets a little more complex as effective porosity is introduced. The term "effective porosity" means different things to different people, and it is necessary to be more specific. The core laboratories often call effective porosity the oven dried interconnected porosity, leaving out the volume of isolated pores. For a log analyst, $\phi_e \to 0$ as $V_{sh} \to 1$ ($\phi_e = \phi_t - V_{sh} \cdot \phi_{sh}$). In NMR log analysis, a 100 psi air-brine capillary pressure define a cut-off to effective porosity on the T_2 distribution [6]. Reservoir engineers think of effective porosity as hydrocarbon filled porosity that will function as a path for flow, given a small differential pressure. Suddenly we can find our self in a situation where we do not longer compare apples to apples.

Either way, effective porosity is neither defined nor measured directly on cores. It adds an additional stage to the log processing, and will be influenced by errors in clay volume and clay porosity as they are transferred into the effective porosity.

All the bound water (section 2.3) add up to the total porosity, as it is a part of the pore space and does not consist of matrix material. Item 1-3 can be defined as clay bound water, but all 4 can be classified as non-effective pore space. That means the relative permeability of this water is so much smaller than for the free water and it will never be produced under normal reservoir conditions. This leads to the concept of effective porosity, defined as:

$$\phi_E = \frac{V_p - V_s}{V_b} \tag{13}$$

where V_S is the Sorbed/Bound water. V_p is the pore volume and V_b is the bulk volume.It is worth mentioning that all this water would be collected during a Dean-Stark measurement, so that the terms effective porosity and total porosity could be mixed up coming from the laboratory.

Hill et al. [8] showed that it is possible to quantify the amount of bound water in a shaly sand sample in the laboratory and then correlate it to other parts of the formation. The equation uses the NaCl concentration and the cation exchange capacity of the clay minerals as follows:

$$1 - \frac{\phi_E}{\phi_T} = \frac{V_s}{V_p} = \left(\frac{0.084}{\sqrt{C_o}} + 0.22\right) Q_v \tag{14}$$

Together with capillary pressure experiments, all 4 types of bound water can be measured, and total porosity can be transformed into effective porosity on the cores.

On logs, the total porosity is calculated into effective porosity by the formula:

$$\phi_E = \phi_T - V_{sh} \cdot \phi_{sh} \tag{15}$$

2.5 The Net-to-Gross Ratio

Not many aspects of the petroleum industry can beat the Net-to-Gross ratio when it comes to appearing simple, while hiding such great amounts of confusion and ambiguities. The first source is in the definition of "Net". Different authors define Sand, Reservoir and Pay differently and a specification of the terms is therefore needed to avoid confusion. Figure 9 shows that within the total evaluation interval known as Gross rock, we find Net Sand, Net Reservoir and Net Pay [25].

Net Sand can be viewed as all rock that could be a potential reservoir. This would exclude for example evaporites, mudstone and unfractured basement rock. Net reservoir is the portion of rock within the potential reservoir that holds porosity and permeability above a critical value. Net pay is a subinterval within the gross rock thickness that in addition holds sufficient amounts of recoverable hydrocarbons. The net pay subintervals are often added together to give a total net pay, and then divided by the gross thickness to give a Net-to-Gross ratio. On a larger scale, this Net-to-Gross ratio is used for executive summaries and given to the media when a discovery has been made. The Net-to Gross ratio contributes to the calculation of volumes in place and of the estimated ultimate recovery from the field as in equation 16.

$$EUR = \left(\frac{A \cdot h \cdot NTG \cdot \phi \cdot S_o}{B_o} \right) RF \tag{16}$$

<table>
<tr><th>Gross Rock</th><th>Net Sand</th><th>Net Reservoir</th><th>Net Pay</th></tr>
<tr><td rowspan="3">All rock within the evaluation interval</td><td rowspan="2">Potential reservoir, All Sand</td><td rowspan="2">Sands that would contain HC if above the OWC</td><td>Above critical amounts of recoverable hydrocarbons</td></tr>
<tr><td>Subcritical hydrocarbon content</td></tr>
<tr><td>Subcritical porosity and permeability character</td><td></td></tr>
<tr><td></td><td>e.g. Evaporites, mudstones, unfractured basement</td><td></td><td></td></tr>
</table>

Figure 9: *Definition of different Net's used in the Net to Gross ratio [25].*

For other purposes, such as reservoir simulation, the global net-to-gross ratio is of little importance. We need to keep track of where every subinterval of pay is located for the simulator to describe the reservoir behaviour as correct as possible. Before we can do that, we need to look into how net pay is quantified. In an attempt to identify non-producing zones, limiting "cut-off" values were in the past (or still are) applied to the petrophysical logs. The problem with the

petrophysical cut-offs are that they have been used by the industry for over 60 years [24], and there are still no academic well defined procedure for identifying or applying them.

Typical cut-off parameters are V_{sh}, used as an identifier for Net sand. Then a ϕ cut-off is applied for the Net reservoir before a S_w cut-off defines Net pay. In the search for the perfect definition of Net Pay, there have been cut-off values assigned to almost every kind of parameter possible to obtain. The range goes from economical considerations [24] to the colors of UV light core photos [16]. This has evolved into some rule of thumb parameters, such as cut-off of 1 md for oil reservoirs and 0.1 md for gas reservoirs. Or more consistent with Darcy's equation in the form of fluid mobility as [19]:

$$\left(\frac{0.01md}{0.05cp}\right)^{gas} = \left(\frac{1md}{5cp}\right)^{oil} \tag{17}$$

As cut-off values are applied to logs with poor vertical resolution, the problem with by-passed pay arises. In a thin, inter-bedded, laminated sand-mudstone system, it is hard to know what hides behind the bulk porosity from the density log [7]. As the density log averages good and bad zones, the good sands will be hidden in the log response. The bulk porosity from the log might end up under the limiting porosity value, causing the whole section to be ruled out.

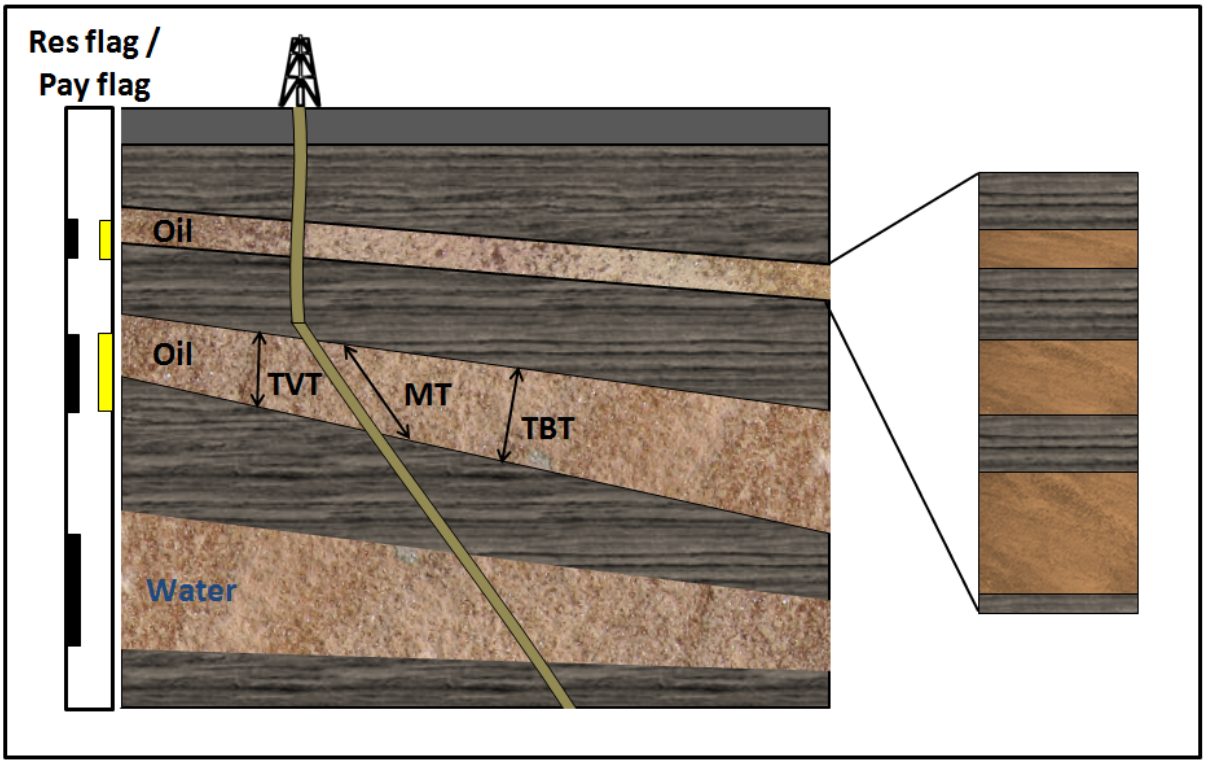

Figure 10: *Net to Gross cross section of a reservoir. Shale laminations may exist on a smaller scale within the net reservoir.*

It is worth noticing that well deviations and bed dipping play a role when net thickness is determined. Even if the well is deviated updip or downdip makes a difference [25]. In figure 10 we can see that measured thickness (MT), true vertical thickness (TVT) and true stratigraphic bed thickness (TBT) all complicates the determination of Net Pay. This get even more complex if bed dip and well deviations are in different planes.

2.5.1 Fractional Net to Gross at petrophysical log scale

Reservoir rocks have variable sand and shale content. Different sands have different reservoir qualities. Differing between net and non-net is an important step before using pore volume logs in a geomodel. One way is through effective porosity adjustments ($\phi_E = \phi_T - V_{sh} \cdot \phi_{sh}$) , another is through a continuous Net to Gross curve.

The fractional Net-to-Gross curve is not as simple as $1 - V_{sh}$ as a function of depth. It is a measure of the sand fraction with potential for hydrocarbon within the investigated volume. To estimate this, there are several approaches, and some of these involve the use of V_{sh} (See section 2.2.1).

There are several methods that can be applied to describe a fractional Net to Gross estimate at an petrophysical log scale.

1. Thomas & Stieber The Thomas and Stieber method (covered in section 2.5.2) gives V_{sh} and in addition ϕ_{sand} from the GR vs. Porosity cross-plot [17]. If the gamma ray log for some reason can not be used, another shale indicator may replace it. The method will honor sands on a lower scale than the bulk measurement. Another benefit with the Thomas & Stieber method is that, because of the simple input, data is almost always available to perform an analysis.

2. 3D resistivity tool Shaly laminations will make an impact on resistivity logs. Because the clay minerals have a layer of ions attached to their surface, they are more conductive than sand. Conventional resistivity tools measure resistivity mainly in the horizontal direction [9]. The use of a triaxial set of induction transmitters and receivers makes is possible to get a resistivity measurement of the bedding plane, R_H and its orthogonal, R_V. In formations with thin laminated shale, it is now possible to get a value of the resistivity within the sand layers. And this resistivity is closely related to the water saturation. The resistivity are measured either in a series or a parallel with the following equations [9]:

$$R_v = (1 - V_{sh}) \times R_{sand} + V_{sh} \times R_{sh-V} \tag{18}$$

$$R_H = \frac{R_{sand} \times R_{sh-H}}{(1 - V_{sh}) \times R_{sh-H} + V_{sh} \times R_{sand}} \tag{19}$$

The 3D resistivity tool can also take the shale anisotropy into consideration. Anisotropic shale can drag down the sand resistivity and make the estimate of water saturation to high. A crossplot of R_V and R_H makes it possible to determine both V_{shale} and R_{sand} .

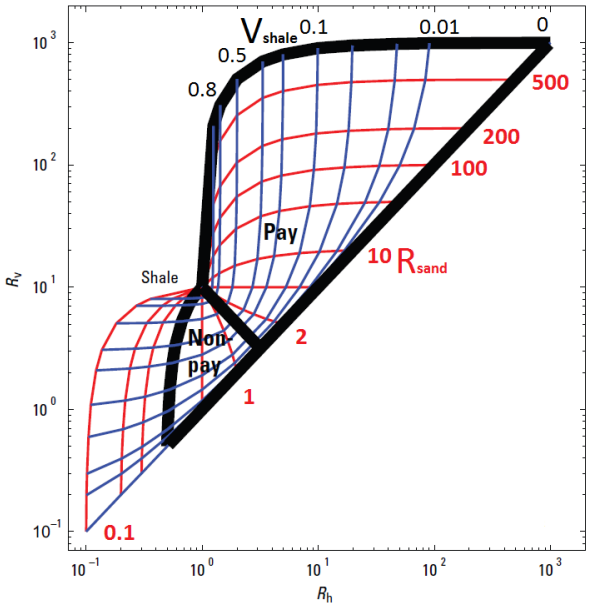

Figure 11: *Cross plot of Rv and Rh (Butterfly plot) discriminate pay from nonpay zones. From Leverdige and Minh, [11] [15].*

3. NMR The NMR log can be used to estimate the amount of clay-bound and capillary-bound water by looking at the components that decay with a time constant faster than 33 ms. Fast relaxation times indicate that fluids are in small pores. A cut-off smaller than 10 ms is often used to look on shale bound water only. Cut-offs as low as 3 ms and 5 ms is in the literature used to estimate clay bound water [21] [14]. Total porosity can then be used as a Net to Gross measurement if the free fluids are Hydrogen Index corrected.

4. Image Logs The image tools provide high resolution measurements that are converted into images. As long as contrast between net and non-net can be seen on a fine scale with orientation in the borehole, images can be created. To obtain a fractional Net to Gross curve, the amount of sand within a 0.4 meter interval may be integrated to fit the scale of other log measurements. It is however hard to use images as the only input to the Net to Gross curve, but they can provide good support for other methods that are formalized. Figure 12 shows an example of an image log from Ivar Aasen. It shows thin shale laminations (Black) on a fine scale, based on gamma ray, photoelectric factor and density logs.

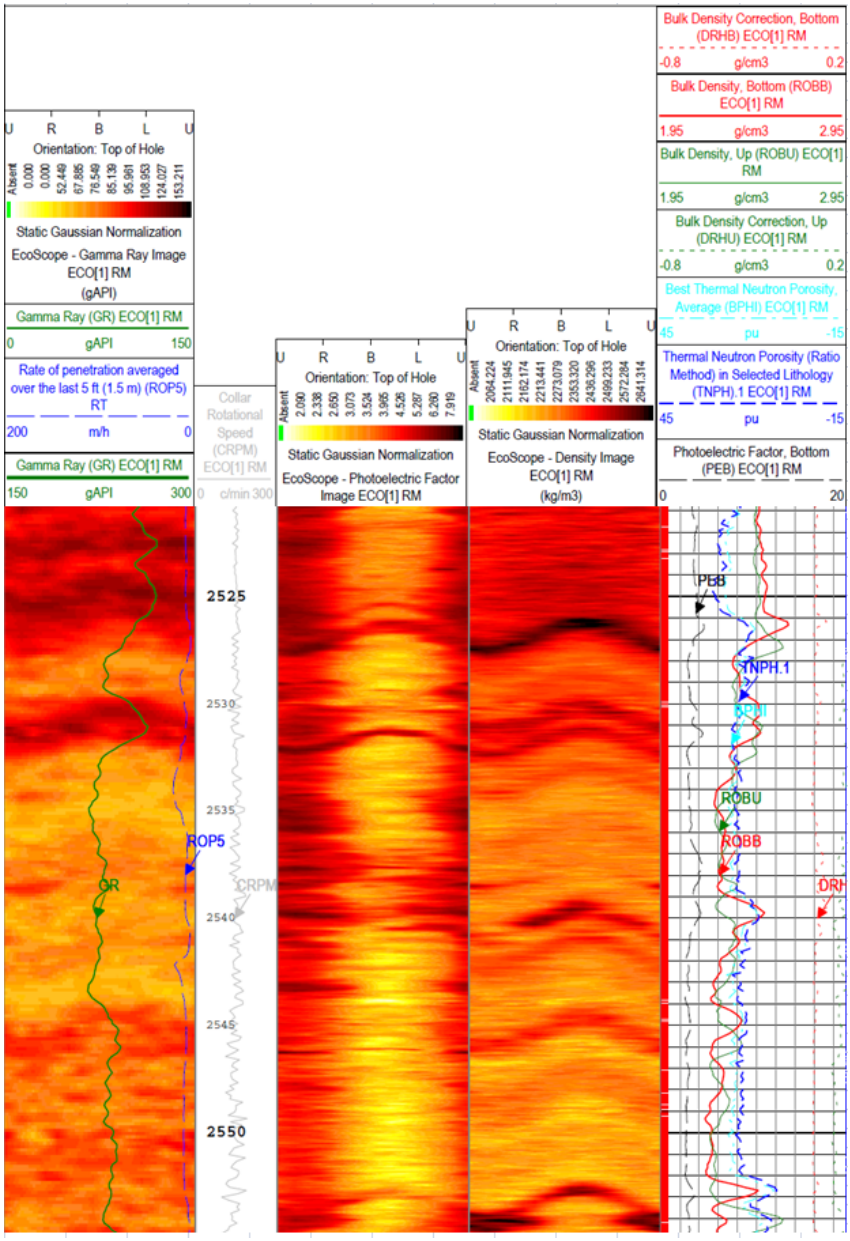

Figure 12: *Image log from 16/1-16A, Ivar Aasen. Thin shale laminations is shown in black on images created by gamma ray, photoelectric factor and density logs.*

2.5.2 Thomas and Stieber method

A volumetric method for shaly sands developed by Thomas and Stieber [22] is based on a crossplot of gamma ray response vs. porosity and helps determine the shale configuration, the sand fraction and the sand porosity. It is based on the expected response for the three different shale distributions and creates a triangle between 100% shale, 100% clean sand and the theoretical case where all the pore space is filled by dispersed shale. The values for clean sand and shale is taken from core analysis, and then combined to create the 100% dispersed point. The trend of porosity with sand volume can then be used to determine the type of shale distribution [6]. This is helpful as sand with good porosity, but much dispersed shale, can be ruled out as non-net. It is also helpful as it gives estimates for the sand porosity, used to match

cores and estimate sand permeability.

Thomas & stieber is one of the methods available to construct a fractional Net-to-Gross curve, and it was used in this study. More specifically it was multiplied by the PHIT Sand estimate at every depth increment (Waxman & Smits, PHIT case). The method does not determine the thickness of the individual shale laminations, but returns a value for the volume investigated. Figure 13 shows an example where a point with a normalized gamma response of 0,26 and a hydrocarbon corrected porosity of 0,22 can be graphically solved for $V_{sh} = 0,2$ (NTG=0.8) and $\phi_{sl} = 0,25$

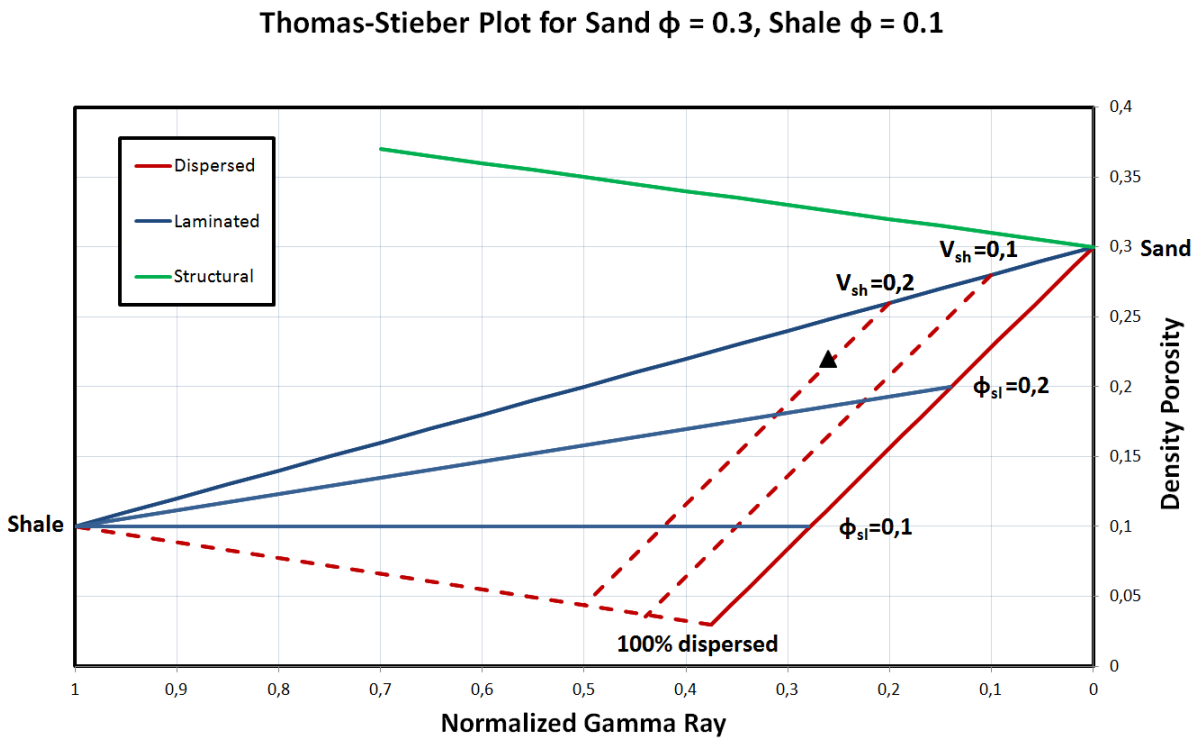

Figure 13: *Thomas-Stieber analysis with a point indicating* $V_{sh} = 0.2$ *and* $\phi_{sand} = 0.25$

The density porosity equation (equation 3 in section 2.1.2) assume a clean formation, and is not corrected for shale which has a different matrix density. One way of correcting it is to iterate on the Thomas & Stieber plot because ρ_{ma} is dependent on the NTG ratio. As the NTG ratio is read from the chart based on ϕ_D, an iterative process of adjusting ρ_{ma} with the previous NTG ratio will return a new NTG ratio. This becomes increasingly important as NTG ratios get low, and we move further away from the clean sand originally assumed in eq 2 and 3. As seen on the plot in figure 13, the sensitivity of the porosity in the important laminated sand layers, ϕ_{sl}, increase as the lines move closer together. Luckily the sensitivity increases in the direction of less productive parts of the formation.

2.5.3 Logging in a laminated sand/shale formation

To illustrate the effect of averaging bulk measurements figure 14 show the values read in a laminated formation. It contains 50% sand, with good porosity and permeability, and 50% shale. The log will average porosities and read 15% as the total porosity. If we calculate

effective porosity to compensate for shale, we end at 10%, assuming a shale porosity of 10%. The porosity of the 30 cm sand is 20%, and has the permeability of a 20% porosity sand. The Thomas & Stieber method described in section 2.5.2 will return the 20% sand porosity together with a fractioanl net to gross of 50%.

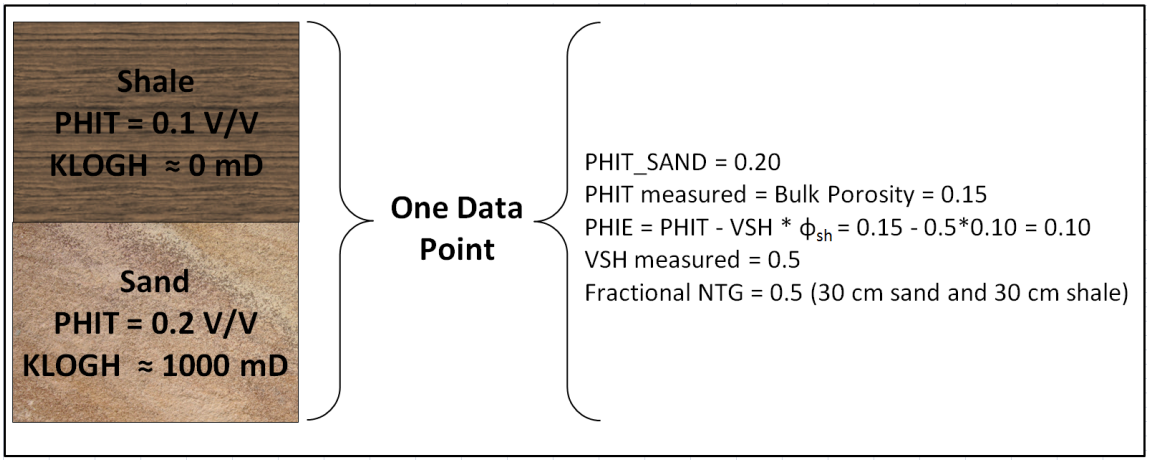

Figure 14: /
The averaging effect of bulk measurements on porosity illustrated on a 60 cm interval containing 50% shale.

Figure 15 shows cores from well 16/1-11 and that the Ivar Aasen field has sections of shale, laminated sands and good sands. When logging sections like the one in the middle, seen in figure 16, properties of the 3 sands will be averaged together with the shale. Using the Thomas & Stieber method, it is possible to obtain an estimate of net to gross ratio, sand porosity and the amount of dispersed shale within the log resolution showed in the red square. But it is impossible to separate the 3 sands from each other; they will appear as one sand. In reality, these sands will probably have different porosity and different permeability. Because of the logarithmic relationship between porosity and permeability, the average permeability of these sands will be underestimated. This happens because the high permeability is affected more than the low when the porosities is combined into an average porosity. As a result, sections with more than one sand within a log resolution are likely to have underestimated permeability even while trying to correct for this.

On the other side, there are effects pulling in the opposite direction. When porosity is measured using a Boyle's law porosimeter, two chambers with known volumes are filled with gas. One contains the core sample and the difference in pressures before and after relates to volumes and porosity. If isolated pores are present, they will not be filled with gas. When logged in the well, these pores will be recorded just as any other pore volume. Permeability correlations are then made by using the cores with underestimated total porosity, and the logs will overestimate permeability. In sand reservoirs, like Ivar Aasen, the presence of isolated pores is as good as absent. In carbonates however, this is an effect that one should be aware of.

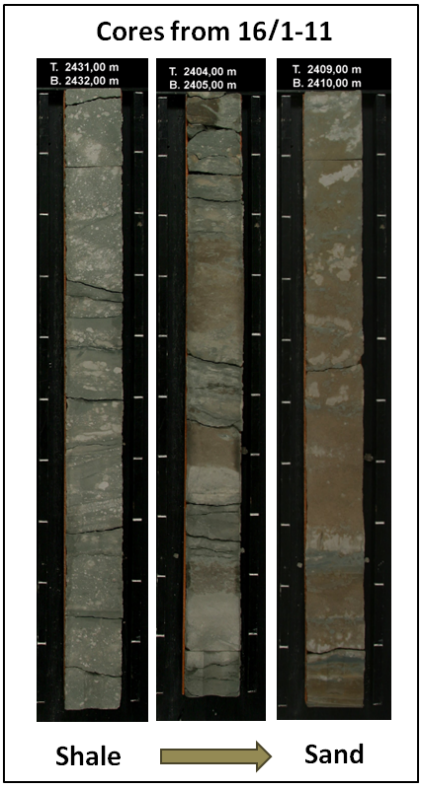

(a) Cores in normal light

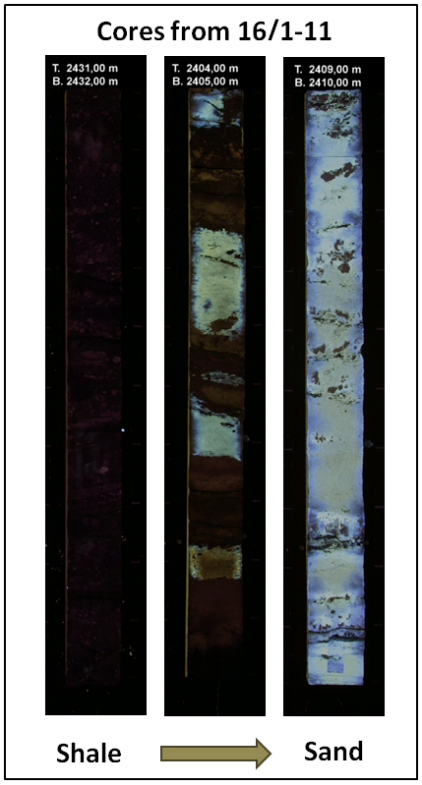

(b) Cores in UV light, showing traces of hydrocarbon

Figure 15: *Core photos from well 16/1-11, Ivar Aasen. Shale is represented to the right, an oil-bearing laminated sand in the middle and an oil-bearing clean sand to the right.*

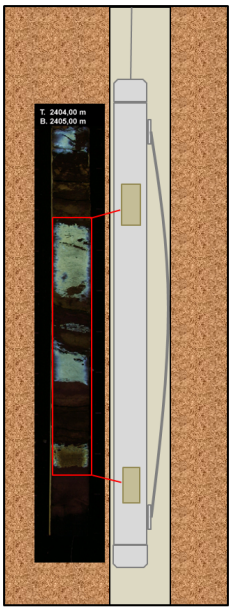

Figure 16: *A CNL (Compensated neutron log) with vertical resolution of 60 cm, logging a laminated shale section*

2.6 Permeability

In 1856, Henry Darcy published his work in improving the waterworks of the town Dijon, by designing a filter large enough to process the daily water requirements [12]. His experiments consisted of flowing water through a sand pack, while recording flow rates and a pressure drop. With the relationship in his equation, Darcy's law (eq 20), came a parameter describing the sandpacks ability to transmit fluids. This is the permeability, (k). The result of Darcy's law and permeability is an introduction of a time-scale to oil recovery calculations. This makes it a fundamental input to geomodels and reservoir simulators.

$$Q = -A\frac{k}{\mu}\frac{\partial \Phi}{\partial x} \tag{20}$$

In Darcy's law Q is the flow rate, A is the cross sectional area, μ is fluid viscosity, k is permeability and $\frac{\partial \Phi}{\partial x}$ is the potential/pressure gradient in the flow direction.

The absolute permeability is a property based on an assumption that only one fluid is present, and it is fully saturating the entire pore space. As soon as more fluids are present, they will have relative permeability dependent on their saturation.

2.6.1 Permeability from core analysis

On core samples, permeability is calculated by laboratories after experiments where gas or liquids are flowed through the plugs. Under normal reservoir conditions, the permeability is only a reflection of the sand structure and pore throat sizes, but in the laboratories the case is different. Air is usually flowed through the cores at close to atmospheric pressures, and a slippage effect between the air molecules and pore walls can occur at low flow rates. This is known as the Klinkenberg effect, and it must be corrected for in order to determine absolute permeability.

Permeability can also be corrected for in-situ rock-brine interactions. Some plugs are flowed with both air and brine to establish a basis for correction before the brine absolute permeability is calculated. The brine permeability can be significantly less than the klinkenberg values. This happens if the drying of cores makes the clay minerals shrink and collapse onto the sand grains. That way, air will have an easier path, compared with the situation where the clays are re-saturated by the brine [5]. The effect of overburden pressure also reduces the porosity and permeability as the rock and pore space is compacted.

2.6.2 Permeability from log analysis

An indirect method of obtaining permeability estimates is by making a petrophysical correlation of core porosity vs. core permeability. Other cross correlations can also be made based on water saturation, gamma ray responses, grain density etc [13].

After coring one well, such correlations are made for every zone and rock types. After correcting the surface porosity for overburden stresses, the porosity log can be directly correlated to core permeability. This makes it possible to create permeability distributions in wells that have not been cored. The correlations are capable of providing a reasonable estimate for permeability, but the true permeability distribution is lost as a line is drawn through the data. The porosity

log is also a bulk measurement, leading to underestimation of porosity and permeability in thin laminated sands.

2.7 Water saturation equations

Determination of water saturation, S_w, is one of the main goals of formation evaluation. It is an important parameter in oil volume, relative permeability and net pay determination. It is usually determined from formation resistivity, and numerous models and equations exist in the literature. This section aims to describe these models and differentiate the two methods used in this study to determine S_w. The conductivity of shaly sand reservoirs depend on the formation water salinity and properties of the shale itself. As figure 17 shows, there might be situations where the standard Archie equation is no longer valid. In the equations, effective porosity has been used as input in the Indonesia equation and total porosity in the Waxman & Smits equation. The equations differ in the use of shale input, compared to the basic clean sand Archie equation.

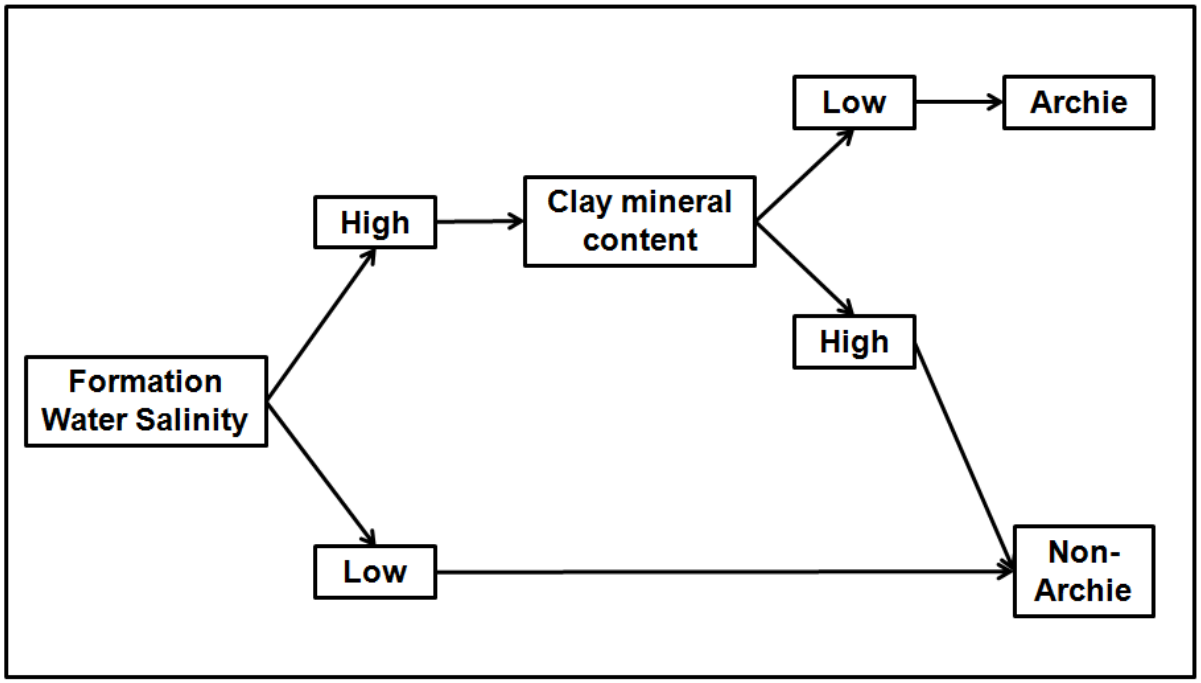

Figure 17: *Flowchart describing situations where standard Archie is not applicable. Inspired by Brandsen [2]*

2.7.1 Archies Equation

The first attempt to determine water saturation from resistivity measurements was done by Archie where he showed that water saturation could be calculated if reliable logs of R_w, R_t and ϕ existed. He noticed that a formations resistivity was proportional to porosity and the water resistivity with a proportional factor, F, called the formation factor. The porosity is adjusted by a cementation exponent, m, and must together with the constant, a, be determined for the different lithologies.

$$F = \frac{R_o}{R_w} = \frac{a}{\phi^m} \tag{21}$$

Archie found an empirical correlation where the water saturation was given as

$$S_w^n = \frac{R_o}{R_t} \tag{22}$$

where n is the saturation exponent. If we combine these equations, we get the Archie equation as:

$$S_w = \left[\frac{a \times R_w}{\phi^m \times R_t}\right]^{\frac{1}{n}} \tag{23}$$

One of the assumptions in Archie equation is that the formation framework has no electrical conductivity. This is not true for rocks containing shale and clay minerals. In shaly formations, the formation factor is no longer constant; it decreases as the water resistivity increases. Another difference in shaly formations is that, m decreases and, a, increases [10].

2.7.2 Indonesia Equation

In 1971, Poupon and Leveaux introduced a method for analyzing logs in shaly formations. They observed that fields with high shale content, <40% , and low water salinity <40,000 ppm, the water saturation tended to be overestimated. To determine the water saturation, they expressed a new relationship between the true resistivity, R_t and the formation parameters affecting the resistivity, $R_w, R_{clay}, \phi, V_{clay}$, and S_w [18]

$$\frac{1}{R_t} = \frac{(V_{clay})^c \times S_w}{R_{clay}} + \frac{\phi^m S_w^n}{aR_w} \tag{24}$$

The equation can be split up, as the first term is describing the clay effect, and the second term is the Archie equation. The paper present two equations, as the first tend to overestimate S_w when the ratio of R_{clay}/R_w is low and the clay content is high. The second equation shifts more of the same samples investigated in the paper to have less than 100% water saturation [18].

$$\frac{1}{R_t} = \left[\frac{V_{clay}^{(1-V_{clay}/2)}}{\sqrt{R_{clay}}} + \frac{\phi^{m/2}}{\sqrt{aR_w}}\right] S_w^{n/2} \tag{25}$$

The authors conclude that the second equation best account for the effect of clay in the range of 40% to 90% on the resistivity of a shaly formation, particularly in the case of low R_{clay}/R_w ratios. However, the equations are 100% empirical and have no physical underpinning.

2.7.3 Waxman & Smits Equation

In 1968, 3 years before the Indonesia equation was introduced, Waxman & Smits introduced a model based on the cation exchange capacity rather than shale volume. A far as the author can tell, their paper "Electrical Conductivities in Oil-Bearing Shaly Sands" [23] was the first attempt to extend the electrical conductivity model to cases where both oil and water was present in shaly sand.

The Waxman & Smits model takes into account that the exchange cations in a given pore will have an increased effect on the conductivity as water saturation decreases and oil saturation increases. The idea is that the water near the surface of clay minerals will influence the conductivity relative to the cation exchange capacity.

The total conductance of the rock can be viewed as two parallel resistance elements. It is the sum of the free electrolyte contained in the pore volume, C_{el}, and the electrolyte resulting from the conductance contribution of the exchange cations associated with the clay, C_c [23].

$$C_{rock} = C_o + C_{el} \tag{26}$$

where

$$C_o = xC_e + yC_w \tag{27}$$

Here C_o, C_e and C_w is the specific conductance's of core, clay exchange cations and equilibrating salt solution, respectively, and x and y are appropriate geometric constants [23].

On a plot of sand conductivity, C_o vs. solution conductivity, C_w, there is a strong influence of the clay term as the formation water salinity is low. Also, the curve is shifted upwards compared to a clean sand relationship where the matrix does not contribute to the conductivity. The sharp increase in conductance with the increasing concentration of electrolyte in the dilute range is attributed to an increasing cation exchange mobility [2]. As we move up the curve, the electrical path through the free electrolytes costs approximately as much energy as en electrical conduction over the clays' surface. This results in a linear relationship with increasing solution conductance.

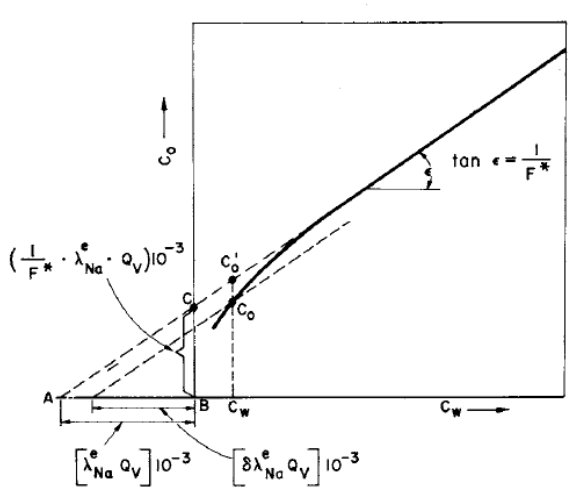

Figure 18: *Core conductivity C_o as a function of equilibrating solution conductivity C_w. From Waxman & Smits [23].*

A note should be made that we are working in the total porosity system with Waxman & Smits equations. Figure 19 shows the hydrated clay exchange ions near the clay mineral surface. The amount of hydrated exchange ions remains the same, when hydrocarbons occupy a fraction of the total pore space. This leads to a higher concentration of the exchange ions in the remaining pore water. The electric current is assumed to follow the same tortuous path along the clay minerals as the ions in the pore water.

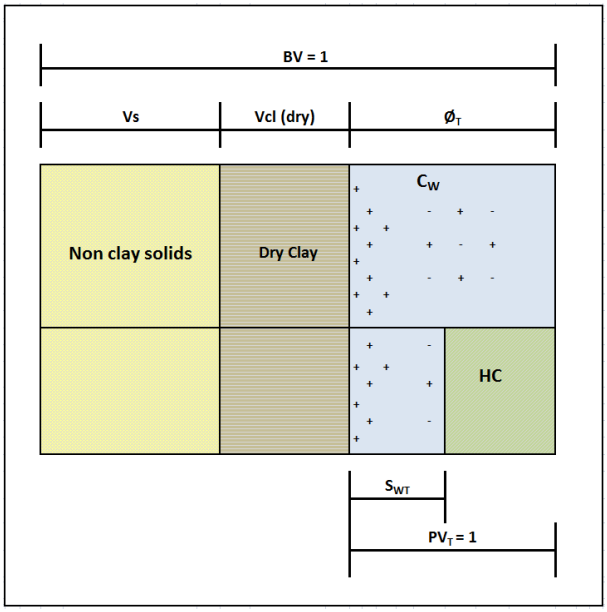

Figure 19: *Waxman & Smits Pore space model. Inspired by PetroSkills [17]*

The general equation can be written as

$$C_o = \frac{1}{F^*} \cdot (C_w + BQ_v) \tag{28}$$

And Waxman & Smits equation expressed with BQ_v and R_t as

$$\frac{1}{R_t} = \frac{S_w^2}{F^* R_w} + \frac{BQ_v R_w}{F^*} \tag{29}$$

The * in the formation factor of equation 28 and 29 is there to tell us it is a shaly sand formation, not a clean sand as originally in Archie's equation (21).

A challenge associated with the Waxman & Smits model is that Q_v is not measured on logs, but must be determined from cores. This is done in a laboratory by flooding a sample with different brines and measuring the resistance over the plug. Q_v can be seen as the segment A-B on the C_o/C_w plot in figure 18 from the Waxman & Smits paper [23].

3 Methodology

The purpose of this study was to investigate the effects petrophysics has on reservoir simulation. To do this, a process similar to the workflow at Det norske oljeselskap was used. The Ivar Aasen field was chosen because of its heterogeneous nature. The amount of available data is also manageable.

The petrophysical work prior to building the geomodels involves evaluation of logs and cores. This process worked as a quality control to the work already done by the petrophysicists at Det norske oljeselskap. All the logs was interpreted and prepared for the base case scenarios, and they where compared to a core reference.

There are numerous shaly sand water equations available. The reason for choosing the Indonesia equation and Waxman & Smits is that they are widely used in the industry, all data was available and they are based on effective and total porosity inputs.

The petrophysical work has been done using version 4.2.2014 of Interactive Petrophysics (IP) by Senergy Software. It is one of the large commercially available software packages used for petrophysical evaluation in the oil industry. Petrel and Eclipse was used as this was the standard at Det norske oljeselskap. A disadvantage, at least with IP, was that the software had to be learned from scratch. With the amount of code-editing, manual iterations and data handling, some minor errors could exist. Also, IP has some short comings, mainly related to saving and loading data. To deal with this a lot of input control, plotting and double checking was done to minimize these errors.

Petrel, Eclipse and other reservoir simulators are tools that should be used with care. If fed the wrong input, they will calculate meaningless results with incredible precision. Even small changes in the inputs, can make a surprisingly large effect on the results. This effect is clearly shown in this study with the sensitivity to volume shale.

As this thesis set out to compare and investigate the differences in shaly sand water saturation equations, and their sensitivity to volume shale, this is where the road splits between all the cases. To build the different geomodels for simulation, unique curve sets for all the appraisal wells, in all the cases had to be made. These curves were the Porosity, Net-to-Gross and Permeability. Water saturation curves are used as one of the cut-offs for Net Pay, but also in porosity calculations based on density readings from the invaded zone.

Figure 20 shows a flowchart of the work done, first on well scale in IP, then on field scale in Petrel

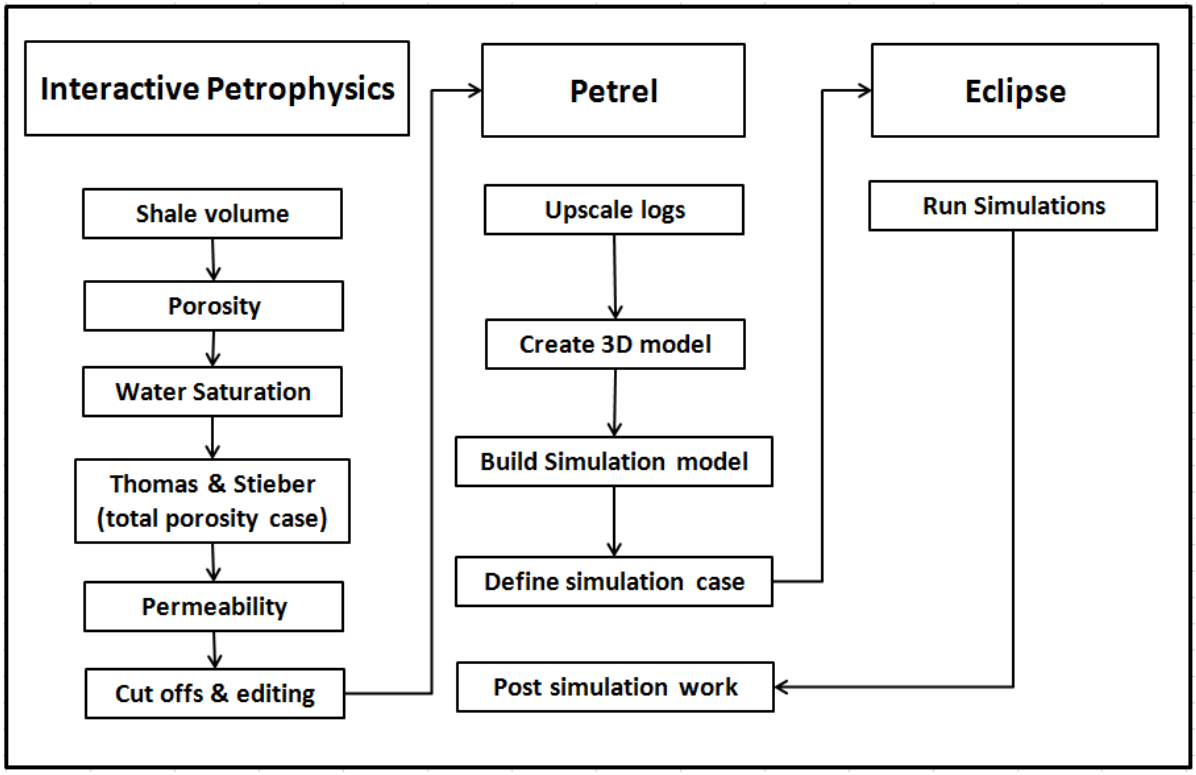

Figure 20: *Flowchart describing the procedure from log interpretation to simulation results.*

3.1 Input to geomodel

In both the effective and total porosity case, the volume of shale is calculated from the same logs, following the same procedures. The density log was used to calculate total porosity, and the Thomas & Stieber method was applied to obtain estimates of sand porosity and the fraction of laminated sands. The sand porosity matched the cores dried to total porosity. In the wells with cores, this sand porosity was used as input to the permeability correlation in the zones that contain good sands. For the other zones and the other wells, total bulk porosity was used as input to the permeability correlation. To adjust the sand porosity and permeability before importing it to the model it was multiplied with the fractional net to gross ratio.

In the effective porosity case, shale is adjusted for at an earlier stage. Porosity is adjusted by subtracting the porosity associated with shale. From this point, the effective porosity is entered as a porosity log to the geomodel and into the permeability correlation without further modifications.

Table 2: *Petrophysical Model inputs*

	Total Porosity	**Effective Porosity**
Volume shale	Neutron / Density, GR	Neutron / Density, GR
Shale distribution	Thomas & Stieber	
Porosity	$\phi_{t,sand} \cdot NTG_{fractional}$	$\phi_e = \phi_t - V_{sh} \cdot \phi_{sh}$
Permeability input	ϕ_t and $\phi_{t,sand}$	ϕ_e
Permeability scaling	$k \cdot NTG_{fractional}$	
Water saturation equation	Waxman & Smits	Poupon & Leveux

3.1.1 Sensitivity of the porosity models

As a first look at the uncertainties and the sensitivities related to the methods, a quick arithmetic comparison of a laminar shale case was made (ref section 2.2.2). Plots of porosity corrected for shale was plotted against volume of shale. The input sand porosity was 0.20, and the shale porosity was set to 0.10 and 0.15. A 10% error in the volume and porosity of shale was investigated.

The equations for total and effective porosity in a laminar shale section are as follow:

$$\phi_T = \phi_{clean\,sand} - V_{sh} \cdot \phi_{clean\,sand} + V_{sh} \cdot \phi_{sh} \tag{30}$$

$$\phi_E = \phi_T - V_{sh} \cdot \phi_{sh} \tag{31}$$

$$\phi_{T,plot} = \phi_{T,sand} \cdot NTG = \phi_{T,sand} \cdot (1 - V_{sh}) \tag{32}$$

The porosity input to the equations is the bulk total porosity from a typical density log (ref section 2.1.2). This is plotted at the black line in figure 21, 22 and 23. One assumption is that the true sand total porosity can be found by the use of the Thomas & Stieber method. In reality, this is an estimate that is affected by uncertainties in volume shale (ref section 2.5.2). The sand total porosity is adjusted by a fractional net to gross curve, affected by the uncertainties in volume shale. This net to gross ratio is obtained by calculating 1-V_{sh}. The sensitivities to volume shale should then reflect the input used in the simulation study.

Based on the equations it looks like the effective porosity case is more robust to uncertainties in shale volume. The difference increases as the Net to gross ratio decreases and difference between sand and shale porosity increases. If the sand and shale porosities is equal, there is no difference in the sensitivities to volume shale. Figure 21 illustrates this where the red lines represent effective porosity and the blue lines estimated sand porosity.

Another uncertainty is related to the shale porosity. Since there is no shale porosity in the Net to Gross ratio, the total porosity has no spread between the curves in figure 22. The uncertainty in the effective case behave the same way as when volume of shale is adjusted, since it is a product of shale volume, shale porosity and the uncertainty in equation 31 that determines the spread. The plots in figure 21 and 22 is a result of equation 31 and 32.

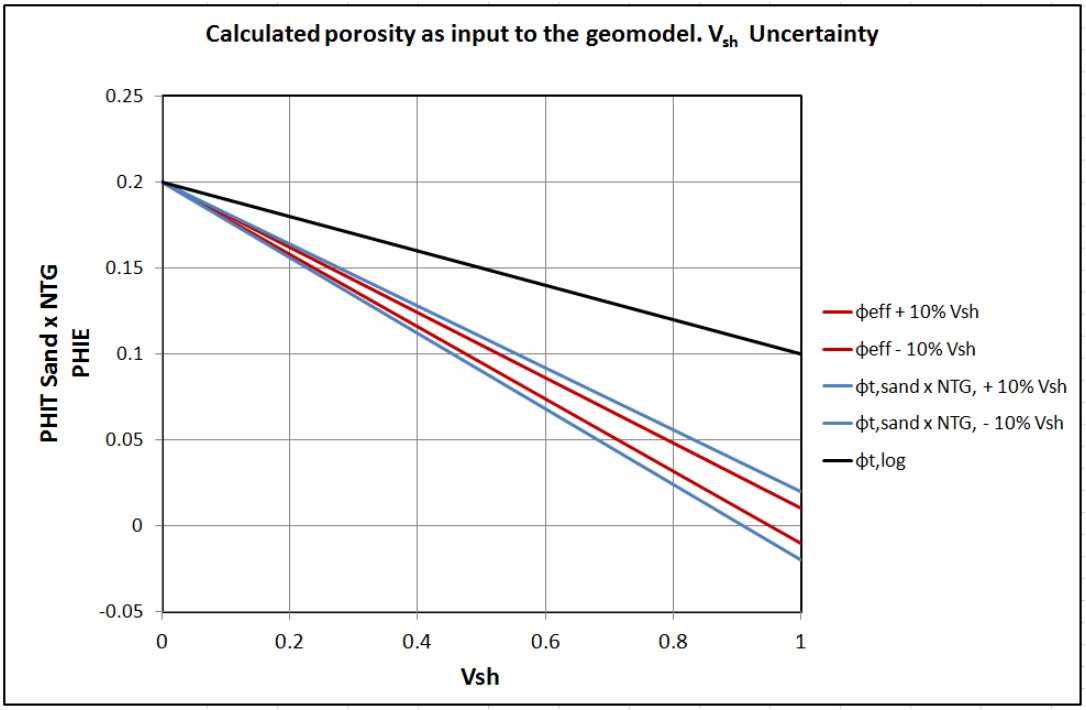

(a) Total porosity is showing a larger spread as volume shale increases. $\phi_{sand} = 0.2$ and $\phi_{shale} = 0.1$

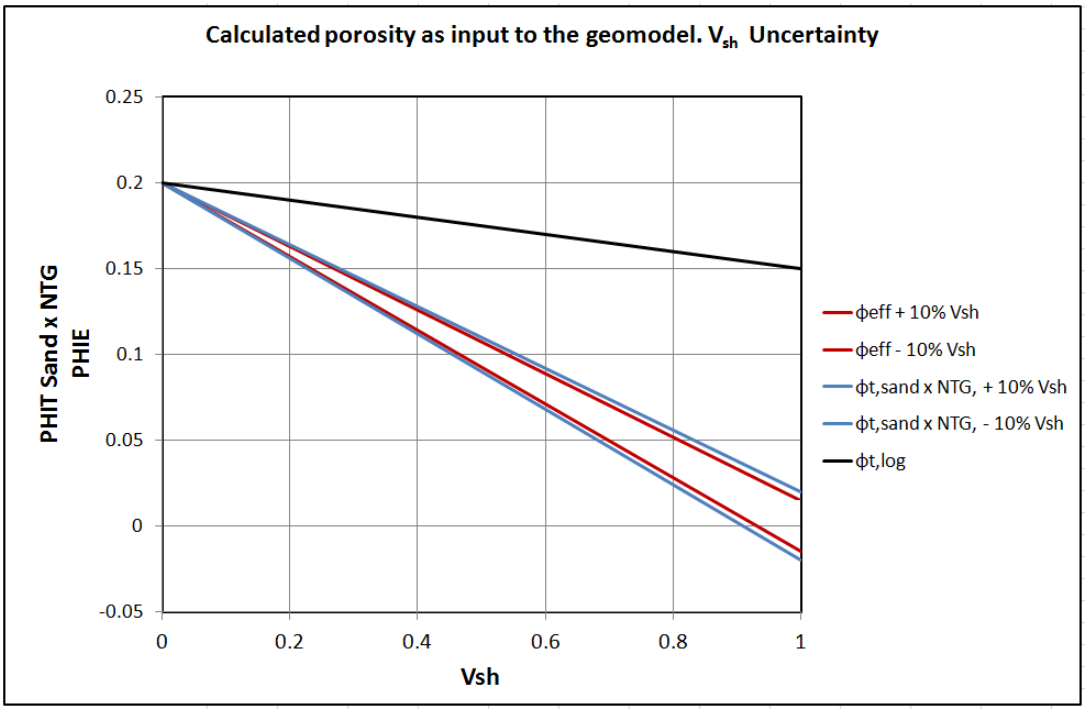

(b) As shale porosity approaches sand porosity, the difference become smaller. $\phi_{sand} = 0.2$ and $\phi_{shale} = 0.15$

Figure 21: *Sensitivity to Volume shale uncertainty. Effective porosity has a smaller spread as volume shale increases.*

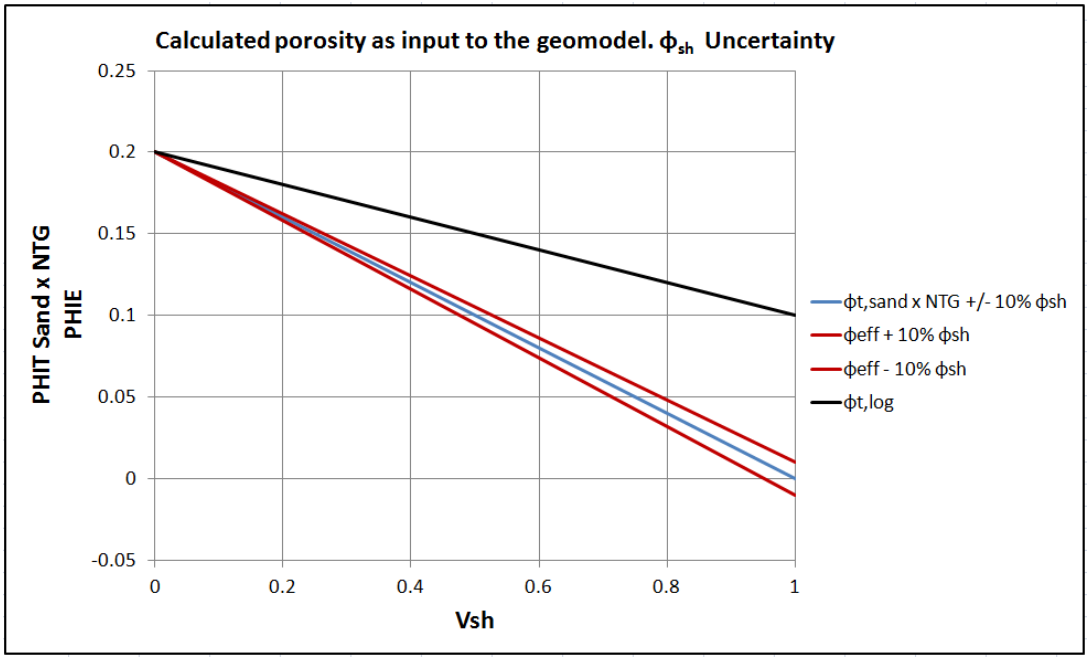

(a) Total porosity is not sensitive to variations in shale porosity. $\phi_{sand} = 0.2$ and $\phi_{shale} = 0.1$

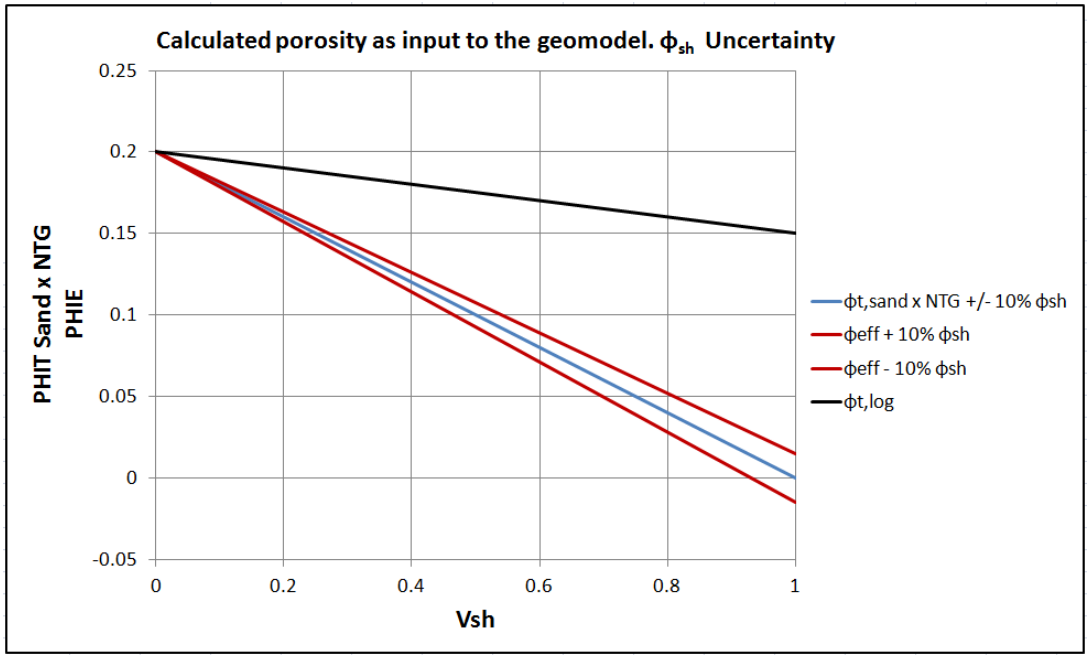

(b) A 10% uncertainty result in a larger spread for effective porosity as the shale porosity increases. $\phi_{sand} = 0.2$ and $\phi_{shale} = 0.15$

Figure 22: *Sensitivity to ϕ_{shale} uncertainty. Total porosity is not affected, and effective porosity is more sensitive as volume shale and shale porosity increases.*

A last case was also investigated where a 10% uncertainty in shale volume was combined with shale porosity variations between 0.08 and 0.12.

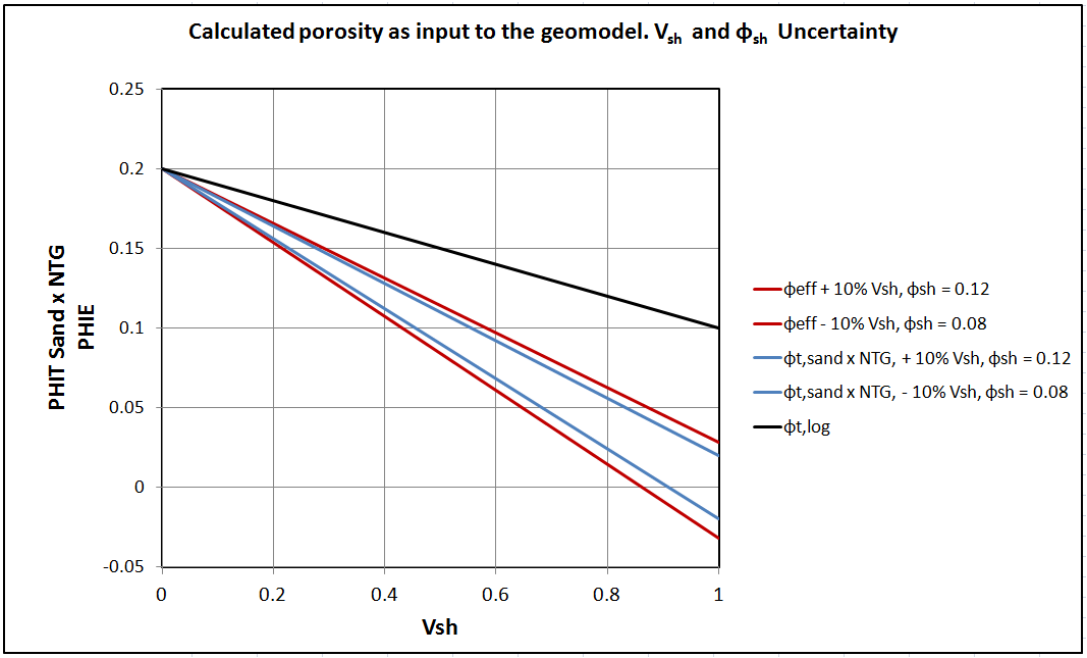

Figure 23: *Uncertainty in both V_{sh} and ϕ_{sh}. Uncertainty in volume shale pulls both lines apart, and the shale porosity add uncertainty to the effective porosity.*

The figures 21, 22 and 23 have shown how the uncertainty in porosity estimates increases as the volume of shale increases. In clean formations, there should not be a big difference between the porosity types. However, as shale volume increases, the differences become clear. The effective porosity is the most robust to variations in volume shale. On the other side, total porosity is not affected at all by variations in shale porosity when not considering the Thomas & Stieber effects.

3.2 Field overview

Ivar Aasen is an oil reservoir with a partial gas cap located North-West of the Utsira High in the North sea. The reservoir depth is approximately 2400 meters, and the water depth is around 110 meters. The reservoir consists of shallow marine sandstones in the Hugin formation, and fluvial sandstones in the Sleipner and Skagerak formations. The field was discovered in 2008.

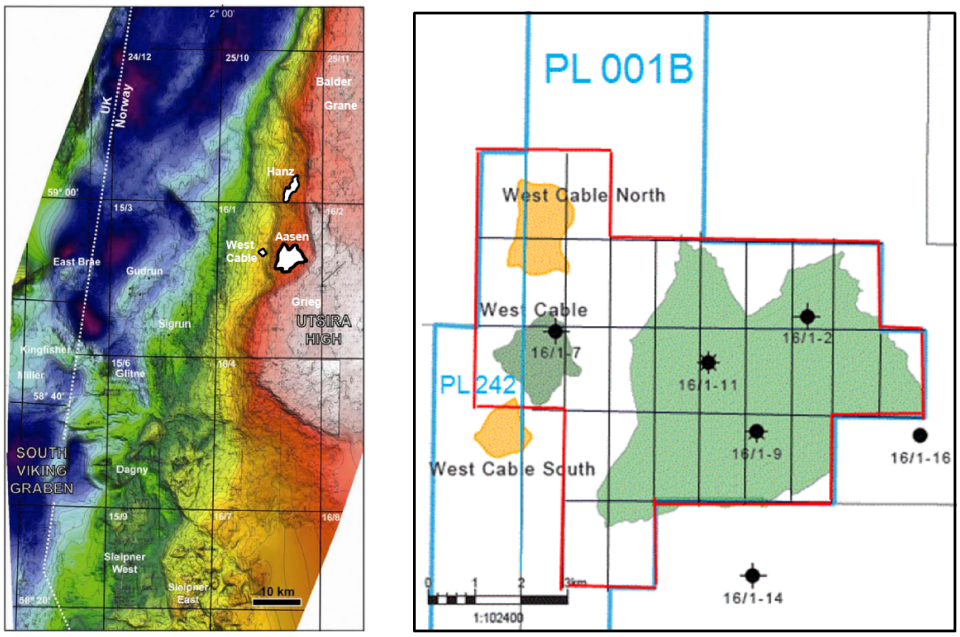

(a) Map showing the location of Ivar Aasen

(b) Field overview including appraisal wells

Figure 24: *Map of Ivar Aasen. The work is not involving West Cable, but is focused on the main Ivar Aasen reservoir [3]*

Figure 24(b) shows the 8 appraisal wells that are used in petrophysical work on Ivar Aasen. The wells are:

- 16/1-2
- 16/1-9
- 16/1-11
- 16/1-11A
- 16/1-14
- 16/1-16
- 16/1-16A
- 16/1-20 AT3

3.3 Shale volume

The first step of the petrophysical evaluation was to calculate the shale volume as a function of depth. This was done by mainly using a Neutron/Density crossplot and picking shale points for the base case, the HI-case and the LO-case. Figure 27 shows the input for the base case. For the zones containing gas, linear gamma ray was used, with input seen in figure 26. The process is described in the background, section 2.2.1. In well 16/1-2 the shale volume was calculated using only gamma ray, since no Neutron/Density log was available. Figure 25 shows an example of shale points from 16/1-9.

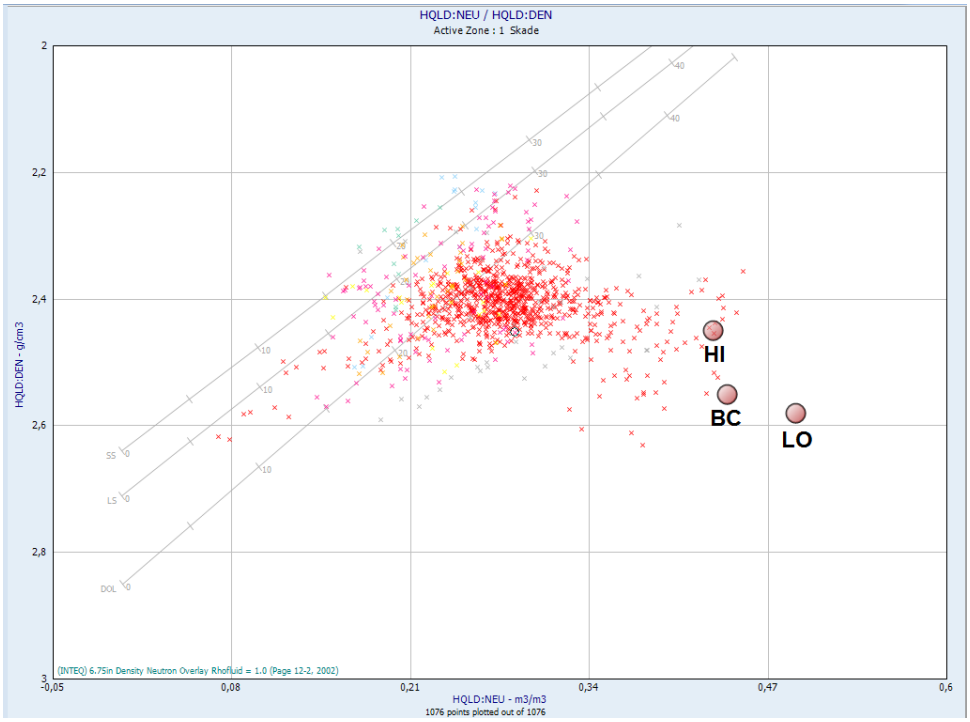

Figure 25: *Neutron Density crossplot from 16/1-9. The points represent values used as input for the shale sensitivity study.*

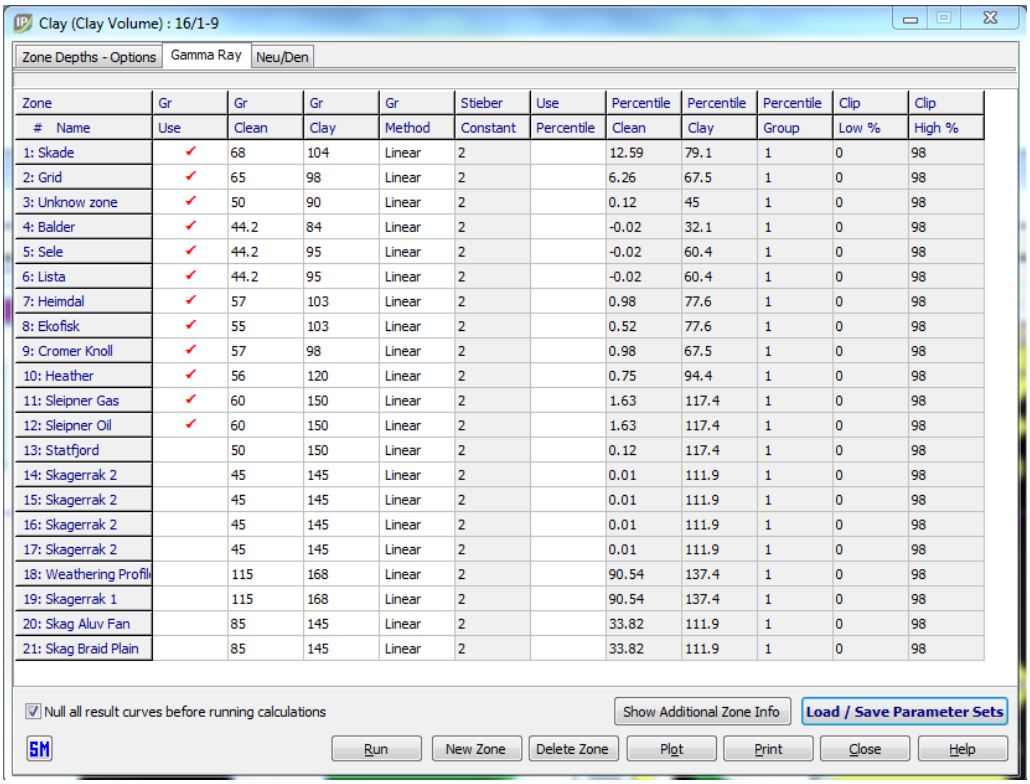

Zone #	Name	Gr Use	Gr Clean	Gr Clay	Gr Method	Stieber Constant	Use Percentile	Percentile Clean	Percentile Clay	Percentile Group	Clip Low %	Clip High %
1	Skade	✓	68	104	Linear	2		12.59	79.1	1	0	98
2	Grid	✓	65	98	Linear	2		6.26	67.5	1	0	98
3	Unknow zone	✓	50	90	Linear	2		0.12	45	1	0	98
4	Balder	✓	44.2	84	Linear	2		-0.02	32.1	1	0	98
5	Sele	✓	44.2	95	Linear	2		-0.02	60.4	1	0	98
6	Lista	✓	44.2	95	Linear	2		-0.02	60.4	1	0	98
7	Heimdal	✓	57	103	Linear	2		0.98	77.6	1	0	98
8	Ekofisk	✓	55	103	Linear	2		0.52	77.6	1	0	98
9	Cromer Knoll	✓	57	98	Linear	2		0.98	67.5	1	0	98
10	Heather	✓	56	120	Linear	2		0.75	94.4	1	0	98
11	Sleipner Gas	✓	60	150	Linear	2		1.63	117.4	1	0	98
12	Sleipner Oil	✓	60	150	Linear	2		1.63	117.4	1	0	98
13	Statfjord		50	150	Linear	2		0.12	117.4	1	0	98
14	Skagerrak 2		45	145	Linear	2		0.01	111.9	1	0	98
15	Skagerrak 2		45	145	Linear	2		0.01	111.9	1	0	98
16	Skagerrak 2		45	145	Linear	2		0.01	111.9	1	0	98
17	Skagerrak 2		45	145	Linear	2		0.01	111.9	1	0	98
18	Weathering Profil		115	168	Linear	2		90.54	137.4	1	0	98
19	Skagerrak 1		115	168	Linear	2		90.54	137.4	1	0	98
20	Skag Aluv Fan		85	145	Linear	2		33.82	111.9	1	0	98
21	Skag Braid Plain		85	145	Linear	2		33.82	111.9	1	0	98

Figure 26: *Inputs to base case shale volume calculations using gamma ray, 16/1-9*

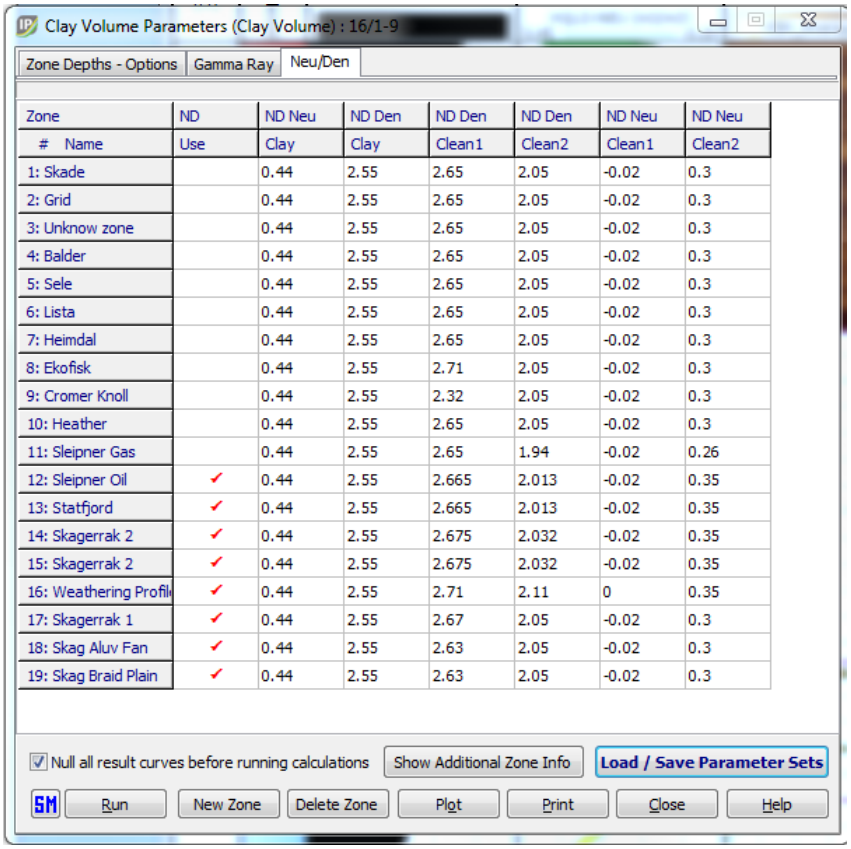

Zone # Name	ND Use	ND Neu Clay	ND Den Clay	ND Den Clean1	ND Den Clean2	ND Neu Clean1	ND Neu Clean2
1: Skade		0.44	2.55	2.65	2.05	-0.02	0.3
2: Grid		0.44	2.55	2.65	2.05	-0.02	0.3
3: Unknow zone		0.44	2.55	2.65	2.05	-0.02	0.3
4: Balder		0.44	2.55	2.65	2.05	-0.02	0.3
5: Sele		0.44	2.55	2.65	2.05	-0.02	0.3
6: Lista		0.44	2.55	2.65	2.05	-0.02	0.3
7: Heimdal		0.44	2.55	2.65	2.05	-0.02	0.3
8: Ekofisk		0.44	2.55	2.71	2.05	-0.02	0.3
9: Cromer Knoll		0.44	2.55	2.32	2.05	-0.02	0.3
10: Heather		0.44	2.55	2.65	2.05	-0.02	0.3
11: Sleipner Gas		0.44	2.55	2.65	1.94	-0.02	0.26
12: Sleipner Oil	✓	0.44	2.55	2.665	2.013	-0.02	0.35
13: Statfjord	✓	0.44	2.55	2.665	2.013	-0.02	0.35
14: Skagerrak 2	✓	0.44	2.55	2.675	2.032	-0.02	0.35
15: Skagerrak 2	✓	0.44	2.55	2.675	2.032	-0.02	0.35
16: Weathering Profil	✓	0.44	2.55	2.71	2.11	0	0.35
17: Skagerrak 1	✓	0.44	2.55	2.67	2.05	-0.02	0.3
18: Skag Aluv Fan	✓	0.44	2.55	2.63	2.05	-0.02	0.3
19: Skag Braid Plain	✓	0.44	2.55	2.63	2.05	-0.02	0.3

Figure 27: *Inputs to base case shale volume calculations using Neutron/Density, 16/1-9*

Figure 28 shows an example from 16/1-11 with traces of GR, Neutron/Density and calculated shale volume as a function of depth. Vertical red and green lines show the shale and clean sand values. The HI and LO shale case will shift the spread of these lines, resulting in a higher/lower calculated shale volume. It should be noticed that cores from 16/1-11 does not contain any obvious 100% shale sections. This makes it harder to establish a safe value for 100% shale.

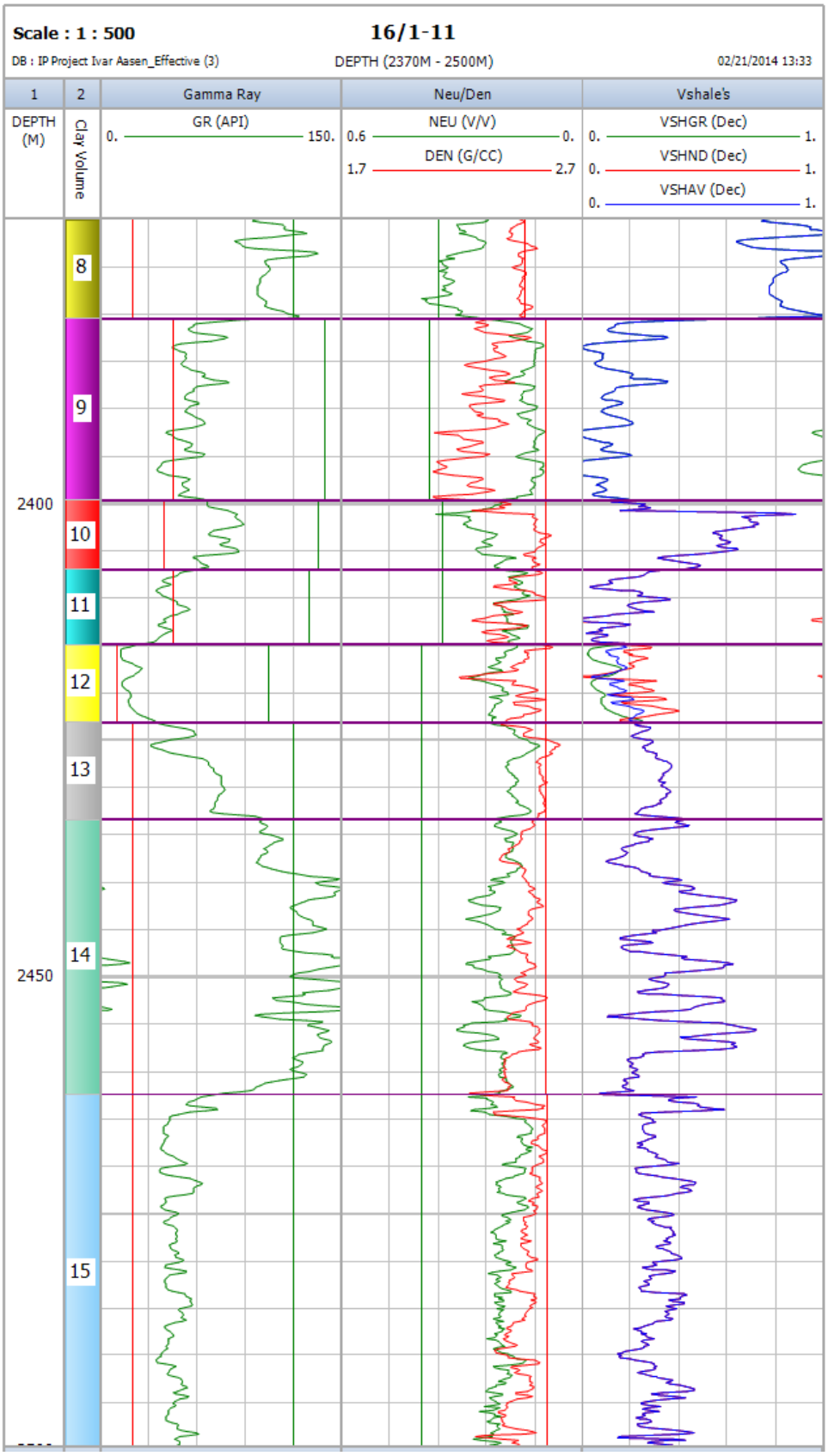

Figure 28: *Volume Shale from 16/1-11. Traces show gamma ray, neutron density and calculated shale content.*

3.4 Porosity and Water Saturation

The next step is calculating porosity and water saturation. Here, a choice is made of using the Indonesia equation or the Waxman & Smits equation and the right set of input parameters must be provided. For porosity calculations, the density log was used, described in section 2.1.2 using equation 2 and 3. Matrix and fluid densities is taken from core and fluid analysis. The cementation exponent, m is described in section 2.7.1, and models how the pore network increases resistivity. In the reservoir zones, it varies between 1.73 in the good sands and 1.83 the bad sands.

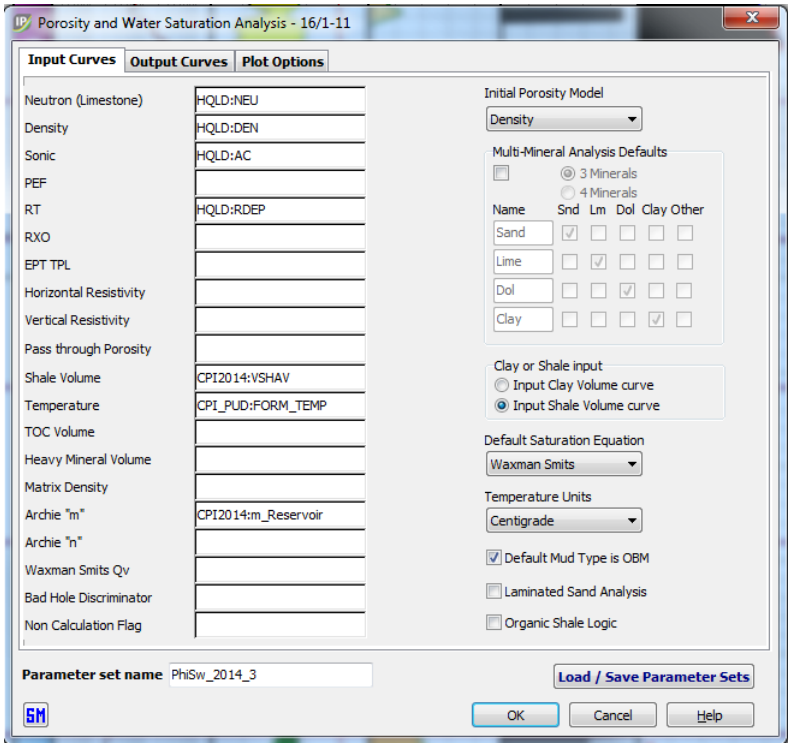

Figure 29: *Porosity calculation inputs, 16/1-11*

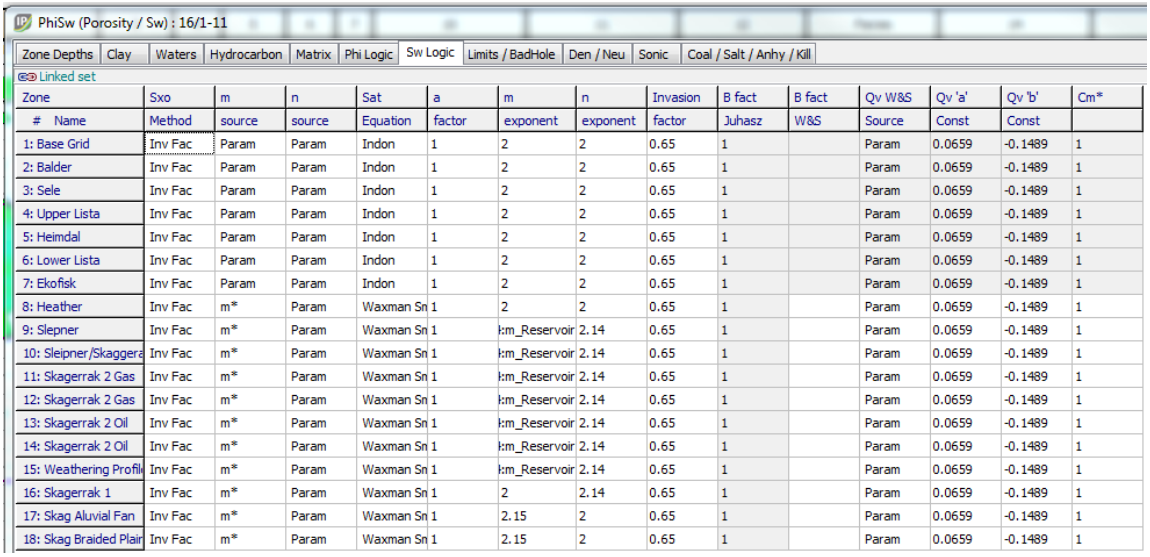

PhiSw (Porosity / Sw) : 16/1-11

Zone Depths | Clay | Waters | Hydrocarbon | Matrix | Phi Logic | Sw Logic | Limits / BadHole | Den / Neu | Sonic | Coal / Salt / Anhy / Kill

Linked set

Zone	Sxo	m	n	Sat	a	m	n	Invasion	B fact	B fact	Qv W&S	Qv 'a'	Qv 'b'	Cm*
# Name	Method	source	source	Equation	factor	exponent	exponent	factor	Juhasz	W&S	Source	Const	Const	
1: Base Grid	Inv Fac	Param	Param	Indon	1	2	2	0.65	1		Param	0.0659	-0.1489	1
2: Balder	Inv Fac	Param	Param	Indon	1	2	2	0.65	1		Param	0.0659	-0.1489	1
3: Sele	Inv Fac	Param	Param	Indon	1	2	2	0.65	1		Param	0.0659	-0.1489	1
4: Upper Lista	Inv Fac	Param	Param	Indon	1	2	2	0.65	1		Param	0.0659	-0.1489	1
5: Heimdal	Inv Fac	Param	Param	Indon	1	2	2	0.65	1		Param	0.0659	-0.1489	1
6: Lower Lista	Inv Fac	Param	Param	Indon	1	2	2	0.65	1		Param	0.0659	-0.1489	1
7: Ekofisk	Inv Fac	Param	Param	Indon	1	2	2	0.65	1		Param	0.0659	-0.1489	1
8: Heather	Inv Fac	m*	Param	Waxman Sn	1	2	2	0.65	1		Param	0.0659	-0.1489	1
9: Slepner	Inv Fac	m*	Param	Waxman Sn	1	:m_Reservoir	2.14	0.65	1		Param	0.0659	-0.1489	1
10: Sleipner/Skaggera	Inv Fac	m*	Param	Waxman Sn	1	:m_Reservoir	2.14	0.65	1		Param	0.0659	-0.1489	1
11: Skagerrak 2 Gas	Inv Fac	m*	Param	Waxman Sn	1	:m_Reservoir	2.14	0.65	1		Param	0.0659	-0.1489	1
12: Skagerrak 2 Gas	Inv Fac	m*	Param	Waxman Sn	1	:m_Reservoir	2.14	0.65	1		Param	0.0659	-0.1489	1
13: Skagerrak 2 Oil	Inv Fac	m*	Param	Waxman Sn	1	:m_Reservoir	2.14	0.65	1		Param	0.0659	-0.1489	1
14: Skagerrak 2 Oil	Inv Fac	m*	Param	Waxman Sn	1	:m_Reservoir	2.14	0.65	1		Param	0.0659	-0.1489	1
15: Weathering Profil	Inv Fac	m*	Param	Waxman Sn	1	:m_Reservoir	2.14	0.65	1		Param	0.0659	-0.1489	1
16: Skagerrak 1	Inv Fac	m*	Param	Waxman Sn	1	2	2.14	0.65	1		Param	0.0659	-0.1489	1
17: Skag Aluvial Fan	Inv Fac	m*	Param	Waxman Sn	1	2.15	2	0.65	1		Param	0.0659	-0.1489	1
18: Skag Braided Plair	Inv Fac	m*	Param	Waxman Sn	1	2.15	2	0.65	1		Param	0.0659	-0.1489	1

Figure 30: *Water saturation calculation inputs, 16/1-11*

For the porosity calculations, ρ_{fl} is based on the saturations and density from the flushed zone. If water based mud was used drilling the well, this is the saturation calculated by the water saturation equation. If oil based mud was used, an invasion factor of 0.65 was applied. This means that the saturation in the flushed zone, $S_{xo} <= Invasion factor$. The empirical formula used by IP is [20]:

$$S_{xo} = \frac{S_w + InvasionFactor}{1 + InvasionFactor} \tag{33}$$

After running the Waxman & Smits, total porosity case, a Thomas & Stieber algorithm covered in section 2.5.2 was executed. This provided estimates for clean sand porosity, needed in the permeability regression.

The code was written in IP and uses shale volume, porosity from the density log, shale porosity and sand porosity as input. It is based on the same approach as the original paper by Thomas & Stieber [22]. The sand porosity changes from 0.285 in the East to 0.275 in the West. Shale porosity is estimated to be 0.11 from core measurements.

Table 3: *Table of porosity inputs for Thomas & Stieber*

Well	Sand Porosity	Shale Porosity
16/1-2	0.285	0.11
16/1-9	0.275	0.11
16/1-11	0.275	0.11
16/1-11A	0.275	0.11
16/1-14	0.275	0.11
16/1-16	0.285	0.11
16/1-16A	0.285	0.11
16/1-20 AT3	0.285	0.11

3.5 Permeability

The next step is the permeability regression. A correlation between core porosity versus core permeability was established for the different facies. Both porosity and permeability is overburden corrected, and the klinkenberg corrected core permeability has been converted to water permeability.

Using either effective porosity (Output from the Indonesia calculation) or total porosity and clean sand porosity (Output from Waxman & Smits and Thomas & Stieber) as input, the permeability can now be estimated. The porosity goes as input along the x-axis in figure 31, and permeability is read along the y-axis. Because of the uncertainty related to the Thomas & Stieber method, estimated clean sand porosity was only used as input in the wells with cores, and only in the facies appropriate for this. In more marginal facies, the total bulk porosity was used as input for the Waxman & Smits case.

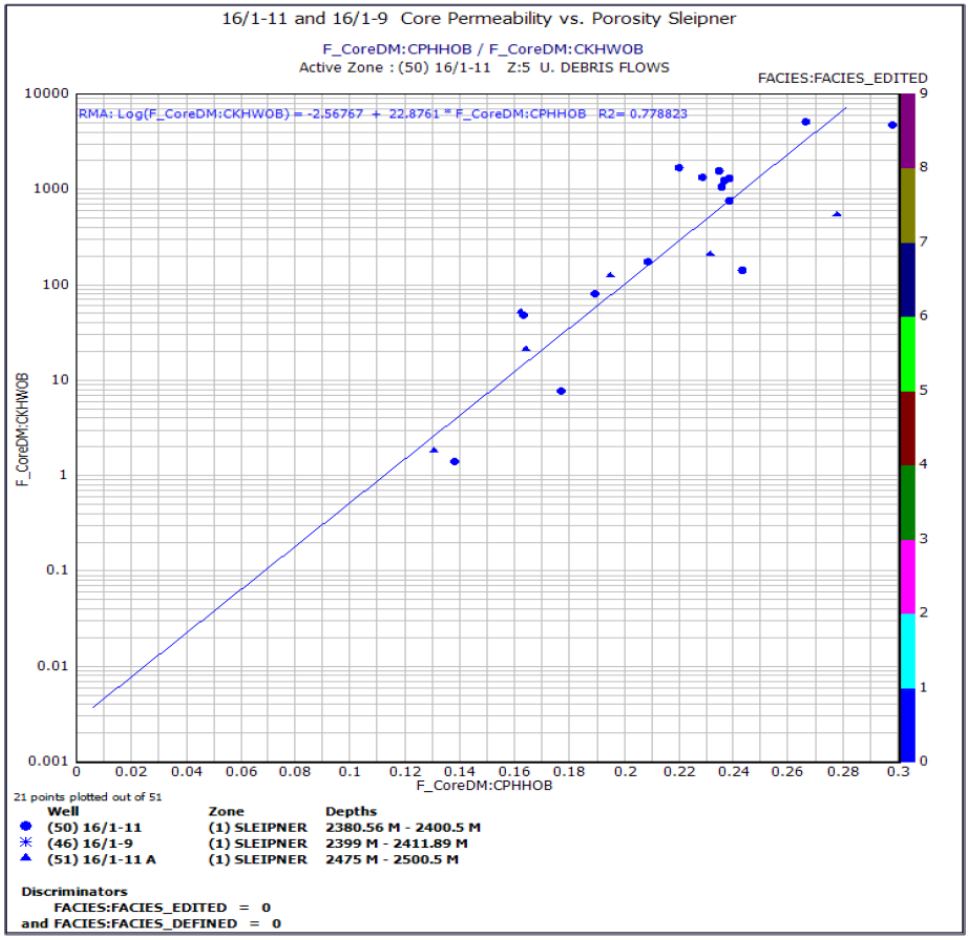

Figure 31: *Porosity - Permeability regression, Sleipner formation. Well 16/1-9 and 16/1-11*

3.6 Cut off's & editing

The next step of the petrophysical evaluation was generating curves/flags for Net Reservoir used as NTG in the Indonesia case. Here, porosity cutoffs of 0.08 and 0.12 were used for gas/liquid zones in the effective porosity case. In the total porosity case, 0.09 and 0.13 was used

to compensate for the added shale porosity. In both cases a shale volume of 0.60 was used as a cut-off.

After this, some minor work was done to the curves, removing negative values and limiting permeability to maximum 10 darcy to prepare them for petrophysical modeling in Petrel.

3.7 Case overview

Figure 32 and 33 is a summary of the most important logs from 16/1-9 and 16/1-11 used and generated while working in IP. It starts with the gamma ray and neutron/density curve, and a shale volume for the base case is presented. Following this, is 5 traces of with the different cases, the HI shale volume (red), the base case (yellow) and the LO shale volume (green). These curves are Res/Pay flag, Shale volume, Porosity, Net-to-Gross and Permeability. The last trace is a pore model after applying the Thomas & Stieber algorithm. It shows laminated clays, total shale, sand, oil and water. Figure 34 is a comparison between the pore models resulting from Waxman & Smits, 34(a) and Indonesia, 34(b). The reason for not applying Thomas & Stieber to the Indonesia case is that it uses effective porosity as input and thereby already compensate for the shale.

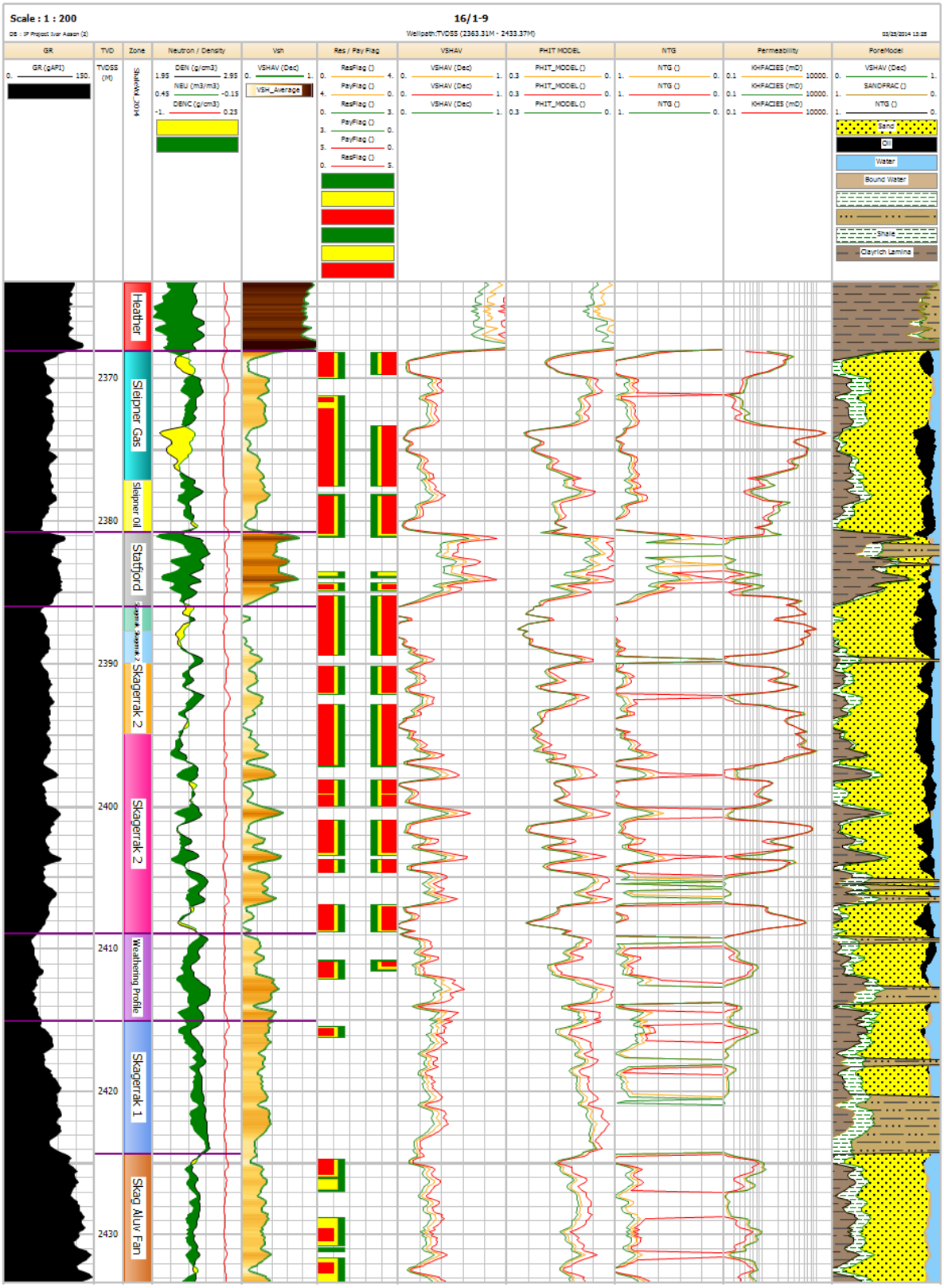

Figure 32: *Model Input using Waxman Smits in 16/1-9. The low shale volume case is colored green, the base case orange and the high shale case red. The traces show gamma ray, depth, formation, neutron/density, Res/Pay flag, volume shale, porosity, Net to Gross, permeability and a pore model.*

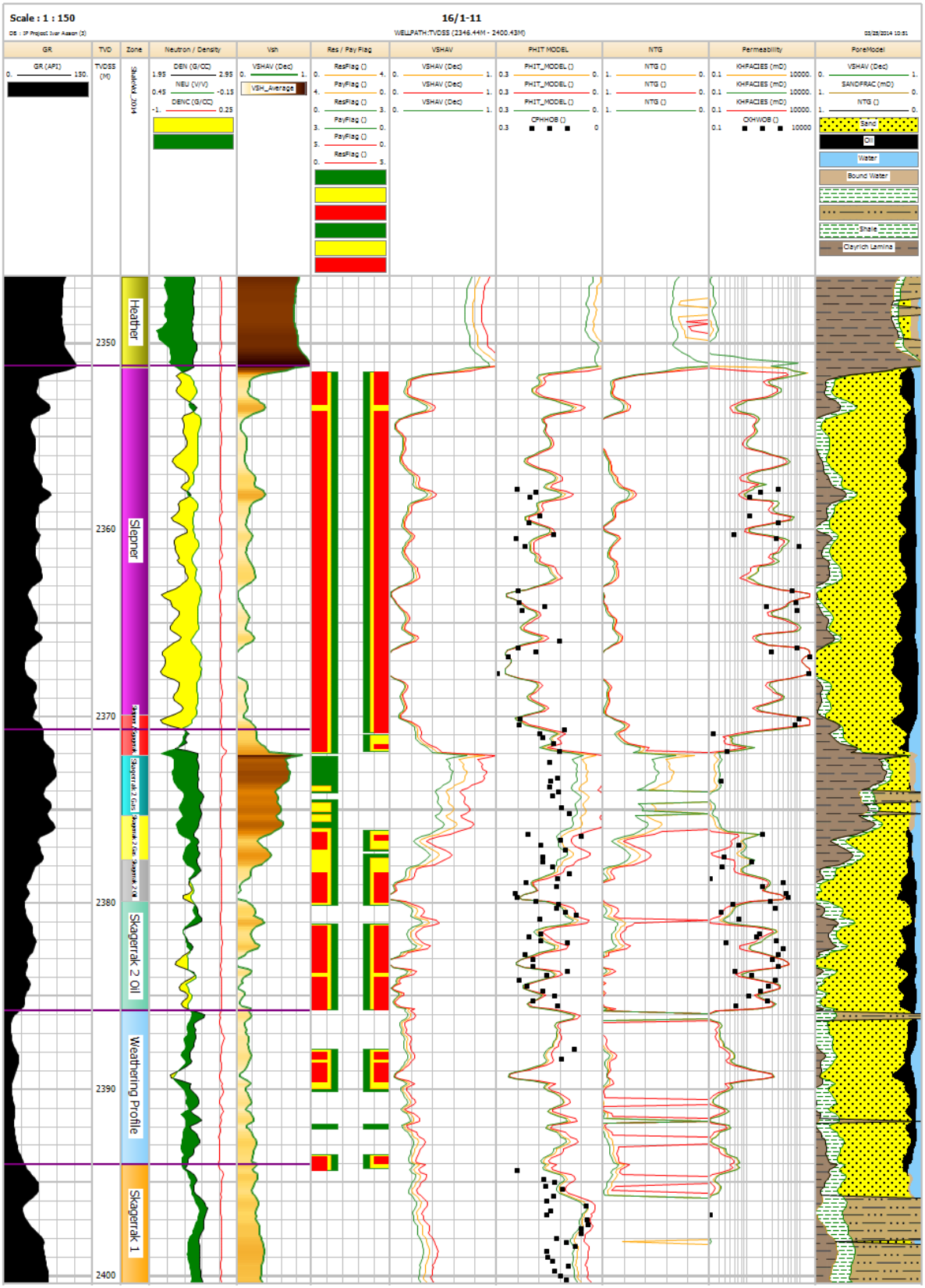

Figure 33: *Model Input using Waxman Smits in 16/1-11*

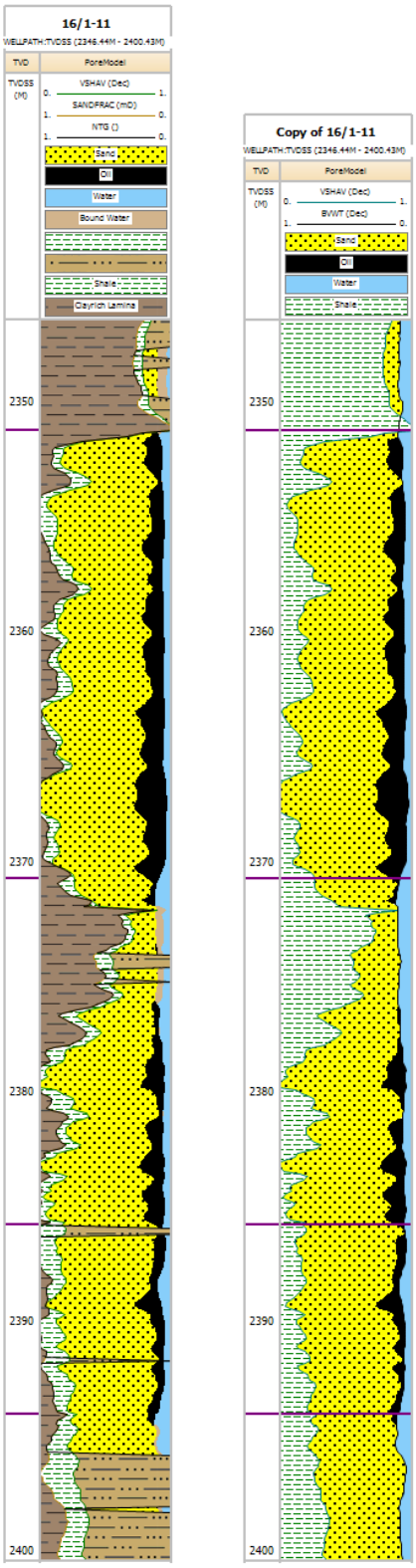

(a) W & S (b) Indonesia

Figure 34: *Comparison of poremodels. The Waxman & Smits interpretation includes volume of laminated and dispersed shale. A slightly higher oil saturation can be seen in the Waxman & Smits model.*

3.8 Upscaling of well logs

The well logs where scaled up in Petrel to fit the vertical thickness of the gridcells. An arithmetic mean was used to average the porosity and net to gross log in a cell. For the permeability, a geometric mean was used. The difference is that an arithmetic mean is based on the sum of the numbers while a geometric mean is based on the product. This is done because zones of low permeability have great influence on the total vertical permeability, and this should be taken into consideration while upscaling. The logs where treated as points, meaning all sample values within a cell are used for averaging, without being weighted. If a layer is close to impermeable, multiplying the other points with its value close to 0 will decrease the total value more than adding a 0 to the rest of the points. If no points are present in the cell, the cell will be undefined. The grid cells penetrated by the well are chosen by petrel as the "Neighbouring cell". This option will average log values from all cells adjacent to the upscaled cell and belonging to the same layer as the upscaled cell. Figure 35 shows the results of upscaling the logs.

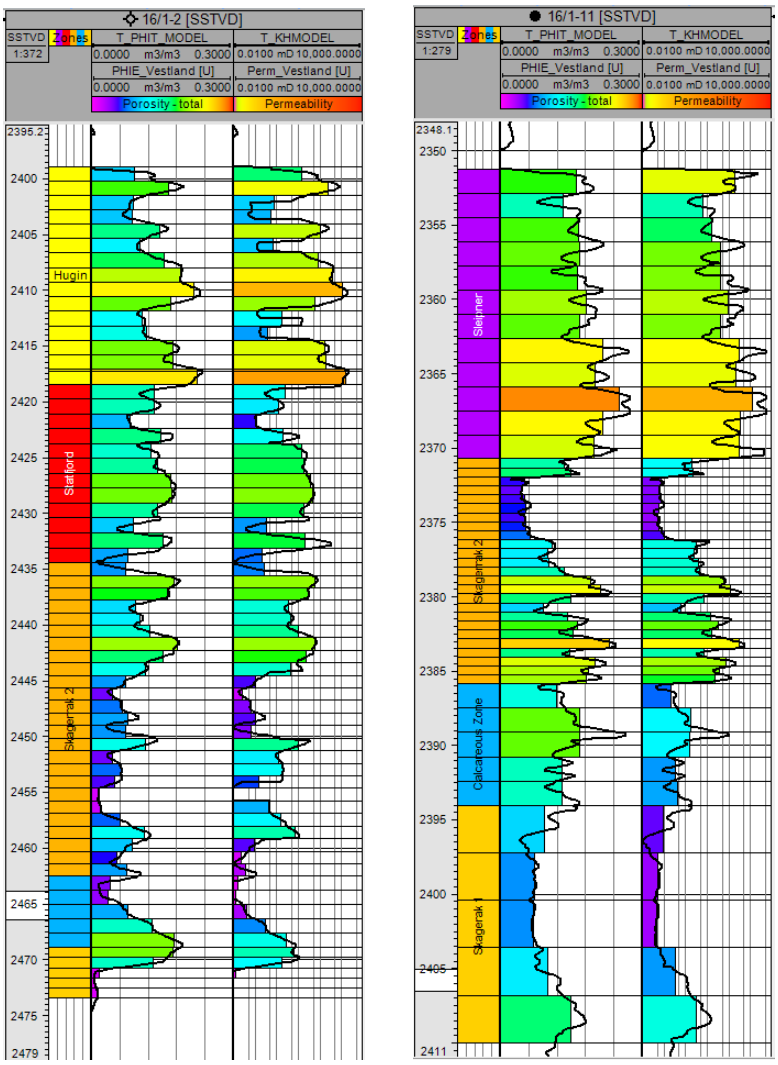

(a) 16/1-2 Porosity and Permeability

(b) 16/1-11 Porosity and Permeability

Figure 35: *Upscaling of well logs in Petrel. The continuous log is displayed together with the result of the upscaling.*

3.9 Creating the 3D model

After the logs was scaled up, the properties (Porosity, Net-to-Gross and Permeability) was used to create a 3D porosity model and a 3D permeability model. The porosity 3D model was used as the secondary variable using collocated co-kriging to build the 3D permeability model for each of the zones. Because the spread of permeability's was reduced to a single line in the permeability regression, a coefficient for co-kriging was limited to maximum 90% correlation to the porosity log for the different zones.

A spherical variogram with dimensions 3000m x 2000m x 3m in the north-west / south-east direction was used as the maximum distance where the sample values was dependent on each other. This can be seen in figure 37(b) as the circular shapes in the porosity distribution. Capillary pressure measurements where used to develop a water saturation function (Leverett J-function), dependent on porosity and permeability from the logs.

$$J\left(S_w\right) = \frac{P_c}{\sigma cos\theta}\sqrt{\frac{k}{\phi}} \tag{34}$$

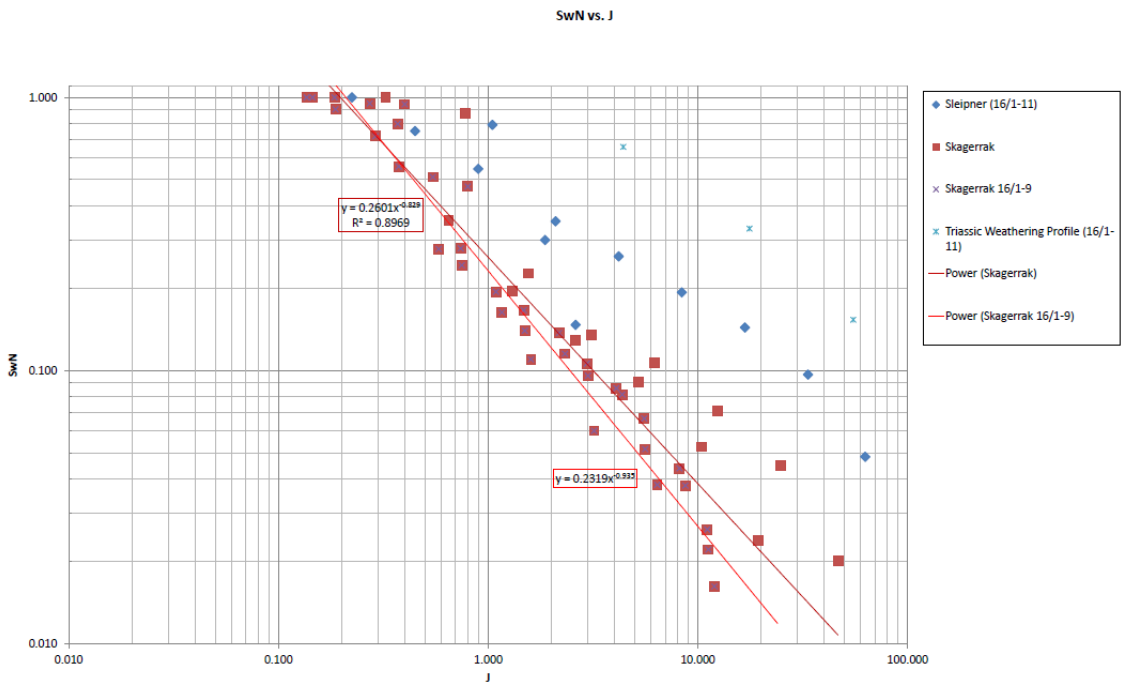

Figure 36: *Normalised water saturation vs. J-function. 16/1-9 and 16/1-11. From PDO [3]*

Figure 37 shows the result of the property distribution, before and after the workflow was run. The porosity, permeability and water saturation property distributions can be found in appendix B.

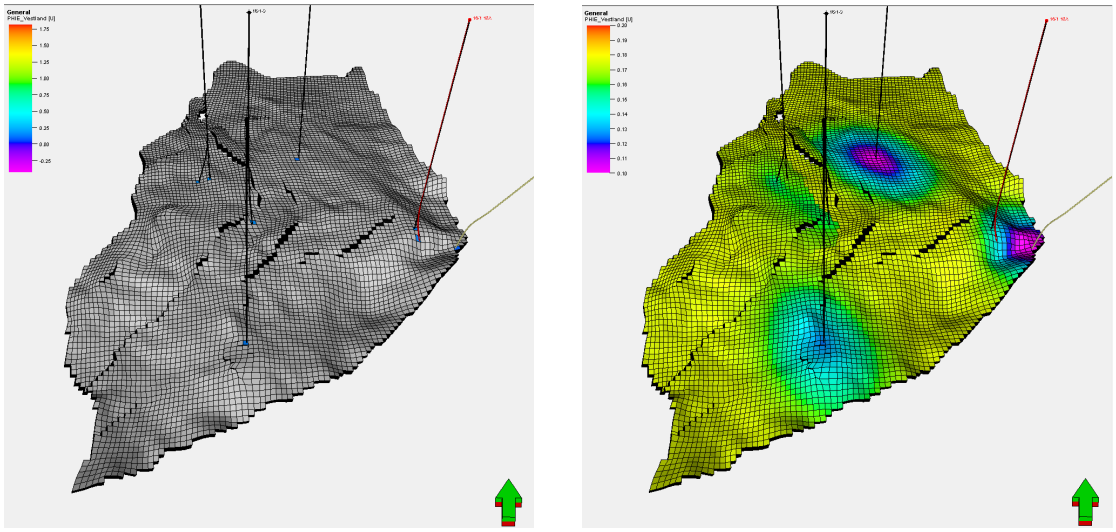

(a) After upscaling logs (b) After running the petrophysical modelling

Figure 37: *Petrophysical modelling: Distributing porosity in the grid around the appraisal wells.*

3.10 Simulation model

The 6 simulation models all share the same 6 oil producers and 6 water injectors. The only difference between the models is the 3 different shale volumes and the shaly sand equations with total or effective porosity used as input. The geometry and properties from the geological model is transferred into the simulation model. The grid is a corner point grid, with approximately 100 x 100 meters in the X and Y direction. The dimensions are 88 x 133 x 74, making a total of 866 096 cells.

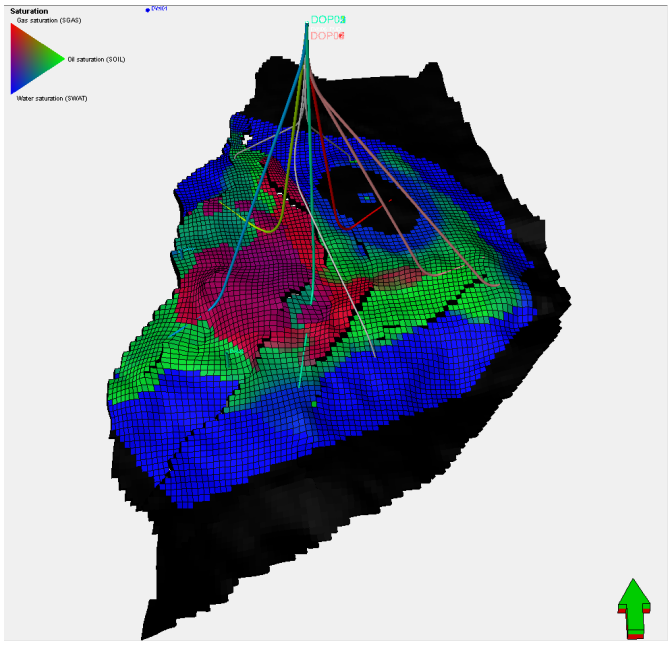

Figure 38: *Simulation model with injectors and producers. The figure shows the aquifer, the oil zone and the gas cap.*

3.11 Production constraints and limits

The Ivar Aasen simulation model is controlled almost the same way as in the PDO [3]. The average reservoir pressure target is set to the initial pressure of 245 bar. In the early production phase, the volume produced will be larger than the injected volume. As a consequence, the pressure will drop, but build up towards the target as more injector capacity become available. Other constraints are as follows [4]:

Field

- Upper limit oil rate = 5 700 Sm^3/d, valid from field start-up
  6 200 Sm^3/d, valid from 01.04.2017
  8 000 Sm^3/d, valid from 01.10.2017
  9 000 Sm^3/d, valid from 01.10.2018
- Upper limit gas production rate = 3 000 000 Sm^3/d (2 500 000 Sm^3/d from production startup until 01.10.2017)

Producers

- Gas lift rate = 150 000 Sm^3/d
- Upper limit oil rate = 3 000 Sm^3/d
- Upper limit gas rate = 1 500 000 Sm^3/d for DOP03 and DOP05 until 01.04.2018; then 500 000 Sm^3/d for all wells
- No limits on water rate
- Lower limit tubing head pressure = 20 bar

Injectors

- Upper limit BHP = 410 bars
- Upper limit water rate = 4 500 Sm^3/d

3.12 Model differences

Permeability An important difference between the models is the permeability. It is the direct effect of inserting effective or total porosity into permeability regressions similar to the one in figure 31. The regression is logarithmic along the Y-axis, meaning a small difference in porosity along the X-axis will become a large permeability difference. The cores from 16/1-11 and 16/1-16 were dried to total porosity. This means the permeability scale is originally correlated to total porosity. Using effective porosity as input will result in underestimating the permeability of the formation. The behavior with higher permeability calculated by total porosity is consistent in all 8 appraisal wells.

The logs were imported into Petrel and compared by plotting them side by side. Figure 39 and 40 shows the logs interpreted for the base case, with both total porosity, Waxman & Smits and

effective porosity, Indonesia equation. Blue shading indicates that the Waxman & Smits case has a higher value than the Indonesia case. The trace to the right is the shale volume used as input for both cases. It plots as a single line for quality control of the input data.

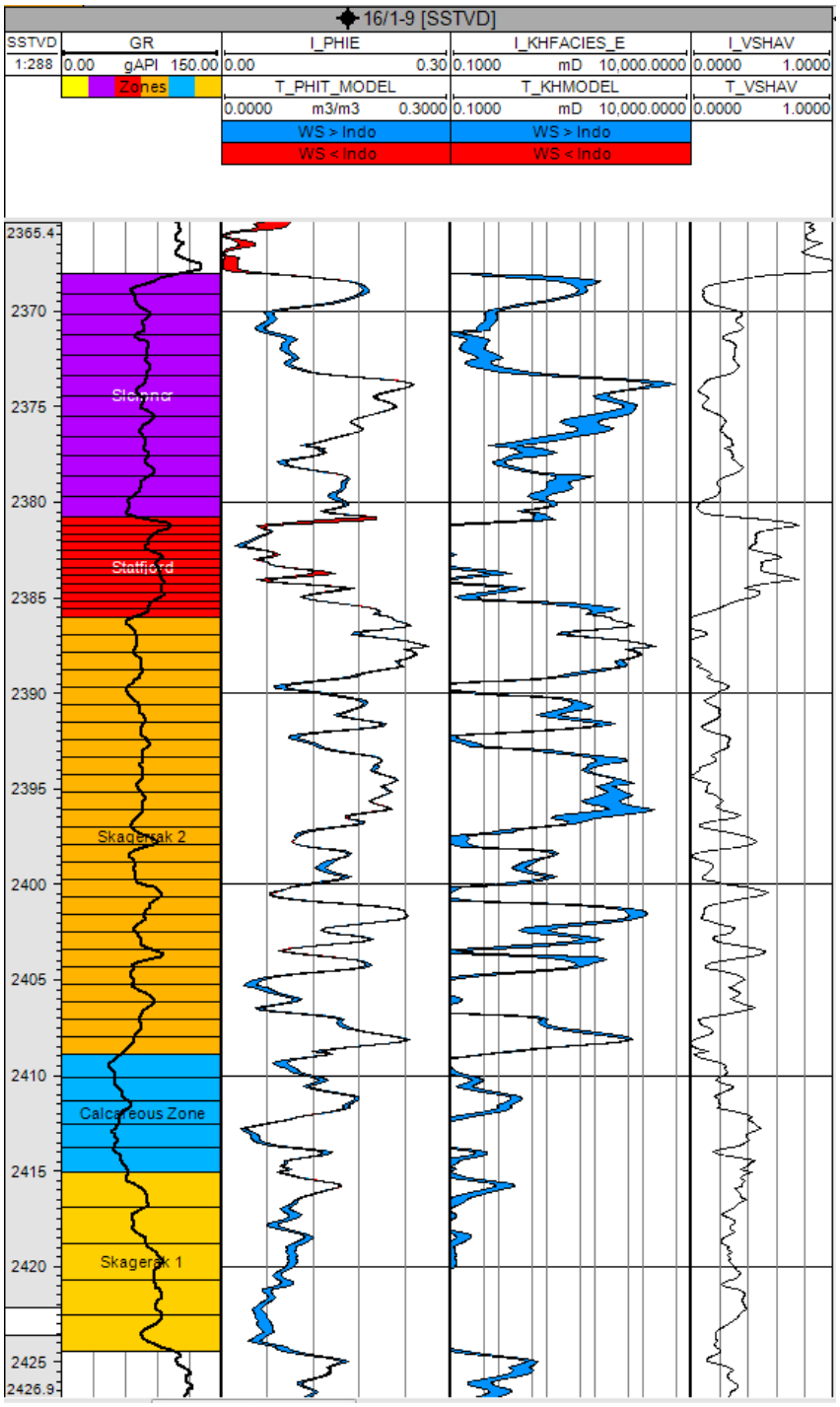

Figure 39: *Comparison of input logs interpreted with Indonesia and Waxman & Smits, well 16/1-9. The small shift in porosity leads to a large spread in permeability, even when plotted on a log scale.*

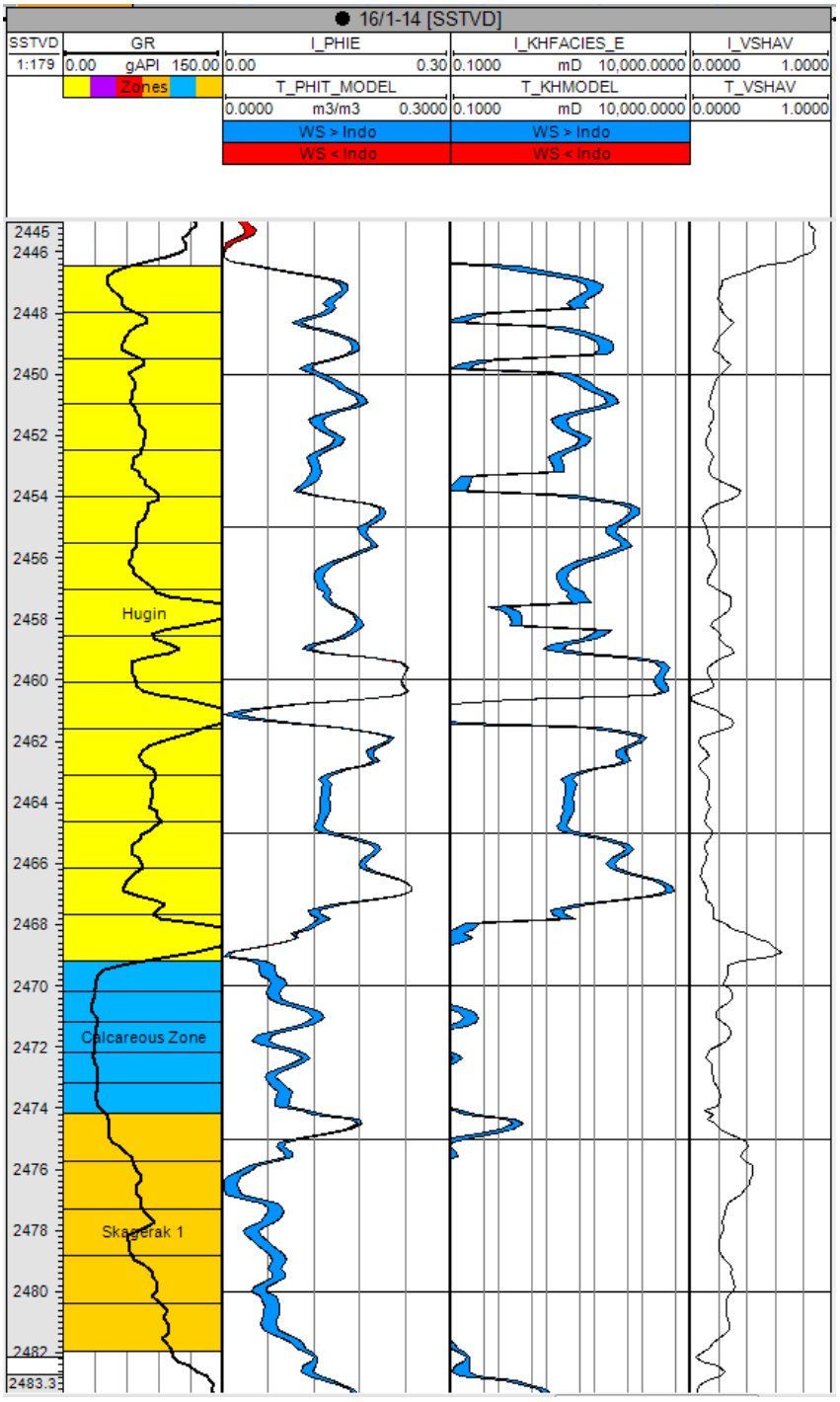

Figure 40: *Comparison of input logs interpreted with Indonesia and Waxman & Smits, well 16/1-14*

Water saturation As the ratio of permeability to porosity is input to the J-function (equation 34, section 3.9), and permeability increases logarithmically, it can be expected lower water saturation as porosity increases. This is also the case; water saturation is constantly lower when using Waxman & Smits and total porosity. Figure 41 shows the distribution with blue representing total porosity and red representing effective porosity water saturations.

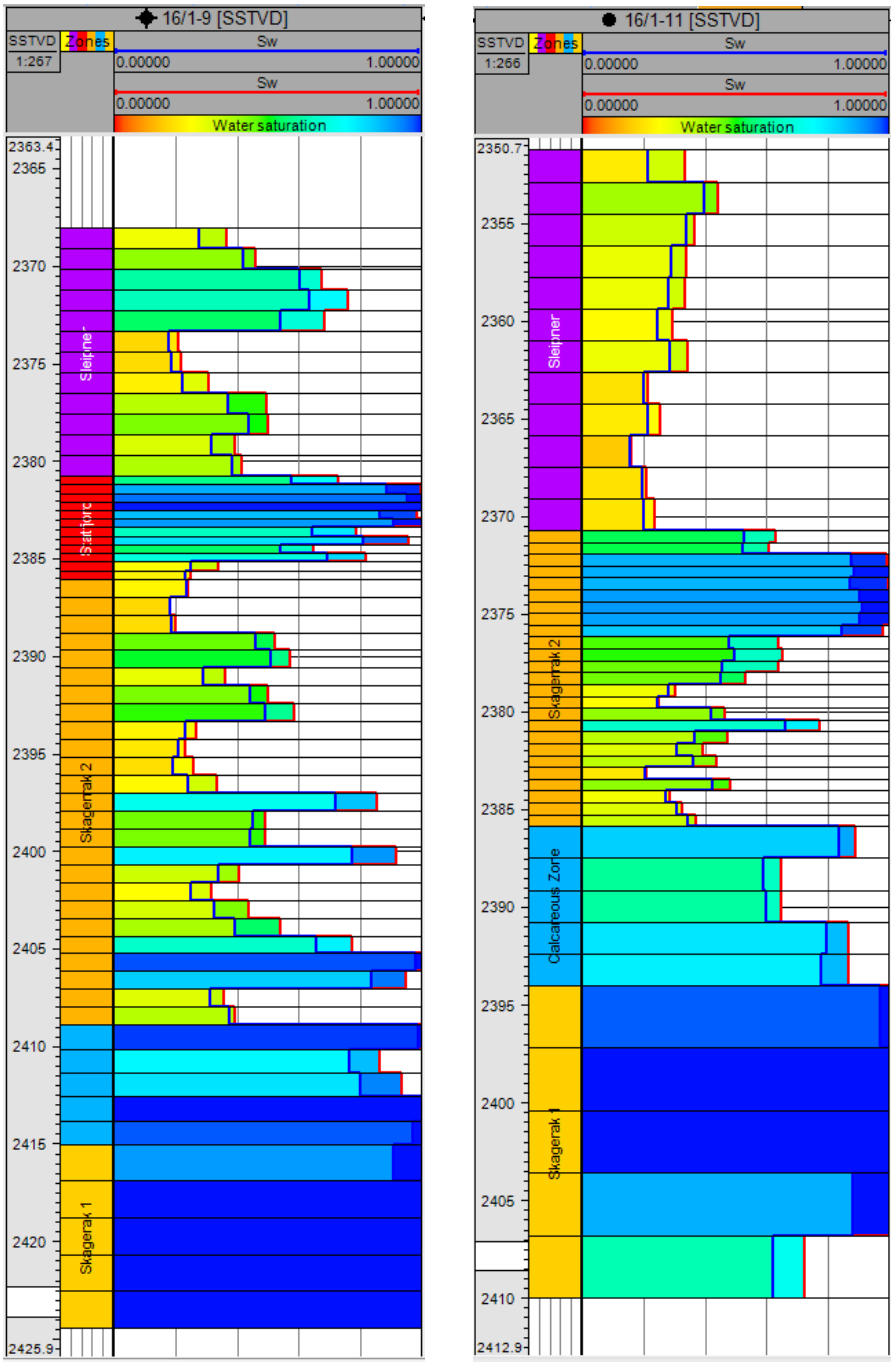

(a) 16/1-9 Water saturation difference (b) 16/1-11 Water saturation difference

Figure 41: *Comparison of water saturations in the model. The red curve illustrates the Effective porosity model, and it is higher through all the layers.*

Relative permeability Besides the obvious economic advantage of having high oil saturation in an oil reservoir, is the relative permeability effect as a function of saturation. An example from well 16/1-9 shows a difference between relative permeability's from 0.36 to 0.61 with the initial water saturation in the two cases. It is hard to directly show the effect this has on the simulation results, as many factors contribute to the results. Knowing the water saturation is initially lower using total porosity, a lower initial water-cut can be expected from the simulation results. The viscosity affecting the mobility of oil and water will not change based on the porosity type input. Figure 42 shows the effect different initial water saturations have on relative permeability.

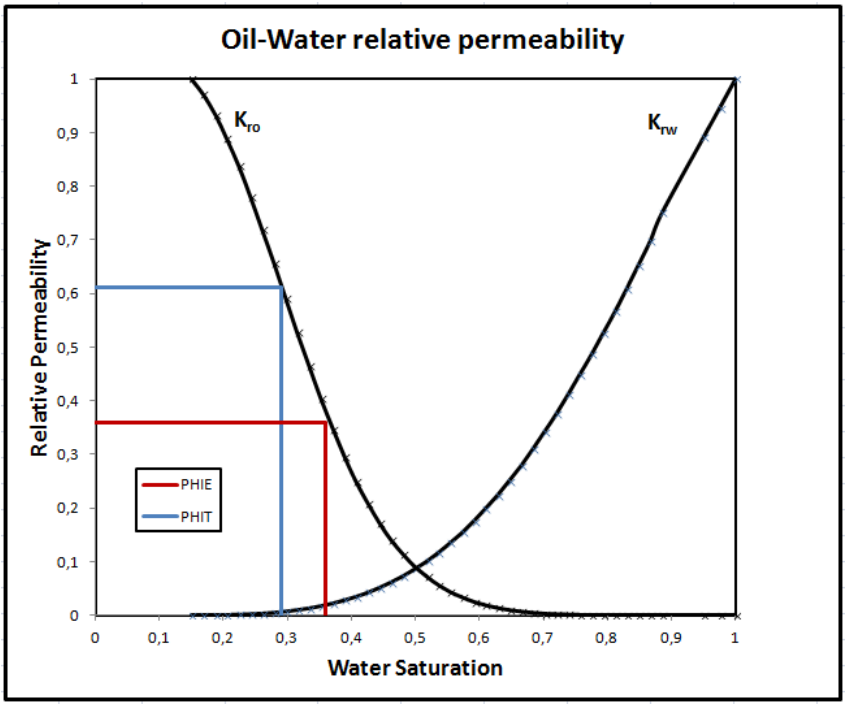

Figure 42: *The effect of water saturation on relative permeability. The curve and input is taken from Well 16/1-9 @ 2391 m TVD. Overestimating water saturations will have a negative impact on the predictions.*

3.13 Log/Core comparison

As cores are available in 16/1-9, 16/1-11 and 16/1-16, a comparison of the calculated porosity and permeability could be made with the core data. In the clean sands with low shale content, a good match is obtained with both effective, total, and estimated sand porosity. When the shale content increases, the effective porosity drops due to the laminated shale fraction. This can be observed in figure 43(a) indicated by arrow number 1. The shale distribution in this area is likely to be laminar based on output from the Thomas & Stieber analysis. Since little shale is distributed in dispersed mode, the porosity should match clean sand total porosity measured on the cores. A decent match is obtained by the total porosity log, and an even better match is made with the clean sand estimate.

When matching the permeability, it is the plugs with high permeability that are the most important. This is because it is the good sands that will contribute the most to production, and obtaining a good match is essential. A good match is obtained by permeability based on clean sand porosity. Figure 43(a) and 43(b) shows this with arrow number 2 and 3. Permeability is plotted on a logarithmic scale, and the permeability log based on effective porosity is often off by one order of magnitude.

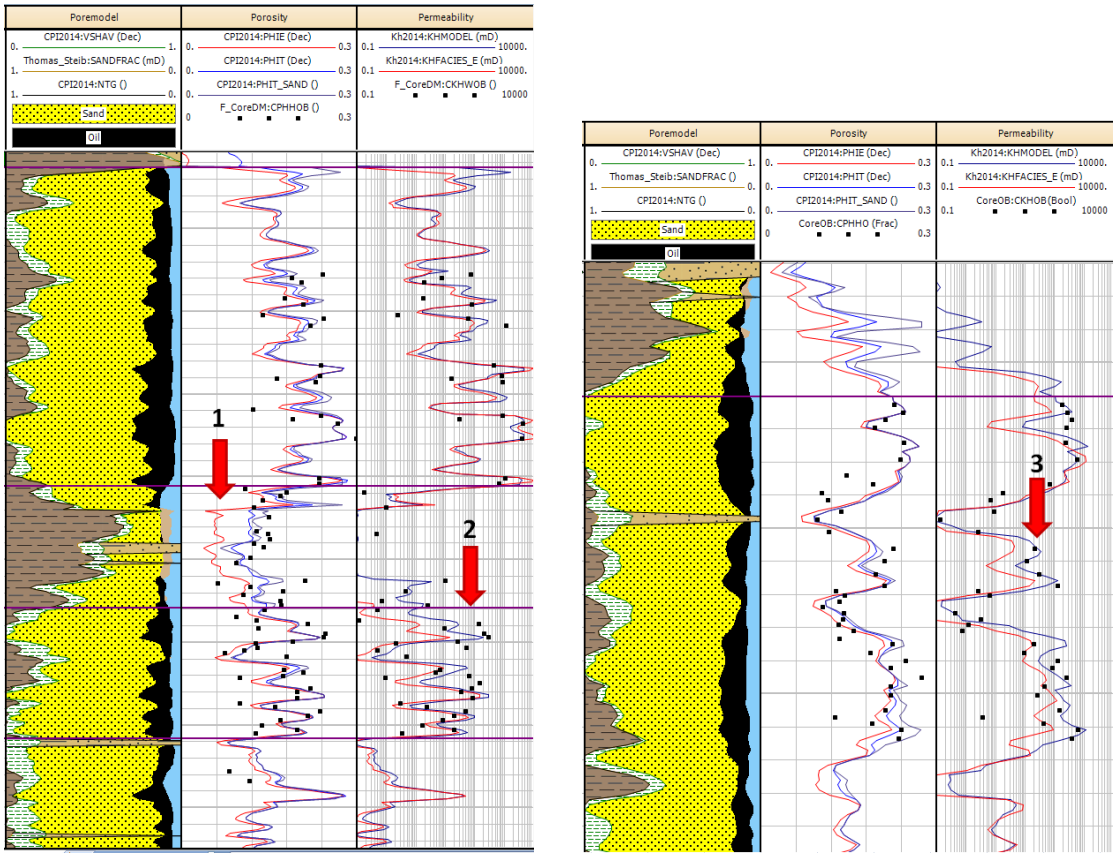

(a) Well 16/1-11 (b) Well 16/1-9

Figure 43: *Log/Core comparison. There is a good match between the logs and cores. The effective porosity values are slightly less than the cores, because they are dried to total porosity. This can be seen in the shaly part of the well sections.*

4 Results

4.1 Simulation results

One of the objectives with this thesis was to investigate the differences, if any, between models based on either total porosity with net to gross or an effective porosity system. The two base cases where run in eclipse with the same grid resolution to avoid numerical dispersion differences between the methods. Porosity, permeability and water saturation where changed in the grid based on either total porosity with net to gross or effective porosity. As figure 44 shows, there is indeed a difference. Initially, the oil production is constrained by the process capacity at the platform. The Waxman & Smits case is able to hold the production plateau for an additional 6 months compared to the Indonesia case. Cumulative production ends on 25 million Sm^3 with total porosity and 22 million Sm^3 with effective porosity, a 13.6% difference if producing to year 2055. This estimated field lifetime is little optimistic, but simulations are run this long for the rates to stabilize. In reality, an economic limit would set a stop to the production at some critical production rate. The recovery factors are approximately 52% in both cases.

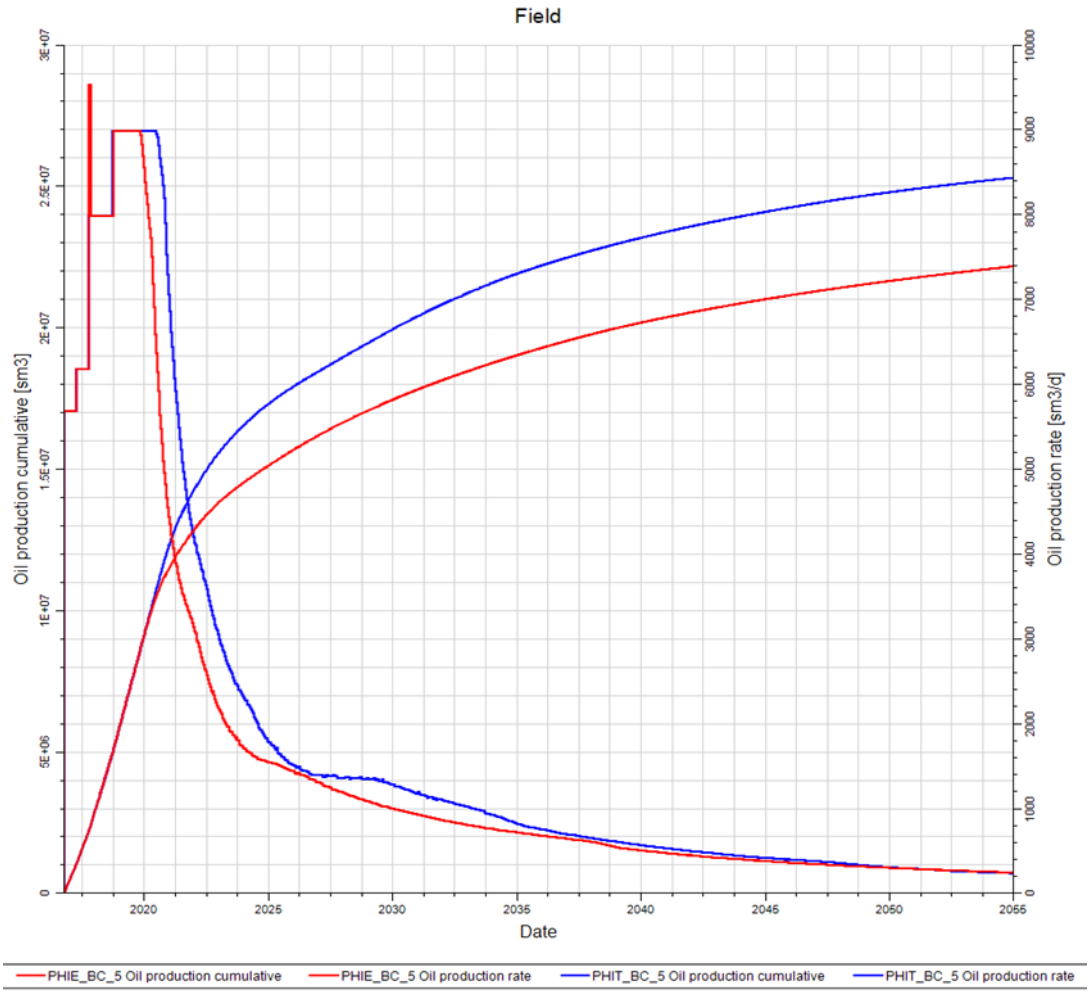

Figure 44: *Base case: Oil production rate and Cumulative oil production. Total porosity shows a significantly higher oil production.*

Cumulative gas production also increases drastically with the total porosity model. Cumulative production increases by 20%, from approximately 5 billion Sm^3 to 6 billion Sm^3, if producing to 2055. Figure 55 in appendix A shows the gas production.

The water production rates appear to be lower during the initial years, then cross over to a stable level of 22 000 Sm^3/d for the total porosity case. The water production rate in the effective porosity case stabilizes at 21 000 Sm^3/d. The water cut, or water-oil ratio, is still less in the total porosity case for an extended period because of the higher oil production rates. Figure 56 and 57 in appendix A shows the water production.

The average reservoir pressure behaves in a similar way in the two cases. The difference is a slightly faster, and 50% higher pressure drop in the total porosity case during the time from end of plateau production to the injectors restore the average pressure. This pressure drop leads to a spike in the gas-oil ratio, as an effect of two things. First, gas comes out of solution as the wellbore pressure drops, and rushes towards the wells because of its favorable mobility. Secondly, the gas-cap will expand and the gas-oil contact will move downwards, closer to the producers. This leads to gas breakthrough, and can be seen in the plot from well DOP02 in figure 61 in appendix A. Figure 58 and 59 in appendix A shows the full field effects of pressure and gas-oil ratios.

Solution GOR at the bubble-point is 162.8 Sm^3/Sm^3, approximately the same as the value the GOR stabilizes at after its spike. In the total porosity case, the GOR stabilizes at 170 Sm^3/Sm^3 and in the effective porosity case it stabilizes at 160 Sm^3/Sm^3.

Water injection is the primary source for pressure support and figure 60 in appendix A shows the water injection rates and cumulative water injected. It shows a slight difference, with higher needs for water injection in the total porosity model. In the early times, water injection is restricted by the individual well capacities of 4500 Sm^3/d.

The oil initially in place in the two cases are different as a result of different porosities and water saturations. Figure 45 shows the total porosity case has an initial volume of 48 million Sm^3 and the effective porosity case 42 million Sm^3. To investigate how much of the increased production was caused by this volume effect, a volume-adjusted simulation was run. This made the models start with exactly the same oil in place. Graphically, it would mean shifting the left start-point of the red Indonesia curve in figure 45 to match the Waxman & Smits start-point.

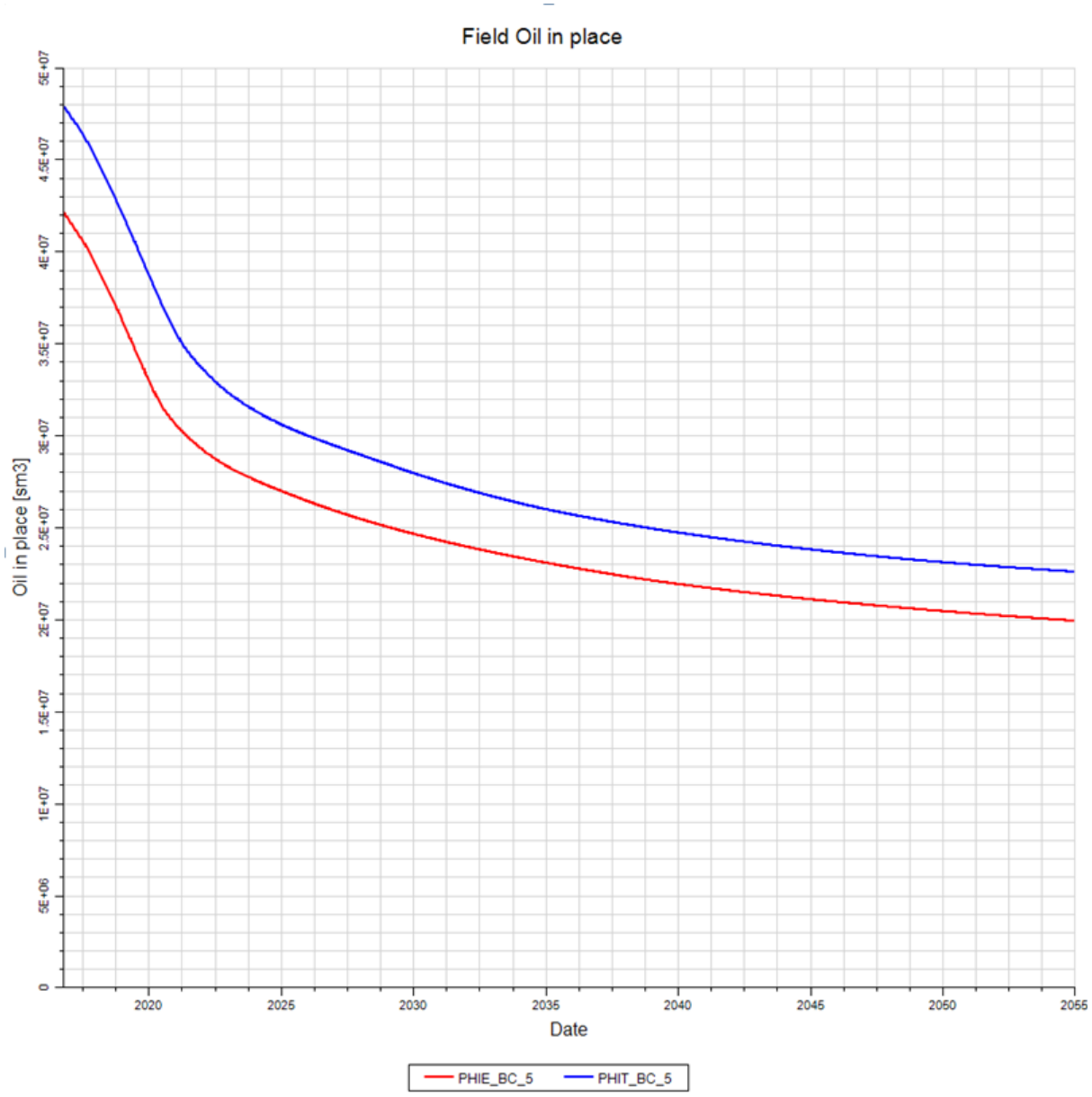

Figure 45: *Base case: Field oil in place. The recovery factors are approximately equal, but total production is higher in the total porosity case.*

With the volume effect gone, the total porosity case still predicts higher recovery than the effective case. This is a result of the total permeability difference and the relative permeability effect.

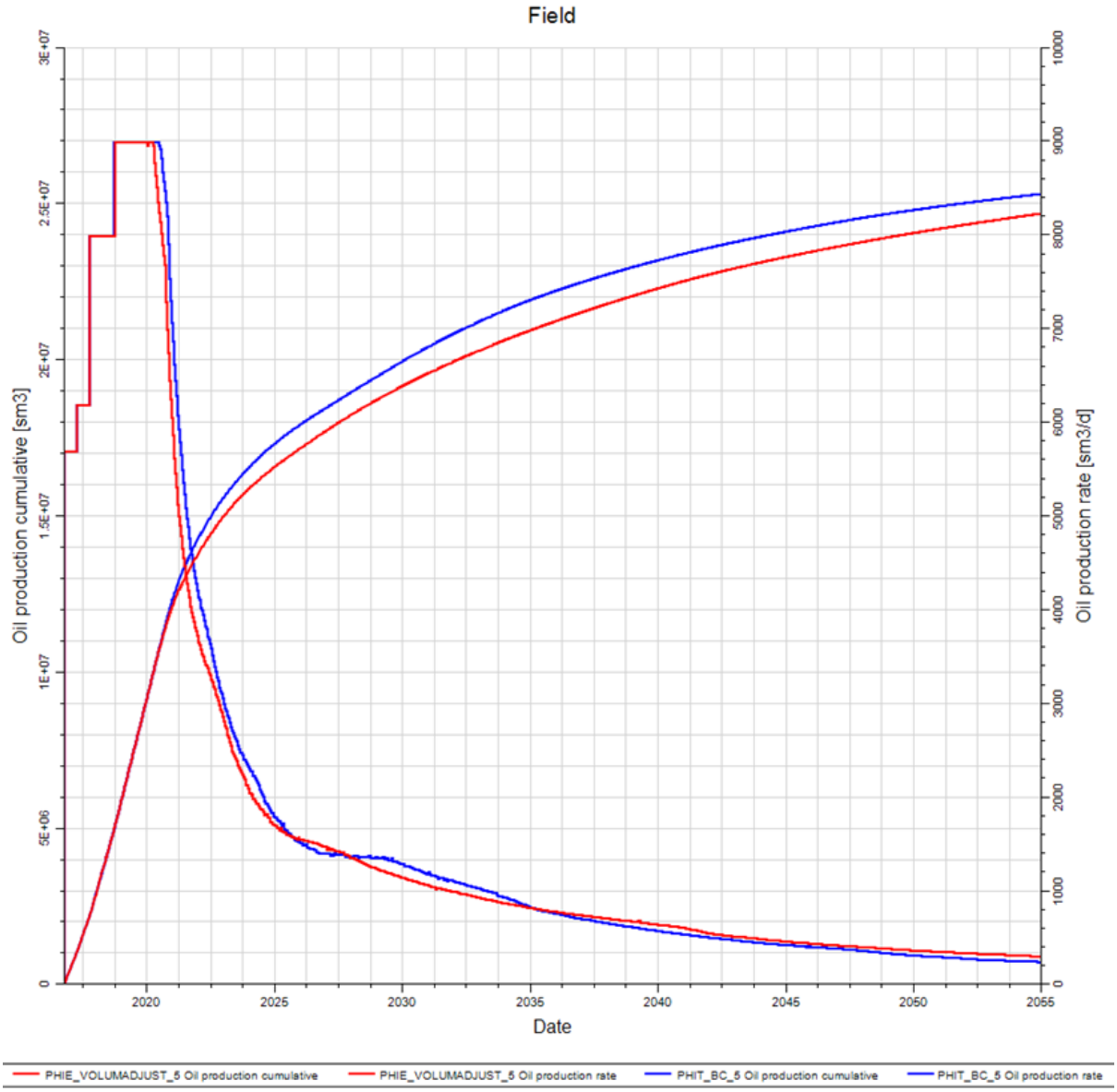

Figure 46: *Volume-adjusted case: Oil production rates and cumulative oil production. A slightly more optimistic recovery is still predicted by the total porosiy model.*

Figure 47 shows the cumulative oil production plotted against the cumulative water injected. This is done to control the mass balance in the cases and find reasons for the additional recovery. There is no big difference in the behavior and the additional oil recovery in the total porosity case is therefore not a result of increased water injection.

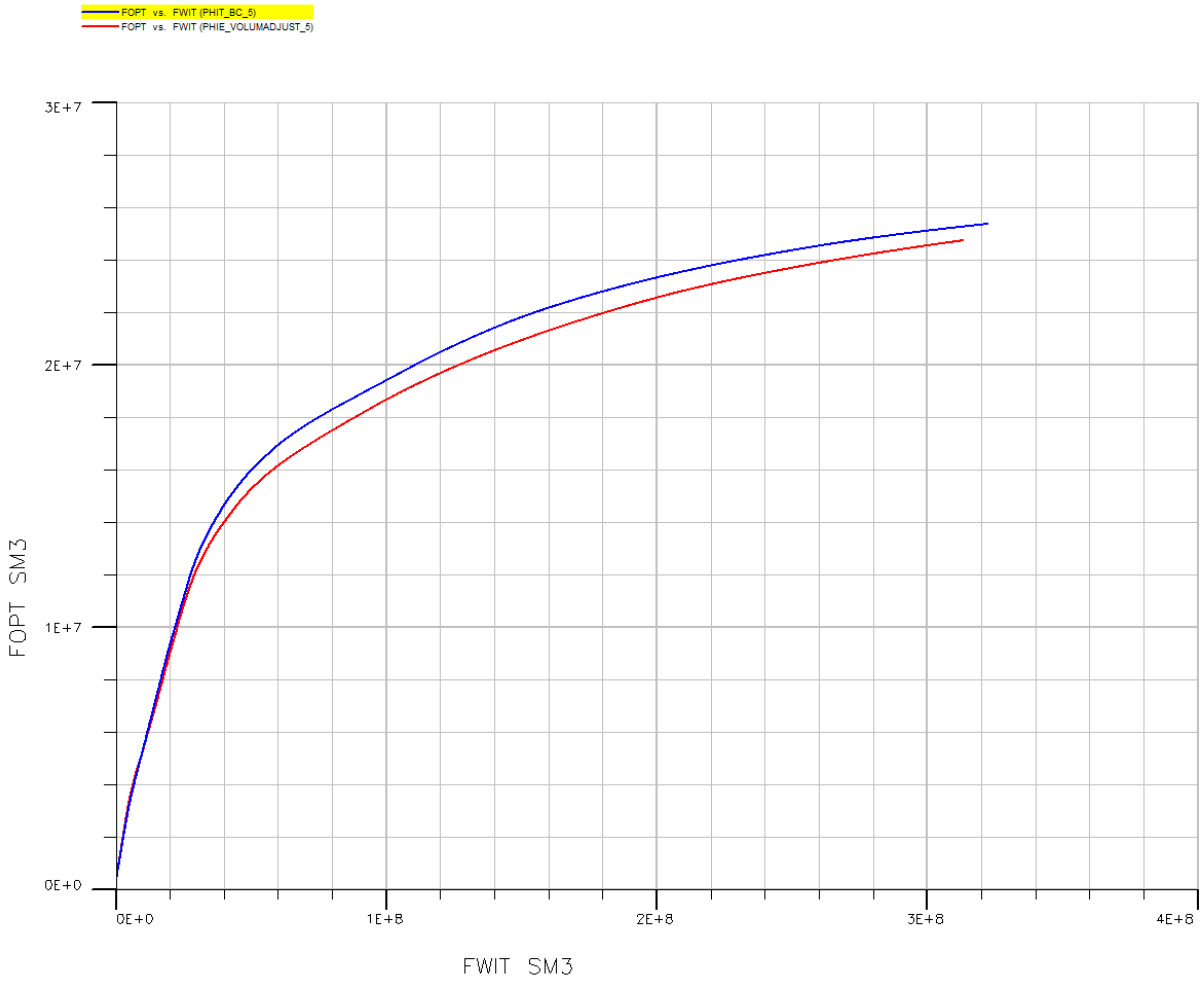

Figure 47: *Volume-adjusted case: Cumulative oil production vs. Cumulative water injected.*

4.2 Sensitivity to volume shale

As simulations were run with both high and low shale volume for total and effective porosity, the sensitivity to volume shale in interpretation was obtained. If the models had different influence on the simulation results, the one with smaller difference between the cases would be more robust to the individual interpretation of the petrophysicist.

Figure 48 illustrates the sensitivity to volume shale and petrophysics in general. The 3 shale-points at the crossplot in figure 25 is the only difference leading to this large spread in the cumulative production.

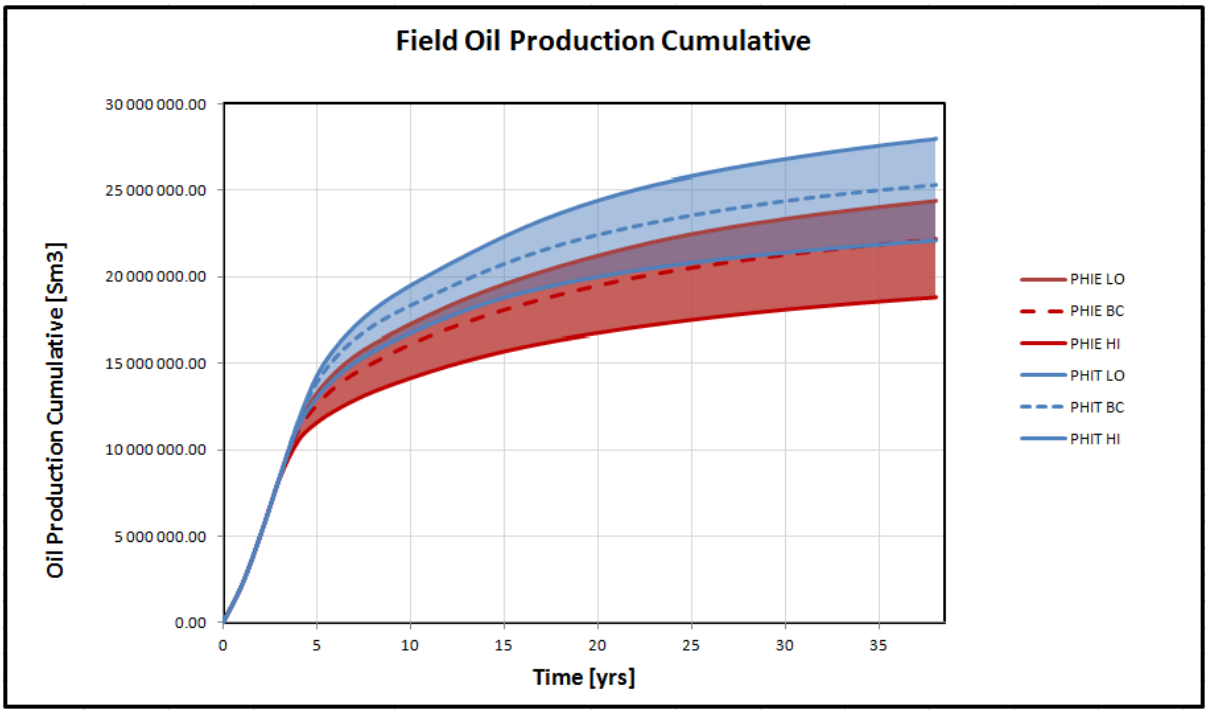

Figure 48: *Spread in cumulative oil production, HI-BC-LO shale volume cases. This figure illustrates the sensitivity to volume shale in reservoir simulations.*

In order of investigating the spread between the curves, a standard deviation of the 3 curves was calculated as a function of time. It shows that although the difference is small, the Waxman & Smits is slightly more reliable during the first half of the simulation, and then the Indonesia takes over as the most robust.

$$\sigma^2 = Var\left[X\right] = \frac{1}{n}\sum_{i=1}^{n}\left(x_i - \bar{x}\right)^2 \tag{35}$$

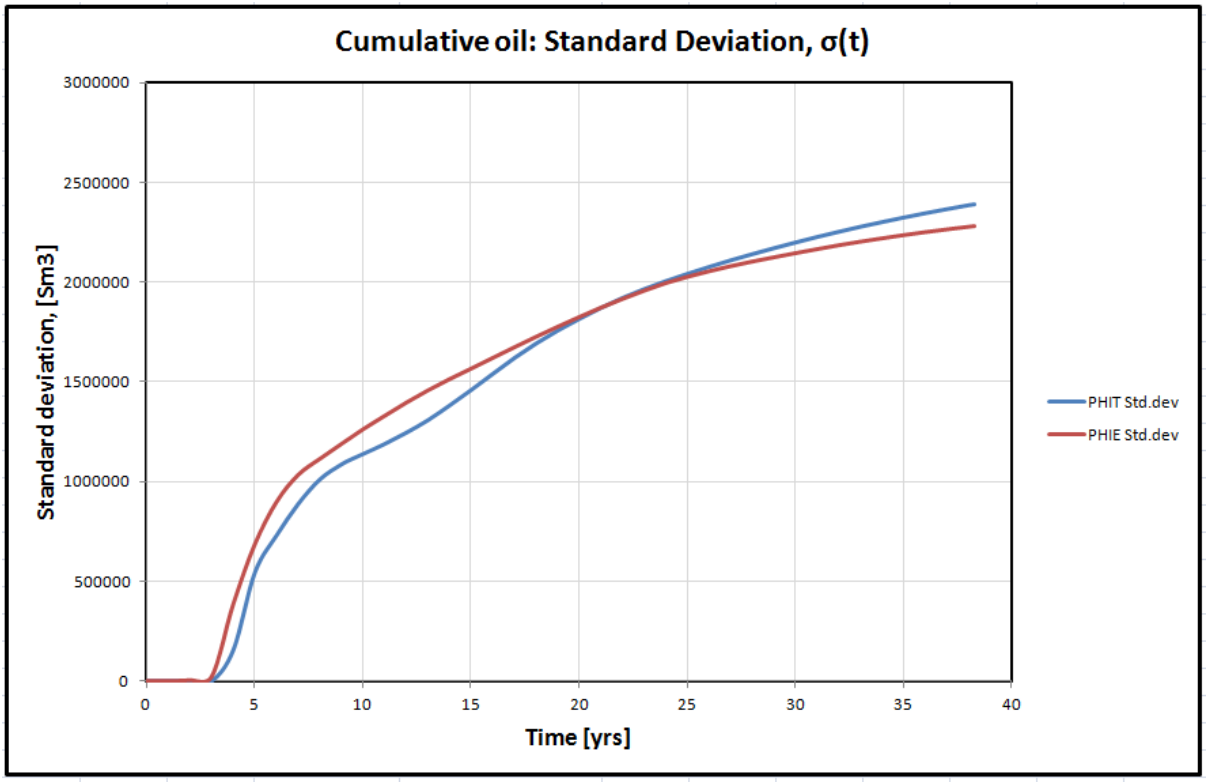

Figure 49: *Standard deviation for the total porosity model and the effective porosity model when volume shale is adjusted. The total porosity model is slightly better during the first 22 years.*

The predicted life of the field from the PDO, based on effective porosity calculations, is approximately 18 years. This is also the time it takes for the standard deviations to become equal.

There is a large difference of the volume in place estimates based on model and volume shale interpretation. The difference between using the effective porosity model with a high shale volume and the effective porosity model with low shale volume is more than 50%. Figure 62 in appendix A shows the volumes in place as a function of time for the different cases.

Table 4: *Different in place volumes based on model and volume shale interpretation*

Values in 1 000 000 Sm^3	**Low shale volume**	**Base case**	**High shale volume**
Total porosity model	53	48	40
Effective porosity model	46	42	35

4.3 Sensitivity to reservoir engineering editing

With the two base case petrophysical models in place, and having proved the impact of shale interpretation error, the effect of some reservoir engineering editing was briefly investigated. This was done to see how the volume shale uncertainty compared to other reservoir parameters frequently discussed among reservoir engineers. The goal again is to see how the two petrophysical models behave compared with each other, and what parameters have the largest impact.

4.3.1 Vertical Transmissibility changes

Initially the vertical permeability in the model was set to be 0.1 times the horizontal permeability. Eclipse calculates transmissibility between cells based on cell geometry, dip angle, permeability and a transmissibility multiplier. Because of uncertainties related to vertical permeability, two simulation runs on both models was run and compared with the base case scenario. The Z-direction transmissibility factors were set to 0.5 and 5 for all 866096 cells in the model.

Figure 50 shows the results, and figure 51 shows the standard deviations. The total porosity model is about twice as sensitive to changes in the vertical transmissibility, compared with the effective porosity model.

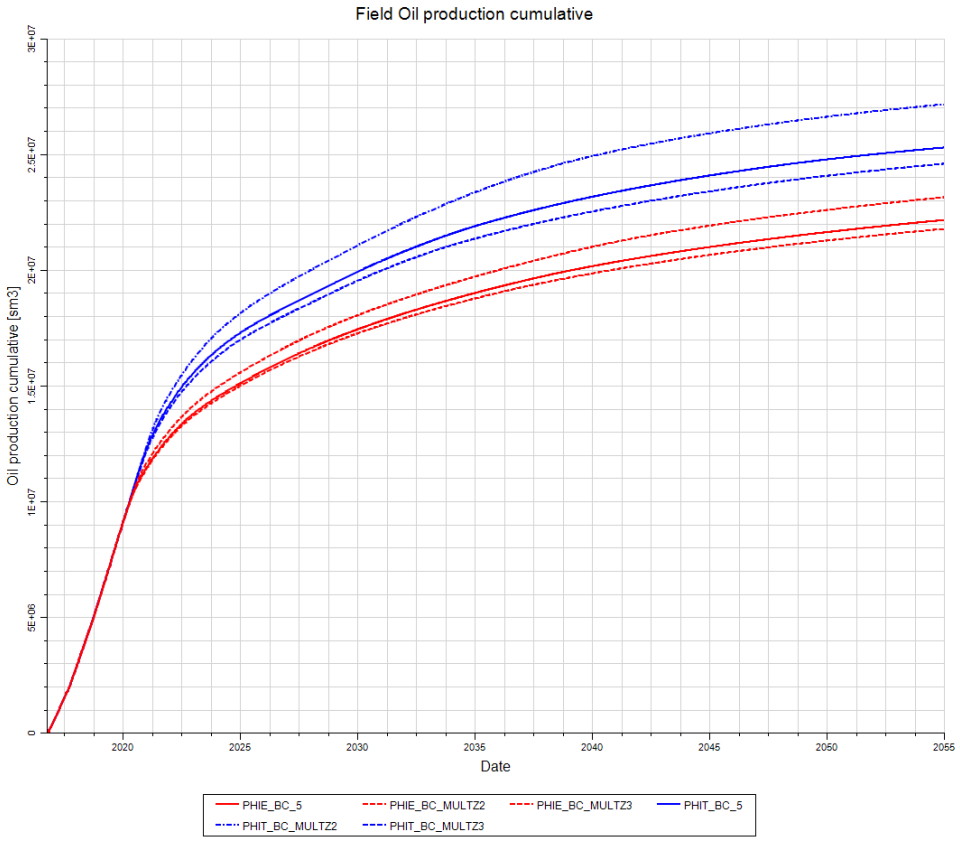

Figure 50: *Effect of vertical transmissibility changes: Cumulative oil production*

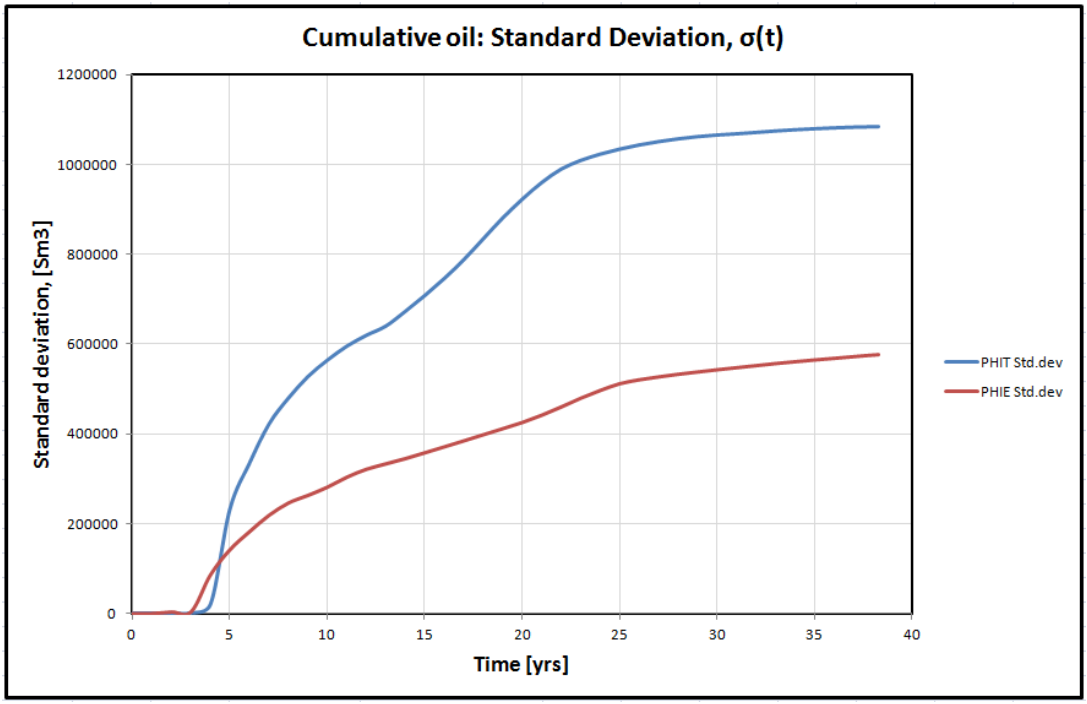

Figure 51: *Standard deviation for vertical transmissibility changes. The total porosity model shows a higher uncertainty than the effective porosity model.*

4.3.2 Sealing faults

The simulations where initially run with no additional flow restrictions across the faults. They are created only by geometric distribution of the flow properties that are shifted within the gird. In two new simulation runs, additional flow restrictions were introduced. The intention was to represent a case of shale smearing or other sealing effects related to faults. A fault transmissibility factor of 0.001 and 0.5 was entered in the models, and a development strategy identical to the base case was run.

Figure 52 show streamlines of the model for the base case scenarios and the sealing fault case. The time of the snapshot is April 2019, about 2,5 years after startup, when all the wells are flowing. The flowline maps look more or less the same to the end of the simulations, since all the wells stay active.

The effect on cumulative oil production with sealing faults was a decrease of 2.3% in the total porosity case and 6.0% in the effective porosity case. The case with a fault transmissibility factor of 0.5 plotted within line-thickness of the base case scenario. Figure 54 shows the standard deviation of the models behavior related to sealing faults.

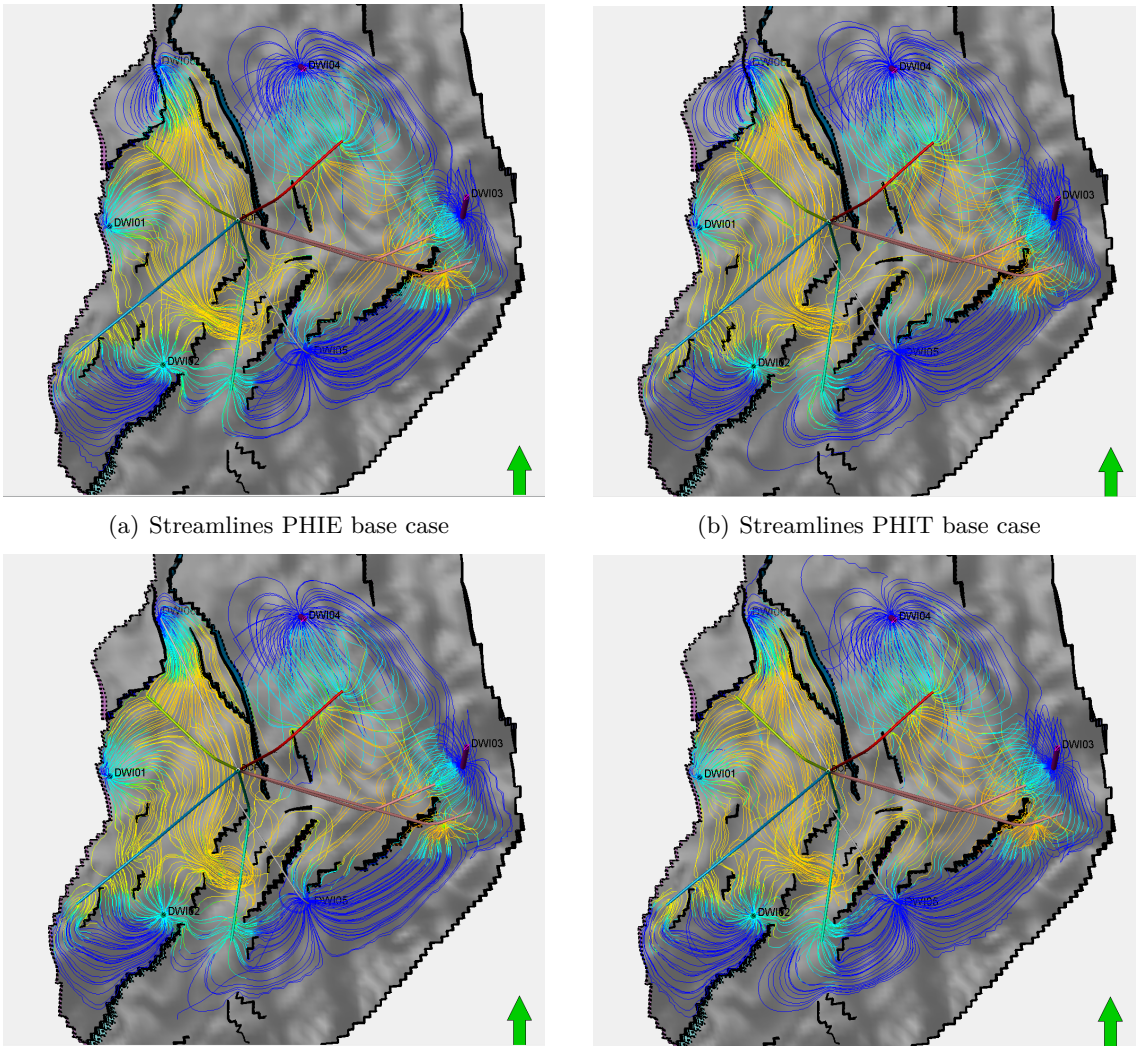

(a) Streamlines PHIE base case

(b) Streamlines PHIT base case

(c) Streamlines PHIE Sealing faults

(d) Streamlines PHIT Sealing faults

Figure 52: *Streamlines with faults open and closed, April 2019. The streamlines does not cross any faults when they are sealing.*

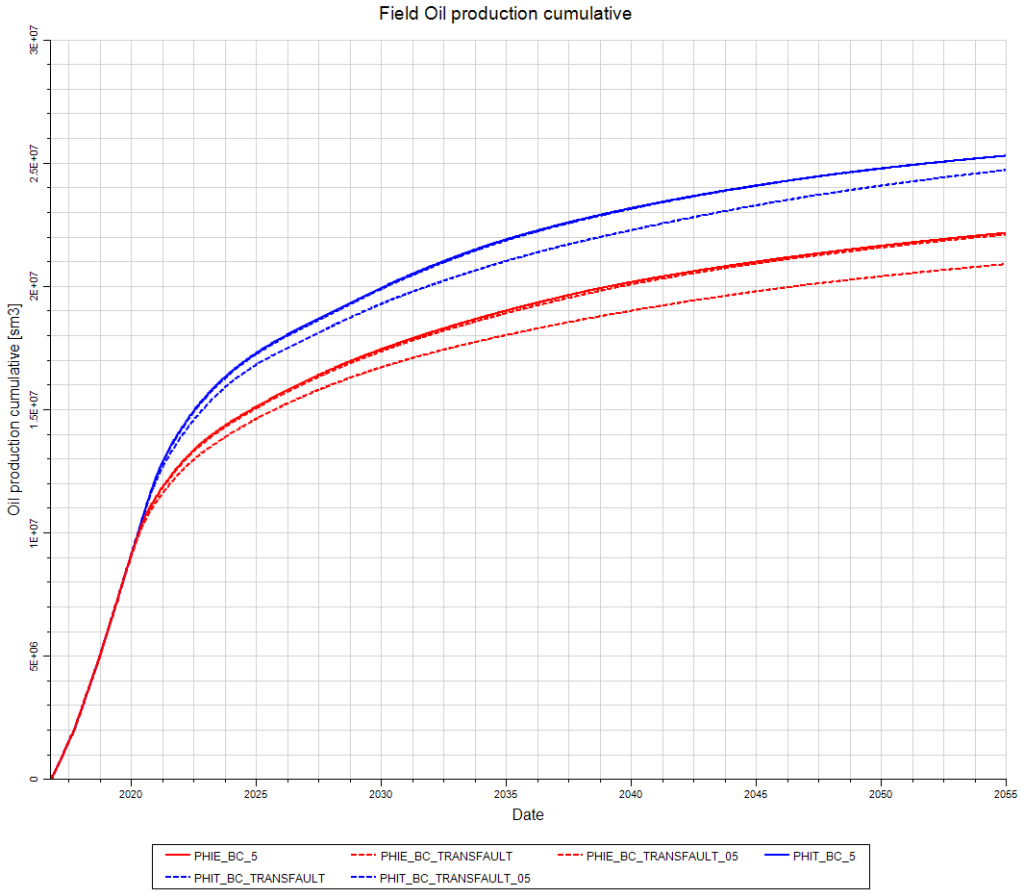

Figure 53: *Effect of introducing sealing faults in the model: Cumulative oil production*

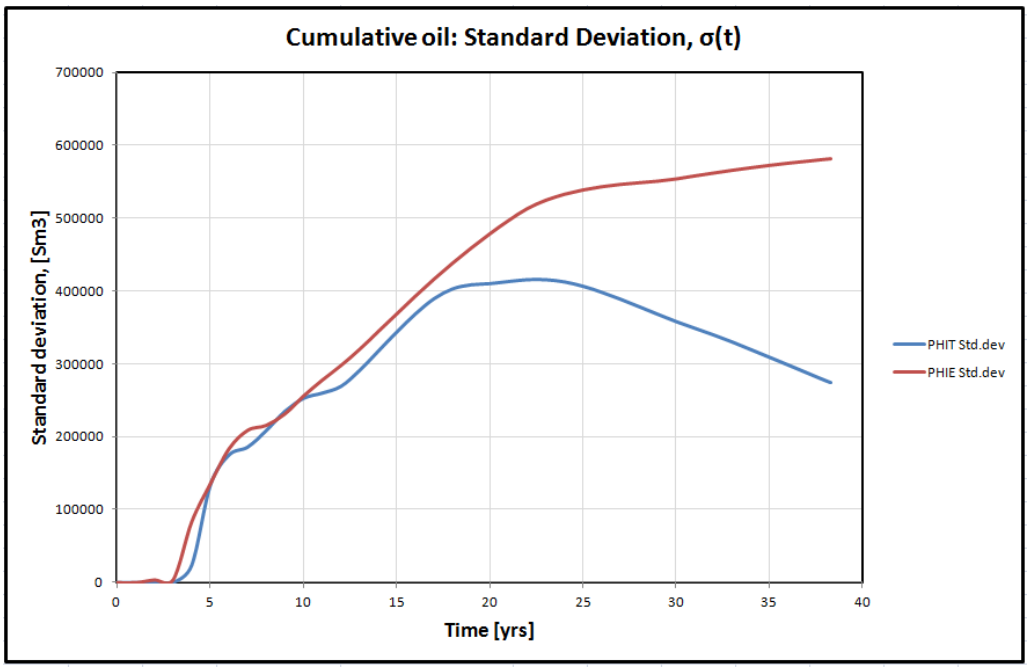

Figure 54: *Standard deviation for fault transmissibility changes.*

To get a perspective of how the different parameters influence the simulation results, table 5 show the difference between the high and low estimates for both models. Volume shale has by far the largest influence on the predicted oil recovery, with an endpoint difference of 5.8 million Sm^3 and 5.5 million Sm^3. The difference between the base cases is also included to compare the effect of model choice to reservoir engineering parameters.

Table 5: *Difference in cumulative oil production between high and low cases for volume shale, vertical transmissibility sealing faults and choice of model. The elements involving petrophysics have the highest uncertainties. Example, sealing faults and volume of shale has almost 4 times larger uncertainties in the effective porosity model, and 10 times larger in the total porosity model.*

Values in 1 000 000 Sm^3	**Total Porosity**	**Effective Porosity**
Volume shale	5.8	5.5
Vertical transmissibility	2.5	1.2
Sealing faults	0.5	1.4
Choice of model (Base case)	3.0	

5 Discussion

The effects of using effective porosity or total porosity times net to gross as input to simulation studies does probably not concern the average petroleum engineer too much. After all, it is only a few percent difference in the porosity values. The importance of this work lies in showing that these few percent really makes a difference, and that there is a difference in the accuracy of the approaches.

The simulations based on the different approaches have provided new and important information on how the models behave. Simulation results shows that the choice between using total or effective porosity has a huge impact on volumes in place and recovery forecasts, with a 13.6% difference in the cumulative oil production. The large difference in volumes between the models is mainly a result of the water saturation distribution based on the porosity and permeability estimates. The difference in production is an effect of permeability, saturations and relative permeability.

A high estimate of volumes in place has a positive impact on the value of a company. A small estimate will on the other hand lead to a higher recovery factor and the associated bragging rights. Volumes are also important in the appraisal stage of development to make a decision between developing a field or abandon it. In addition to the volumes, the distribution of hydrocarbons is important from an economic point of view. Different companies share the costs and revenues based on license boundaries, shares and production allocation. The companies might argue with this in mind that one case is better than the other. The water saturation and fluid contacts can be shifted around in dipping beds, moving hydrocarbons from one license to another. Perhaps this study could prove useful for the companies benefiting from the total porosity scenario.

In general, the total porosity model gives a more optimistic prediction of the recovery. Results show a significant incremental oil and gas production with the total porosity and Waxman & Smits approach. Water production rates and the water cut generally become lower in the total porosity case. The difference in rates is a quantification of the effects induced by different permeability and water saturations in the models. As relative permeability is dependent on water saturation, low water saturation leads to higher oil production rates until water breakthrough. The water injection rates are also of importance, as water injection will affect the operating costs of the platform. The liquid production rates are higher in the total porosity case, and more water must be injected to maintain the pressure support. All in all, the predictions are more optimistic with the total porosity model.

The arithmetic comparison between total and effective porosity in section 3.1.1 showed uncertainties in only volume shale made the effective porosity look more robust. The simulation results from section 4.2 showed that this was not the case, as the standard deviations were approximately equal. The total porosity case has a slightly more robust solution at early times and at the same time holds the plateau for a longer time. This is good news to the economists. Net present value calculations would turn out higher and they would have less uncertainty related to them. This happens as the discounting favors early times, and the future pays less off in NPV. By maintaining the early production rates, the project will return the investments faster.

The other results from the arithmetic comparison suggested that total porosity would perform better when an uncertainty to shale porosity was added. Unfortunately, the amount of work related to simulate this in addition to the work already done was beyond the capacity of the

author. From the arithmetic study one might say the best case effective porosity scenario was simulated in the comparison. With the simulation results in mind it is fair to say that the effective porosity sensitivity to volume shale is the same as total porosity or larger.

One disadvantage with the total porosity method is that the clean sand porosity is estimated using the Thomas & Stieber method. In other words, sand porosity is not measured by the logs; it is derived by the use of shale volume and the density porosity log. Both have uncertainty factors covered in section 2.1 and 2.2, and they will be transferred into the clean sand porosity estimate. This is why total porosity and not estimates for clean sand porosity was used in the permeability correlation in section 3.5 for the zones where uncertainties was too large. These uncertainties are the absence of cores, or zones with very high shale content forcing the data point into the lower left corner of the Thomas & Stieber diagram (figure 13 section 2.5.2). When the net to gross ratio is lower then 0.6, small errors in bulk total porosity can make a huge difference in the clean sand porosity estimate.

With the techniques used to determine porosity on cores and logs, it is hard enough to get the total porosity right. On cores, the possibility of inducing stress and damage clay minerals during the drying process is present. On logs, the bulk measurement hides important information about shale distribution and sand properties. To estimate effective porosity, additional assumptions about the clay-richness and volume of shale must be used. This makes the effective porosity a victim to one of the largest uncertainties related to formation characterization. With the accuracy associated with total porosity measurements compared to effective porosity, the probability of matching the logs and cores is higher. With an acceptable match, the data can be used with confidence as input to the reservoir simulator.

The impacts on the simulations when comparing choice of model, volume shale, sealing faults and vertical transmissibility uncertainties might surprise or scare the general reservoir engineer. The large spread in volume shale runs serves as an acknowledgement of the importance and influence the petrophysical work has on model behavior. The different spreads is of course a result of the magnitude of input variations, but the small difference in shale point input had a surprisingly large effect on the results. This is only as a secondary effect through porosity estimate and the permeability, since volume shale is not loaded into the model directly. The uncertainty introduced by model selection is on the other hand not influenced by subjective input and editing. The 3 million Sm^3 difference in predicted recovery is a result related to the effective or total porosity approach only.

The sensitivities of the shale curves are unfortunately not known, and they could be affected by many factors. If the same study was done on another field, or if wells in the simulation runs behaved different, the results could change. This study, however, showed that the impact should be expected to be significant. In an ideal situation, Monte Carlo analysis could be performed changing parameters such as volume of shale, shale porosity and sand porosity. This would generate a distribution of the simulation results and tornado charts with sensitivity of input parameters could be generated. Sadly, the time it takes to generate one set of results is so large that it becomes impossible to implement in practice.

The vertical transmissibility had a larger spread in the total porosity case than in the effective porosity case. Vertical permeability usually has a high uncertainty, as core plugs are mostly cut in the horizontal direction. In addition to this, cores are cut on a scale that is too small to register continuous shale layers which inhibits vertical flow. To observe these effects, more dynamic flow test measurements would be required. The effect this would have on the models can however be investigated. The standard deviation showed that the total porosity was about

twice as sensitive to these adjustments as the effective porosity.

In the fault transmissibility case almost no production is lost when the transmissibility is reduced by 50%. This might be a result of poor original transmissibility or great placement of injectors and producers, as most of the streamlines lies parallel to the faults. Some streamlines can be seen to cross each other in figure 52. This is not an effect where the reservoir simulator lets to particles exist on the same place to the same time, but a result of a 2D representation of a 3D model. In the case of totally sealing faults, some areas like the North-West corner is cut from the production, leading to a lower total production. There is much uncertainty related to the faults in the model, as the seismic resolution is around 20-30 meters. When the thickness of oil-bearing sands is from 40 meters and down, a fault of 30 meters would have a large impact. Some faults are obvious according to the trained eyes of the geophysicists at Det norske, while others are more subtle. A new fault interpretation based new seismic is performed as this thesis is written, but it is not ready in time to be included. It would probably reflect reality in a better way, but as long as the basic model is kept constant it should have little effects on the results of this study.

6 Conclusion

- For Ivar Aasen, there is a significant difference in in-place volumes and recovery depending on the petrophysical model applied. Of the two models discussed in this study, it is believed that the total porosity based model is closer to reality than the effective porosity model because of its better match with cores. The total porosity model estimates initial volumes in place of 48 million Sm^3 and the effective porosity model only 42 million Sm^3. The difference in cumulative oil production is 13.6%, and it illustrates the possible error related to use of the effective porosity model.
- The petrophysically estimated volume shale parameter have a large impact on volumes and recovery. The total porosity model is slightly less affected by this parameter in early times than the effective porosity model.
- Variations in volume shale has a greater influence on simulation results then adjustments to fault transmissibility and vertical transmissibility factors. Together, volume shale and the choice of model deserve close attention when dealing with heterogeneous formations like the Ivar Aasen field.

Nomenclature

ϕ_s	Porosity, sonic
Δt	Interval transit time
Δt_f	Fluid transit time
Δt_{ma}	Matrix transit time
ϕ	Porosity
ϕ_E	Effective Porosity
ϕ_T	Total Porosity
$\phi_{clean\,sand}$	Porosity, Clean sand
$\phi_{disp\,shaly\,sand}$	Porosity in dispersed shaly sand
ϕ_D	Porosity, Density log
ϕ_{sh}	Porosity, Shale
ϕ_{sl}	Porosity in laminated sand
ϕ_s	Porosity, Sonic log
ρ_b	Density, bulk
ρ_{fl}	Density, fluid
ρ_{ma}	Density, matrix
a	Tortuosity factor
B_o	Formation volume factor, oil
C_o	NaCl concentrations in equivalents / liter
F	Formation factor
$F*$	Formation factor, Shaly sand
m	Cementation exponent
n	Saturation exponent
Q_v	Cation exchange capacity of clay mineral cations, milliequivalents / Pore volume
R_H	Horizontal resistivity
R_o	Water-filled rock Resistivity
R_t	True Resistivity
R_v	Vertical resistivity
R_w	Water Resistivity
R_{sand}	Sand resistivity
R_{shale}	Shale resistivity

S_o	Oil saturation
S_w	Water saturation
V_b	Bulk Volume
V_g	Grain Volume
V_p	Pore Volume
V_S	Sorbed/Bound Water
$V_{sh,\,lam}$	Volume laminated shale
$V_{sh,\,str}$	Volume structural shale
$V_{sh,gr}$	Volume Shale, Gamma ray
V_{sh}	Volume shale
A	Area
EUR	Estimated ultimate recovery
h	Height
NTG	Net-to-Gross
PHIE	Effective porosity
PHIT	Total porosity
RF	Recovery factor

References

[1] Bassiouni, Z. *Theory, Measurment, and Interpretation of well logs.* SPE, 1994.

[2] Brandsen, H. Lecture notes from TPG4180, petrophysics advanced course. *NTNU* (2014).

[3] Det norske oljeselskap ASA. *Plan for Development and Operation, Ivar Aasen* . Det norske oljeselsap ASA, 2012.

[4] Det norske oljeselskap ASA. *Ivar Aasen Field Development Project, Design Basis* . Det norske oljeselsap ASA, 2013.

[5] E. Eslinger and D. Pevear. *Clay Minerals for Petroleum Geologists and Engineers.* SEPM, 1988.

[6] Ellis, D. V., and Singer, J. M. *Well Logging for Earth Scientists.* Springer, 2008.

[7] Flolo, L. H., Menard, W. P., Weissenburger, K. W., Kjarefjord, J. M., and Arnesen, D. M. Revealing the petrophysical properties of a thin bedded rock in a Norwegian sea reservoir by the use of logs, core and miniperm data. *SPE 64273* (1999).

[8] H.J.Hill, O.J.Shirley, and G.E.Kleim. Bound Water in Shaly Sands - Its Relation to Qv and Other Formation Properties. *The Log Analyst* (1979).

[9] Jun, C., HongShen, W., Shusheng, G., and Hui, G. Low resistivity pay evaluation uing triaxial induction in offshore south china. *SPE 131462* (2010).

[10] Langeland, H. *Innforing i boreholsloggings.* PTS, NTH, 1992.

[11] Leveridge, R. M. New resistivity-logging tool helps resolve problems of anisotropy, shoulder-bed effects. *Journal of Petroleum Technology August 2010* (2010).

[12] L.P.Dake. *Fundamentals of Reservoir Engineering.* Elsevier, 1978.

[13] L.P.Dake. *The Practice of Reservoir Engineering (Revised Edition).* Elsevier, 2001.

[14] Minh, C. C. NMR Petrophysics in Thin Sand-Shale Laminations. *SPE 102435* (2006).

[15] Minh, C. C., and Joao, I. Formation evaluation in thin sand/shale laminations. *SPE 109848* (2007).

[16] Perarnau, A. Use of core photo data in petrophysical analysis. *SPWLA* (2011).

[17] PetroSkills. *Shaly Sand Petrophysics.* PetroSkills, LLC, 2010.

[18] Poupon, A., and Leveaux, J. Evaluation of water saturation in shaly formations. *The Log Analyst* (1971).

[19] Ringrose, P. S. Total-Property Modeling: Dispelling the Net-to-Gross Myth. *SPE 106620* (2008).

[20] Software, S. *Interactive Petrophysics User Manual.* Senergy Software LTD, 2013.

[21] Straley, C., and Rossini, D. Core analysis by low-field nmr. *SCA9404* (1994).

[22] Thomas, E. C., and Steiber, S. J. The distribution of shale in sandstones and its effect upon porosity. *SPWLA* (1975).

[23] Waxman, M. H., and Smits, L. J. M. Electrical conductivities in oil-bearing shaly sands. *Pet.Eng J* (1968).

[24] Worthington, P., and Cosentino, L. The Role of Cut-offs in Integrated Reservoir Studies. *SPE 843887* (2003).

[25] Worthington, P. F. Net Pay - What Is It What Does It Do? How Do We Quantify It? How Do We Use It? *SPE 123561* (2010).

A Simulation results

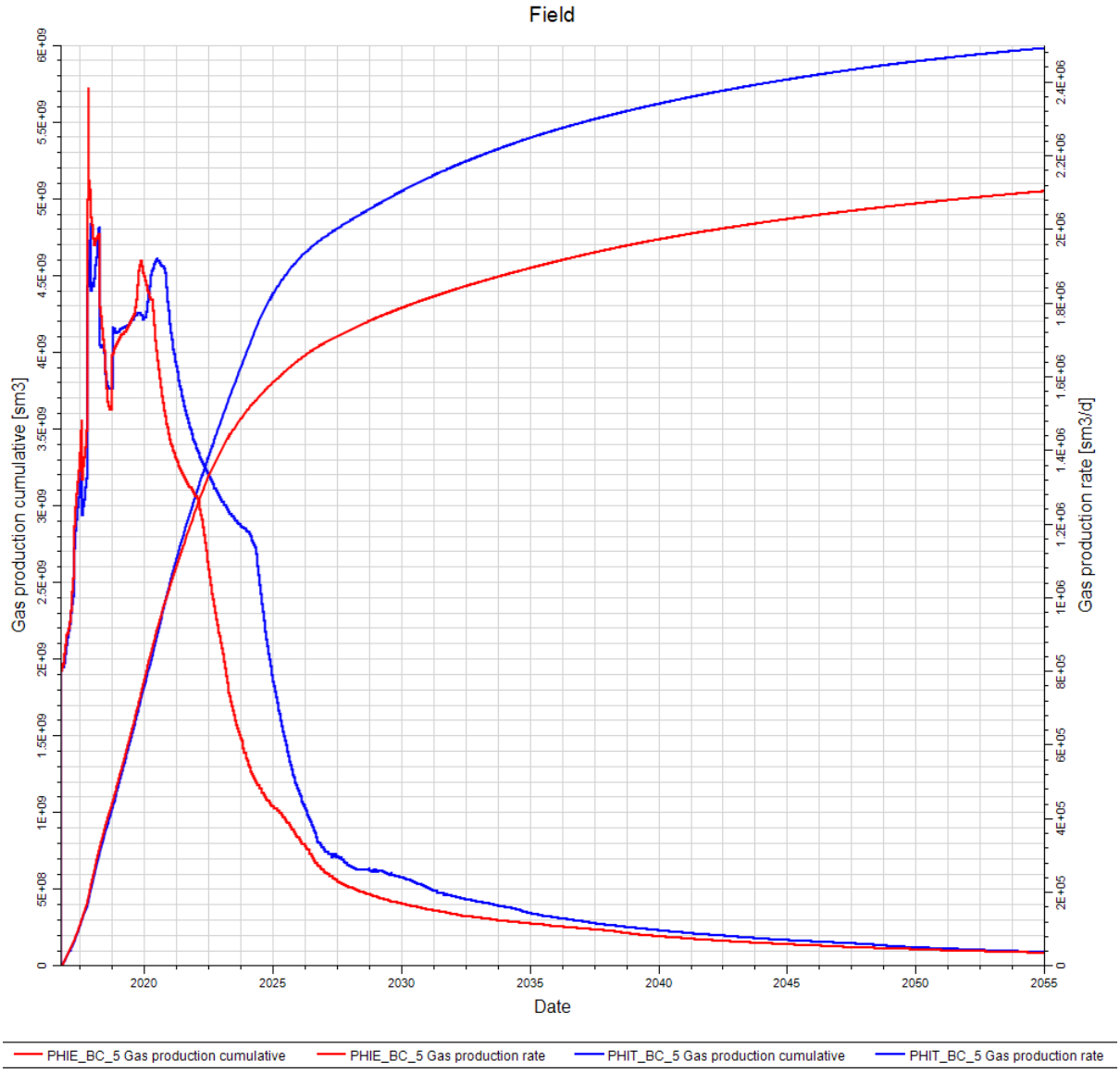

Figure 55: *Base case: Gas production rate and Cumulative oil production*

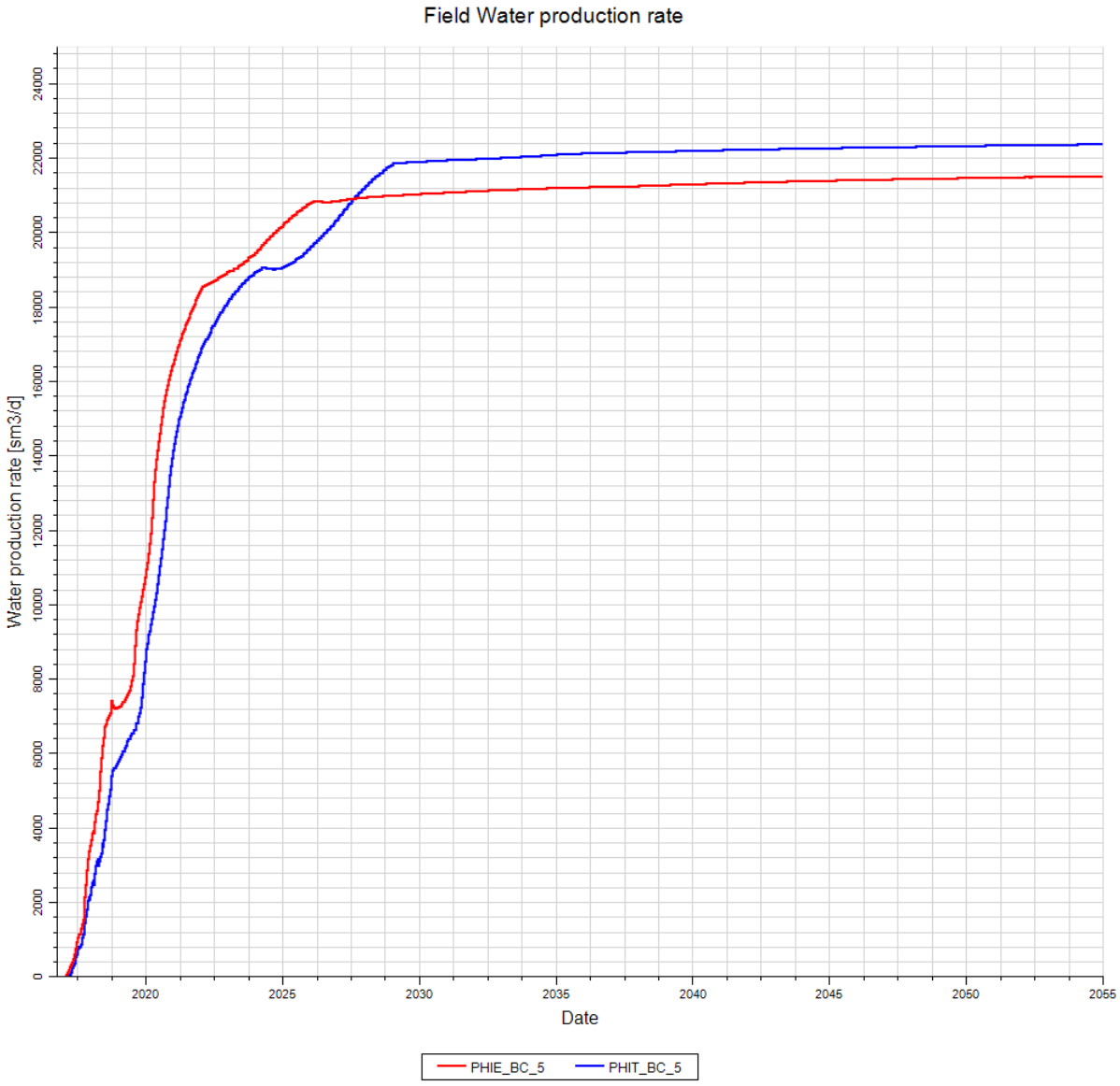

Figure 56: *Base case: Water production rate*

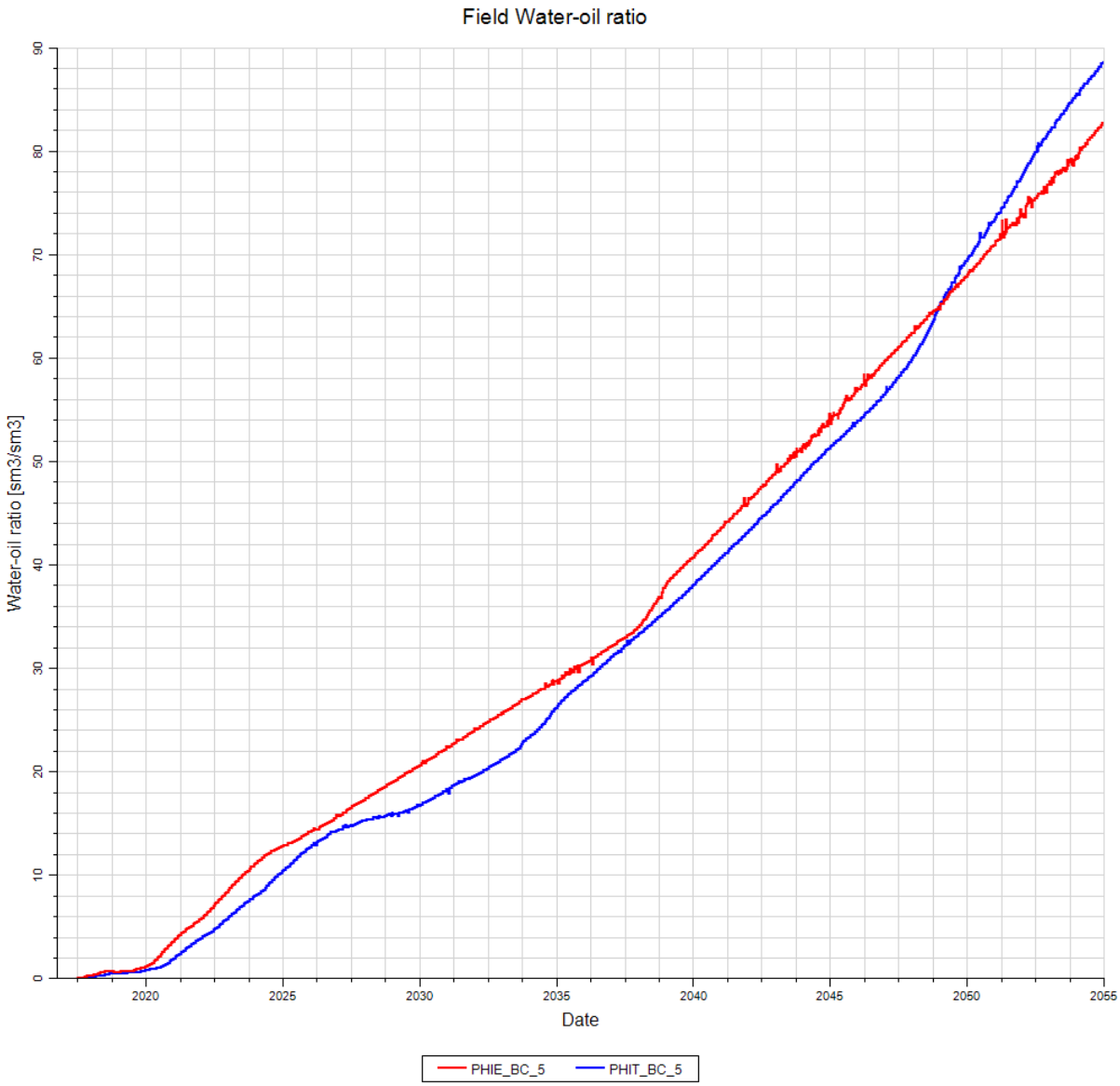

Figure 57: *Base case: Field Water-oil ratio*

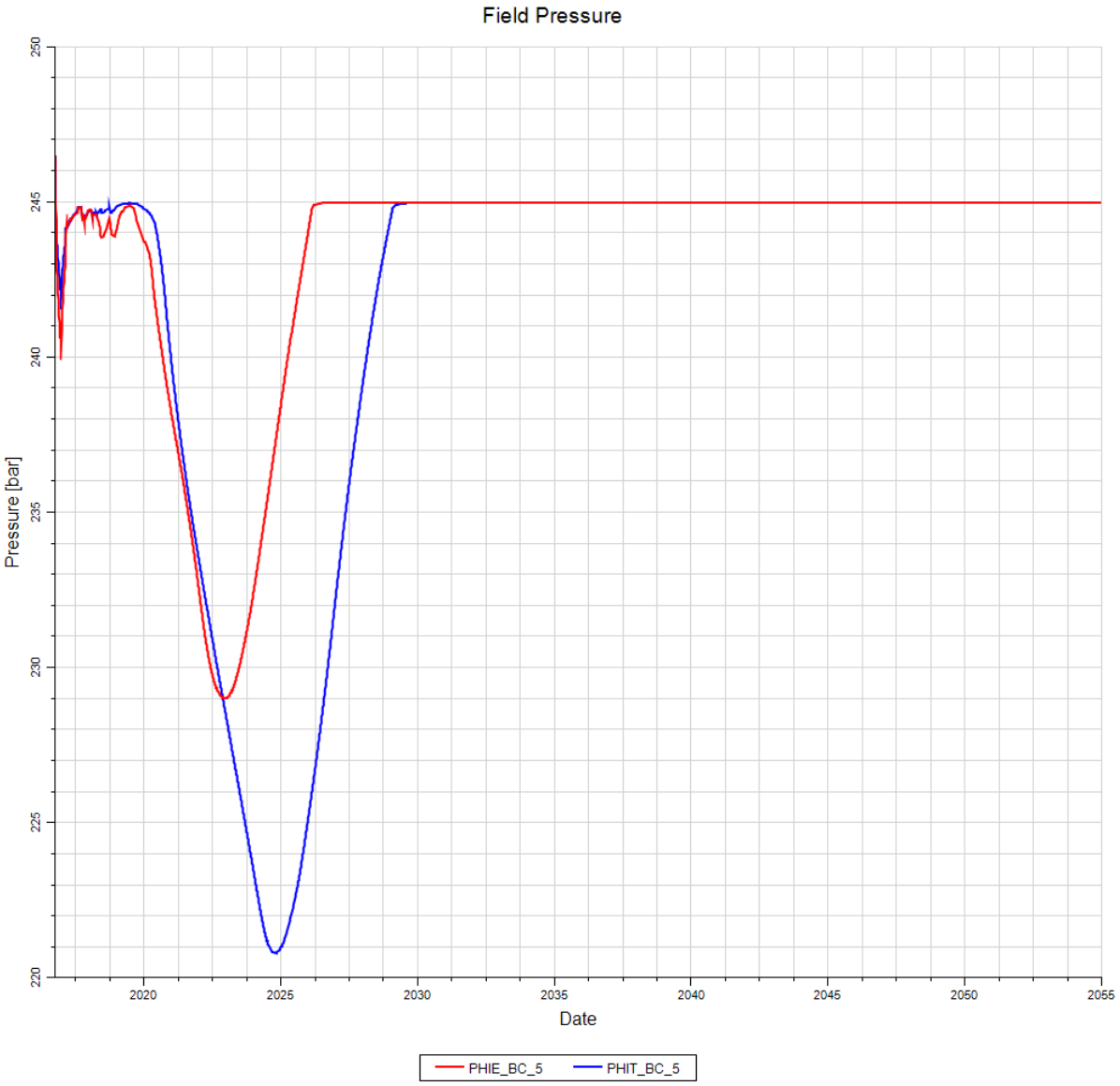

Figure 58: *Base case: Average reservoir pressure*

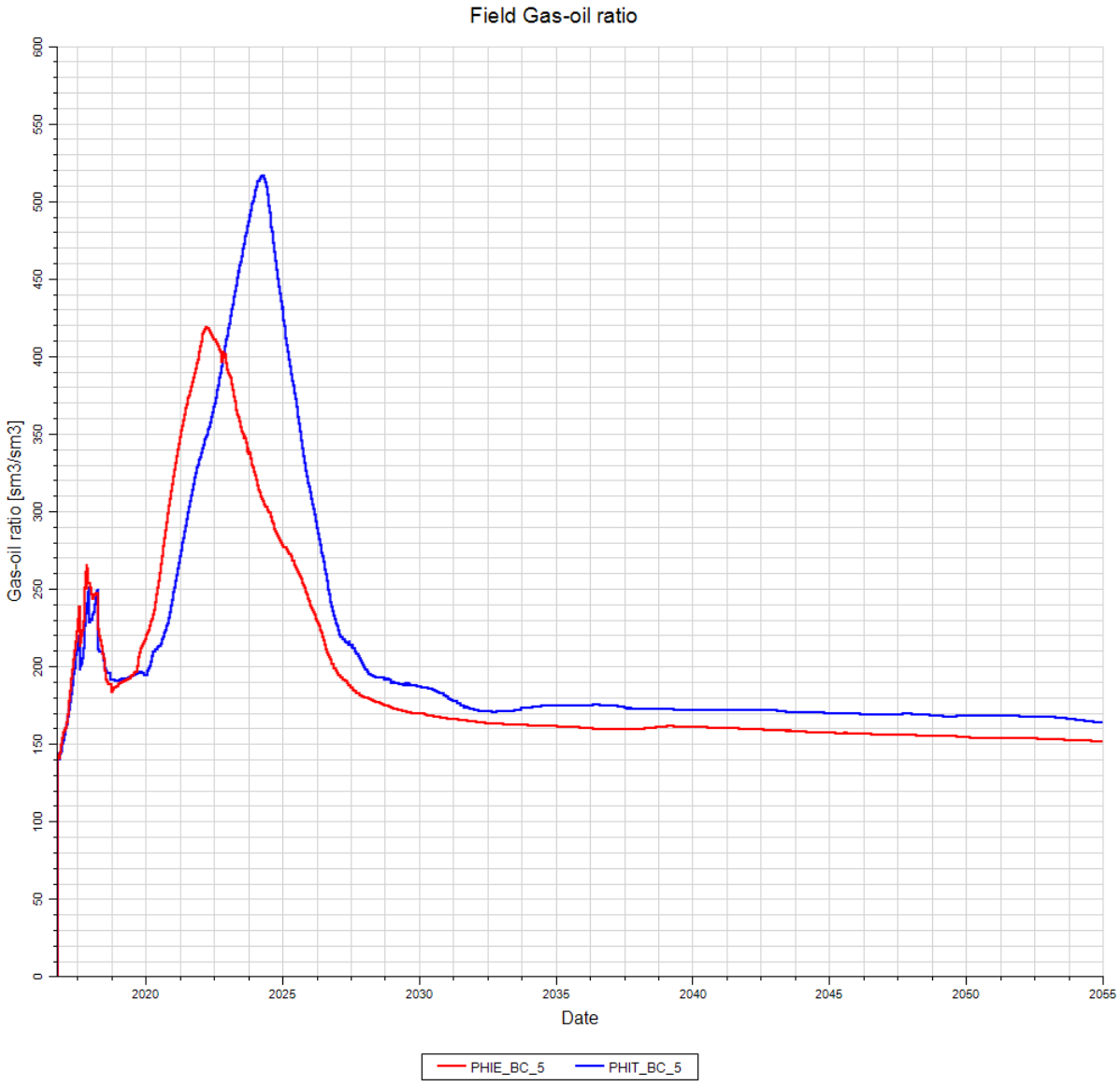

Figure 59: *Base case: Field Gas-Oil ratio*

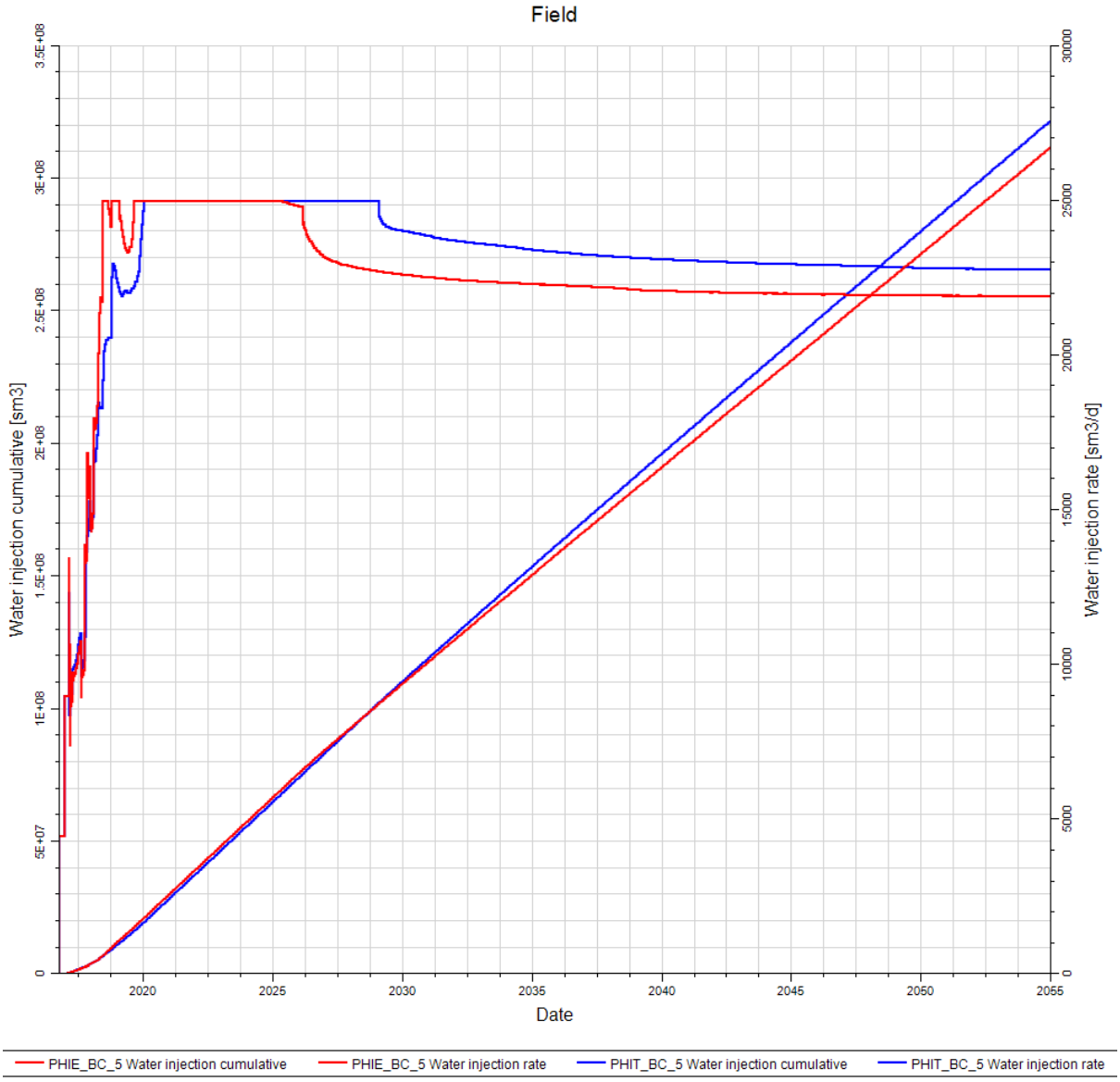

Figure 60: *Base case: Field water injection rate and cumulative injection*

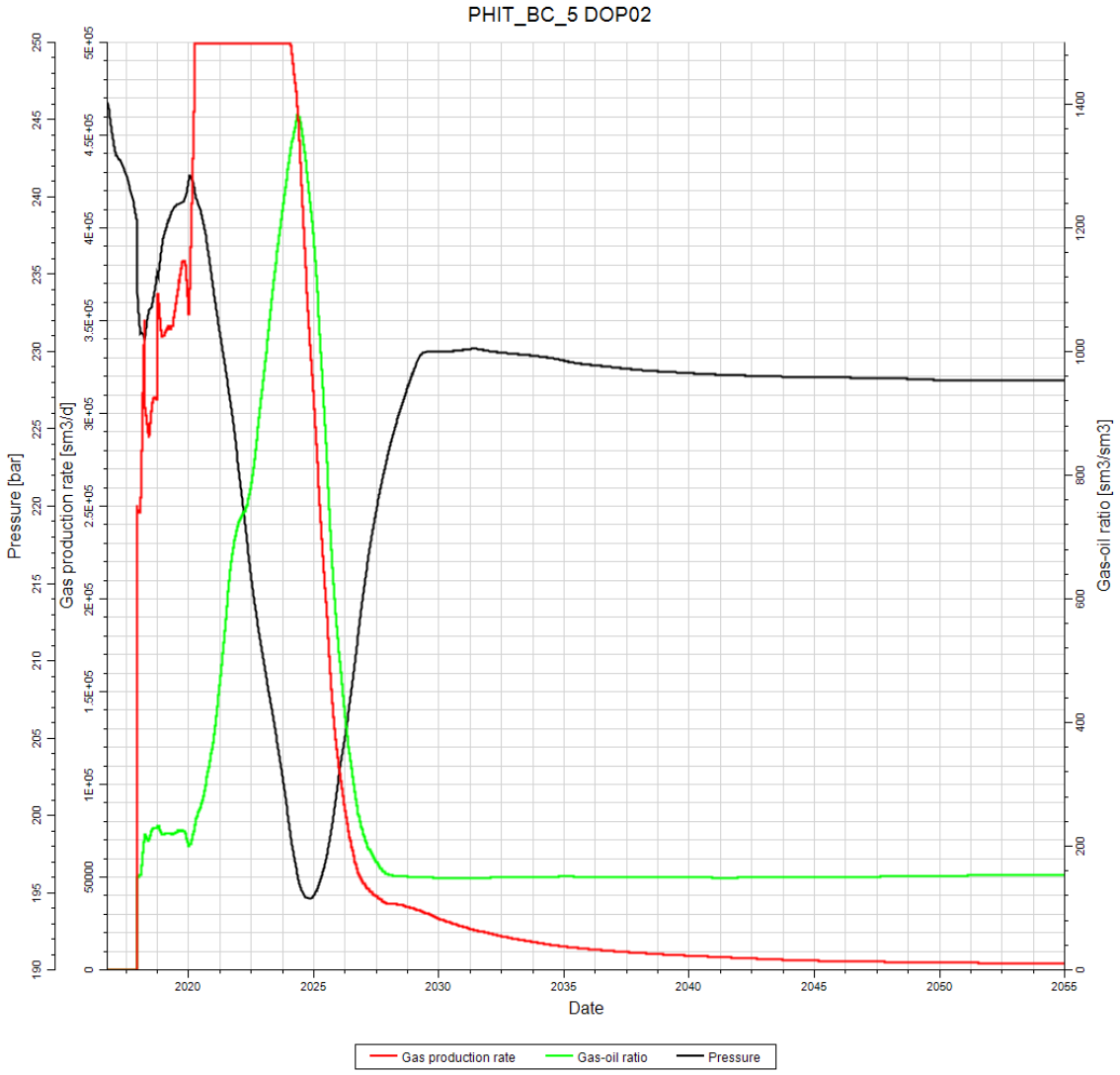

Figure 61: *Base case: GOR, gas production rate and downhole pressure in DOP02*

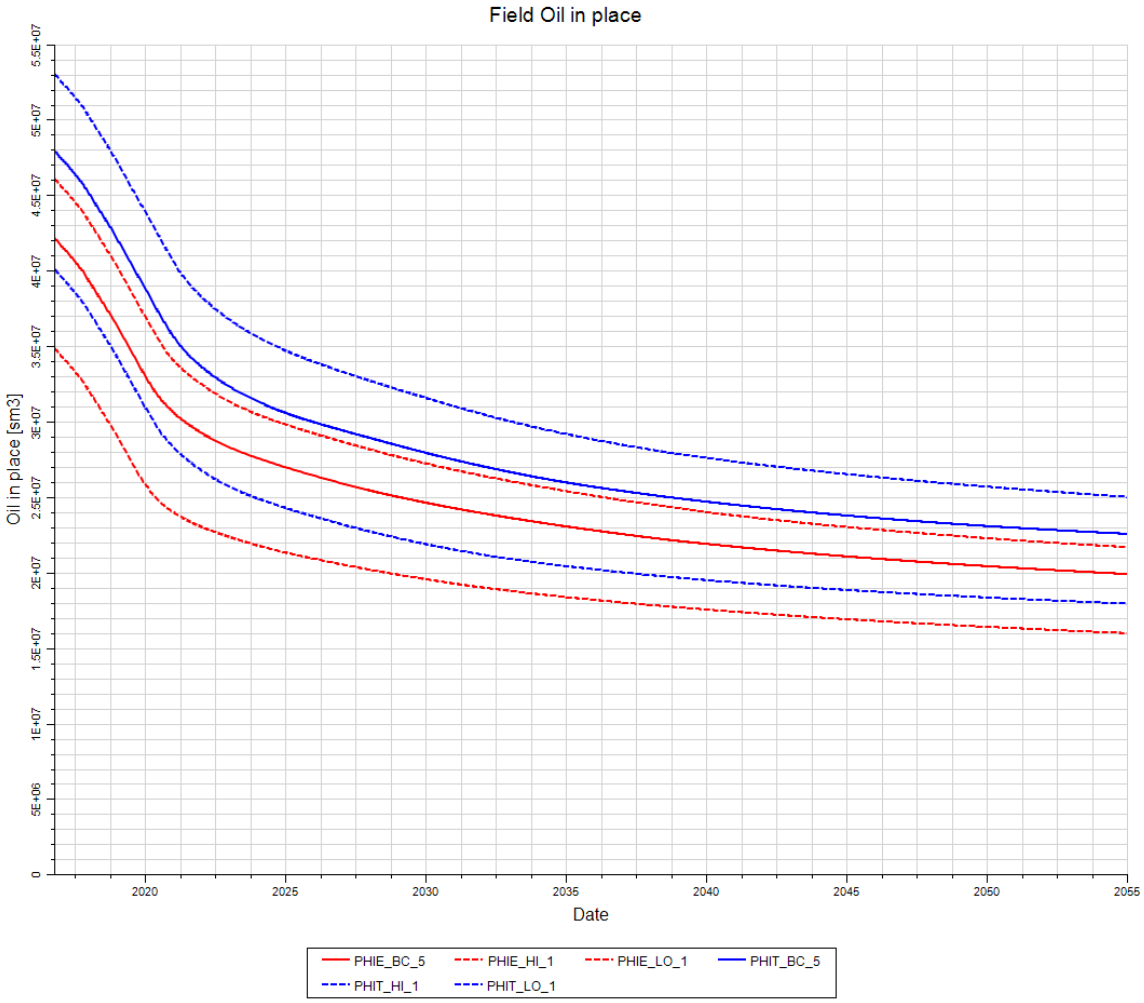

Figure 62: *Shale uncertainty study: Field oil in place*

B Base case Property Histograms

After the well logs had been scaled up and distributed in the 3D grid, some statistics become available. This short section includes statistics for the entire 3D model for the base case with total and effective porosity. A "difference parameter" was created as follow:

$$\text{Difference parameter} = \text{Value in PHIT model} - \text{Value in PHIE model} \tag{36}$$

This histogram works as a filter, with values above 0 meaning the parameters are higher in the total porosity case. Moving away from the center of the histogram means a larger absolute difference.

B.1 Porosity

As seen in the histograms, the porosity in the gridcells is higher in the PHIT grid almost all the time. The negative difference is a result from some minor crossovers in the porosity logs in the Statfjord and Skagerak 2 formations. Figure 39 shows this crossover in well 16/1-9.

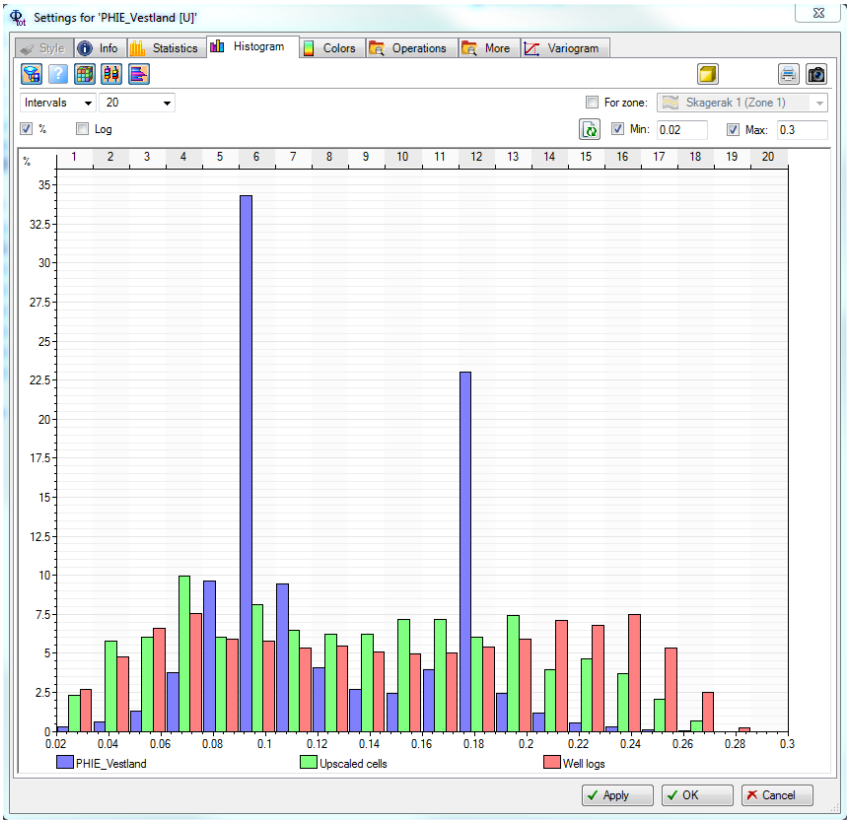

Figure 63: *Porosity, PHIT*

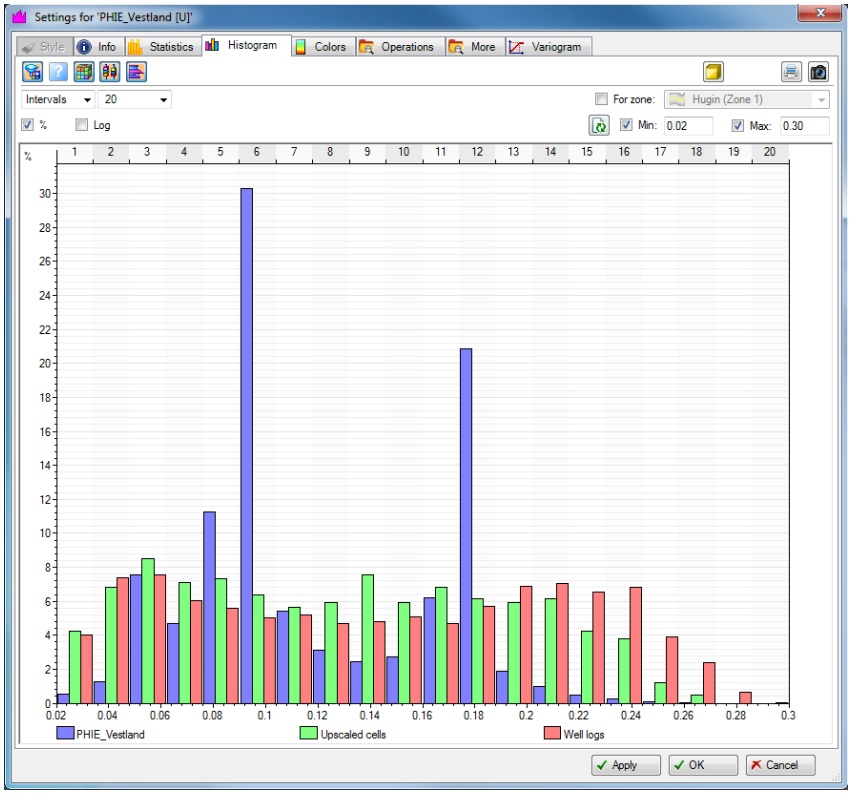

Figure 64: *Porosity, PHIE*

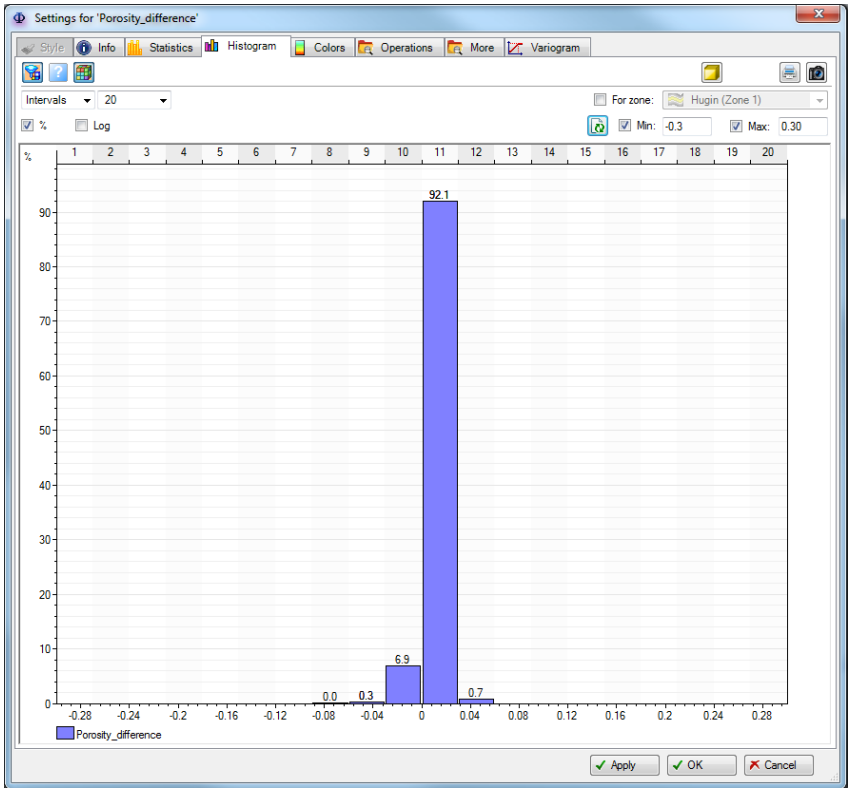

Figure 65: *Porosity difference, PHIT-PHIE*

B.2 Permeability

Permeability is calculated as a function of porosity along the well, and co-kriged with porosity in the petrophysical modeling. It should therefore not be a surprise that permeability is higher in the PHIT case. It is usually minor differences, but cells with up to 2000 md difference exist. These cells have high permeability in both models, so the relative difference is not that extreme.

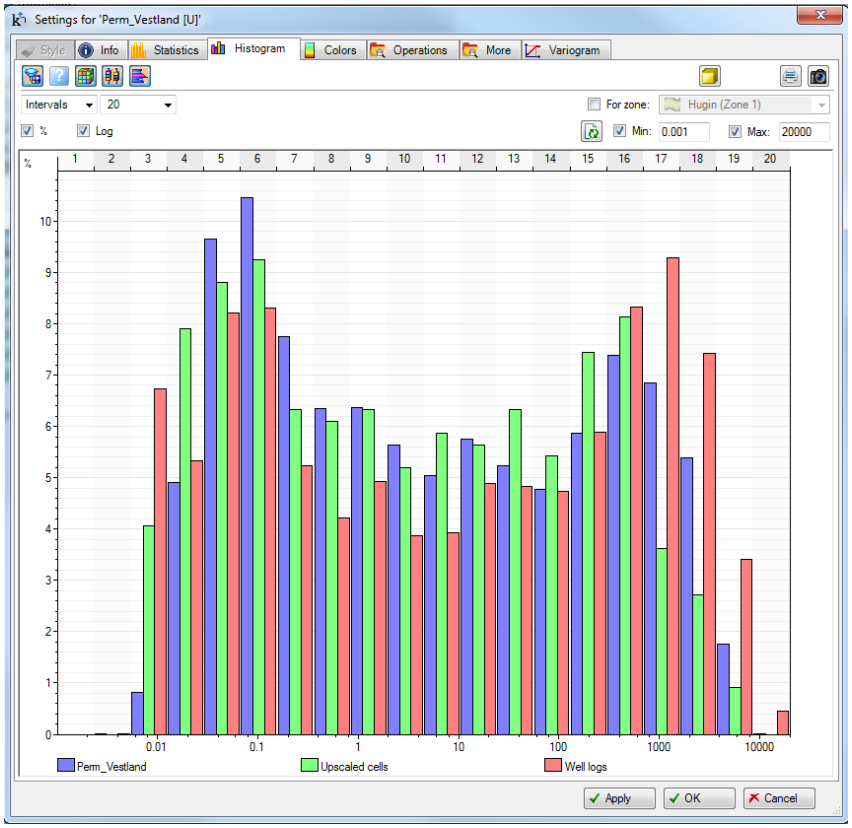

Figure 66: *Permeability, PHIT*

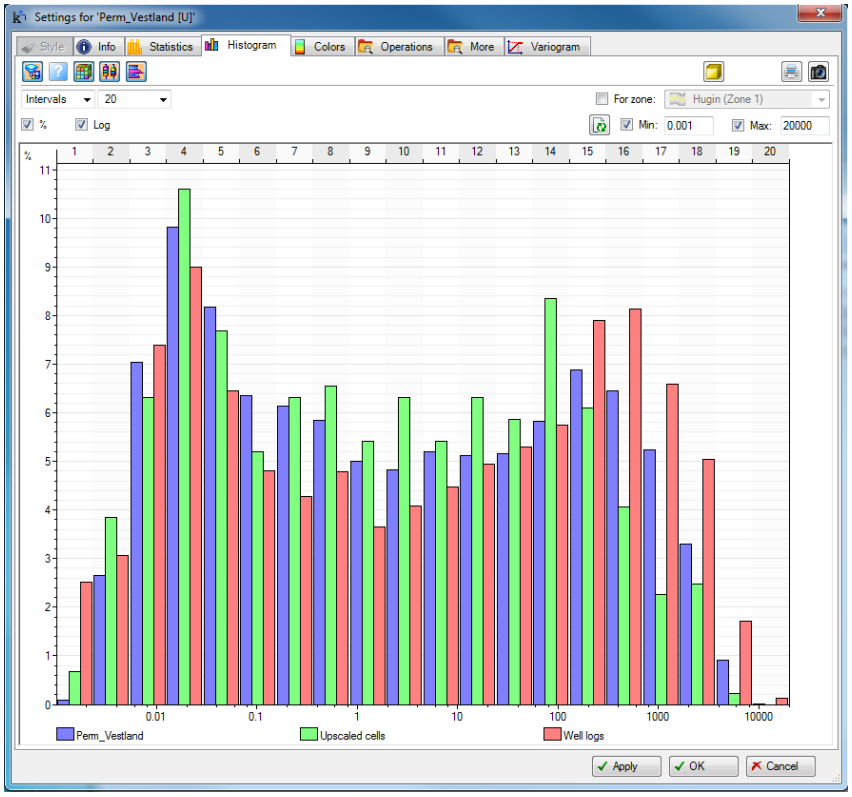

Figure 67: *Permeability, PHIE*

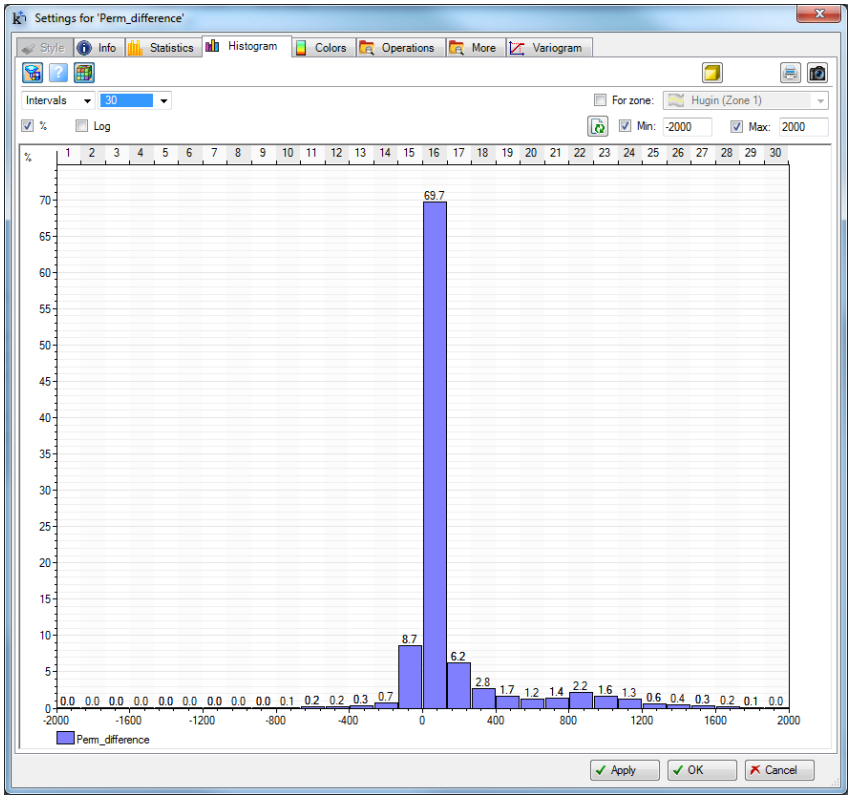

Figure 68: *Permeability difference, PHIT-PHIE*

B.3 Water saturation

The water saturation in the model is calculated based on porosity and permeability with the Leverett J-function. It can be seen that most of the cells in the effective porosity case has higher water saturation than in the total porosity case.

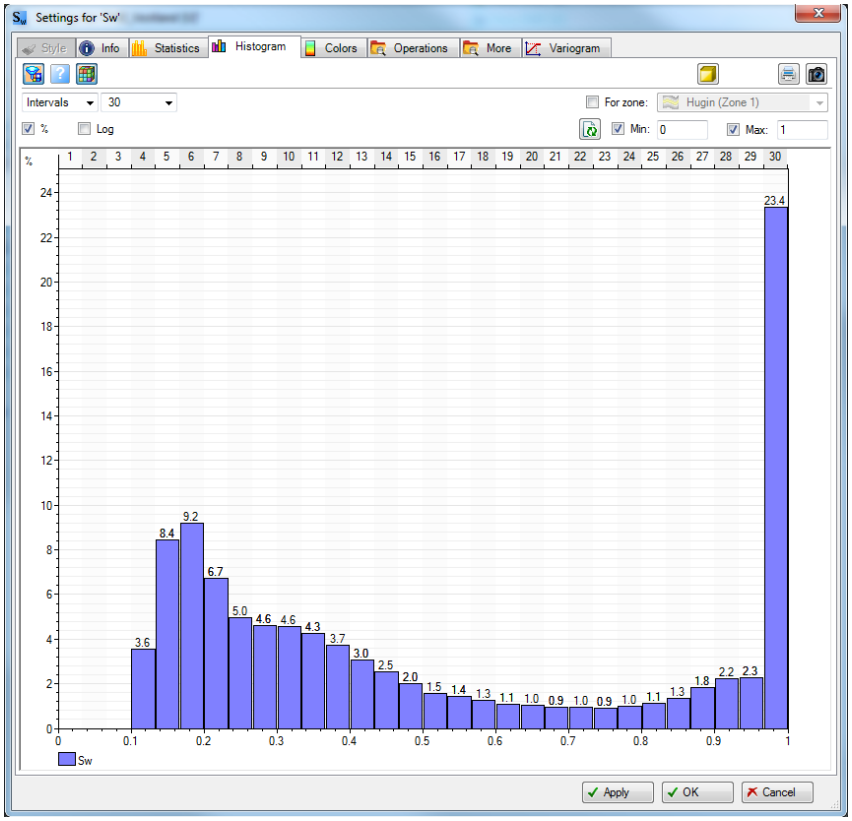

Figure 69: *Water saturation, PHIT*

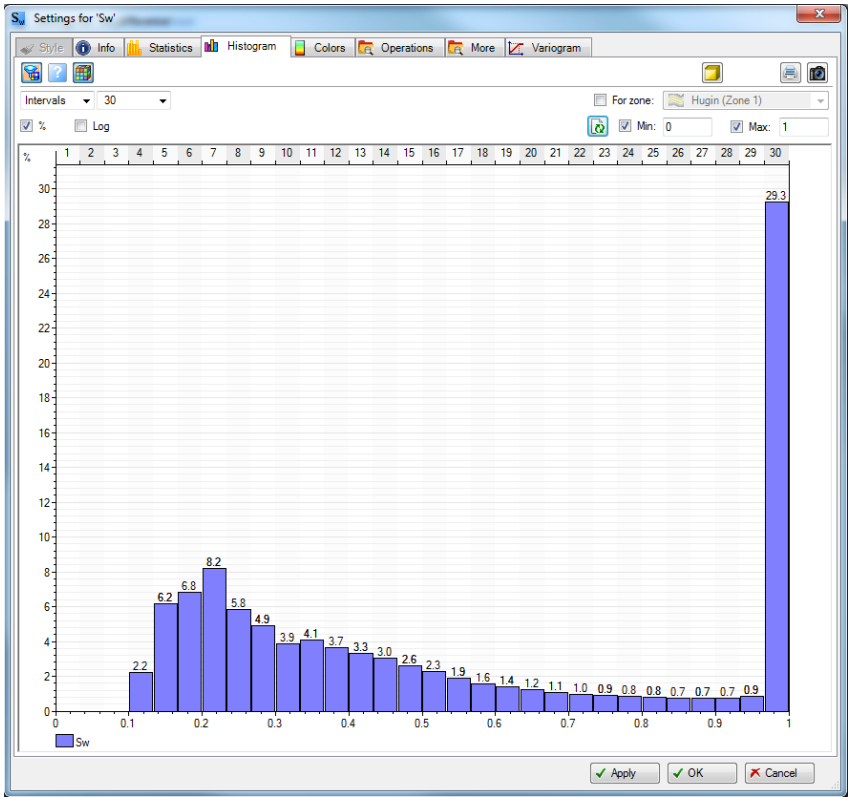

Figure 70: *Water saturation, PHIE*

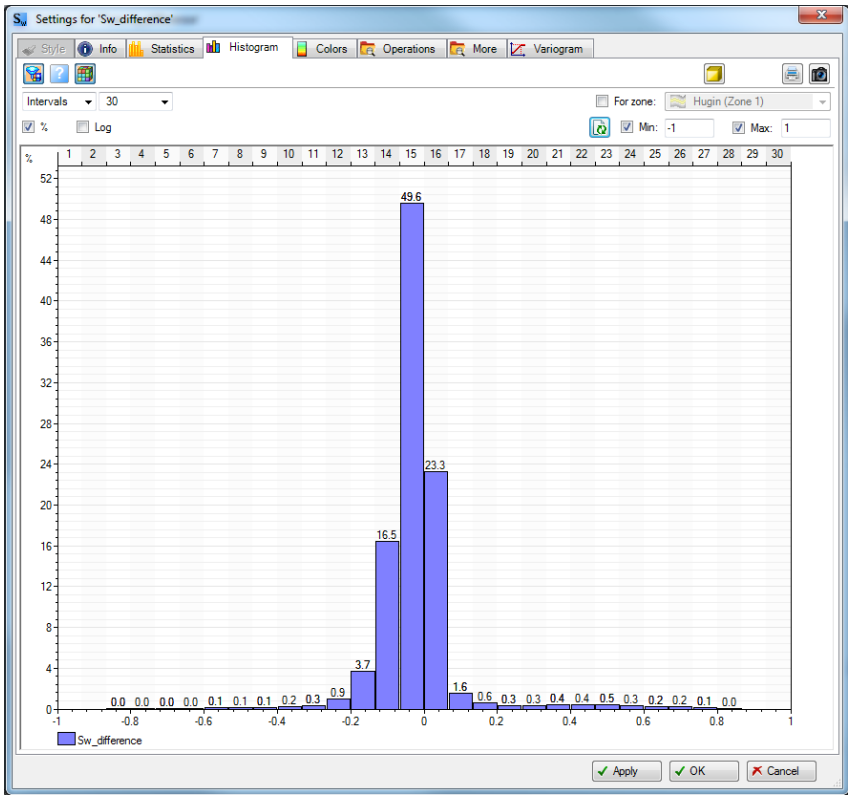

Figure 71: *Water saturation, PHIT-PHIE*

C Log/Core comparison

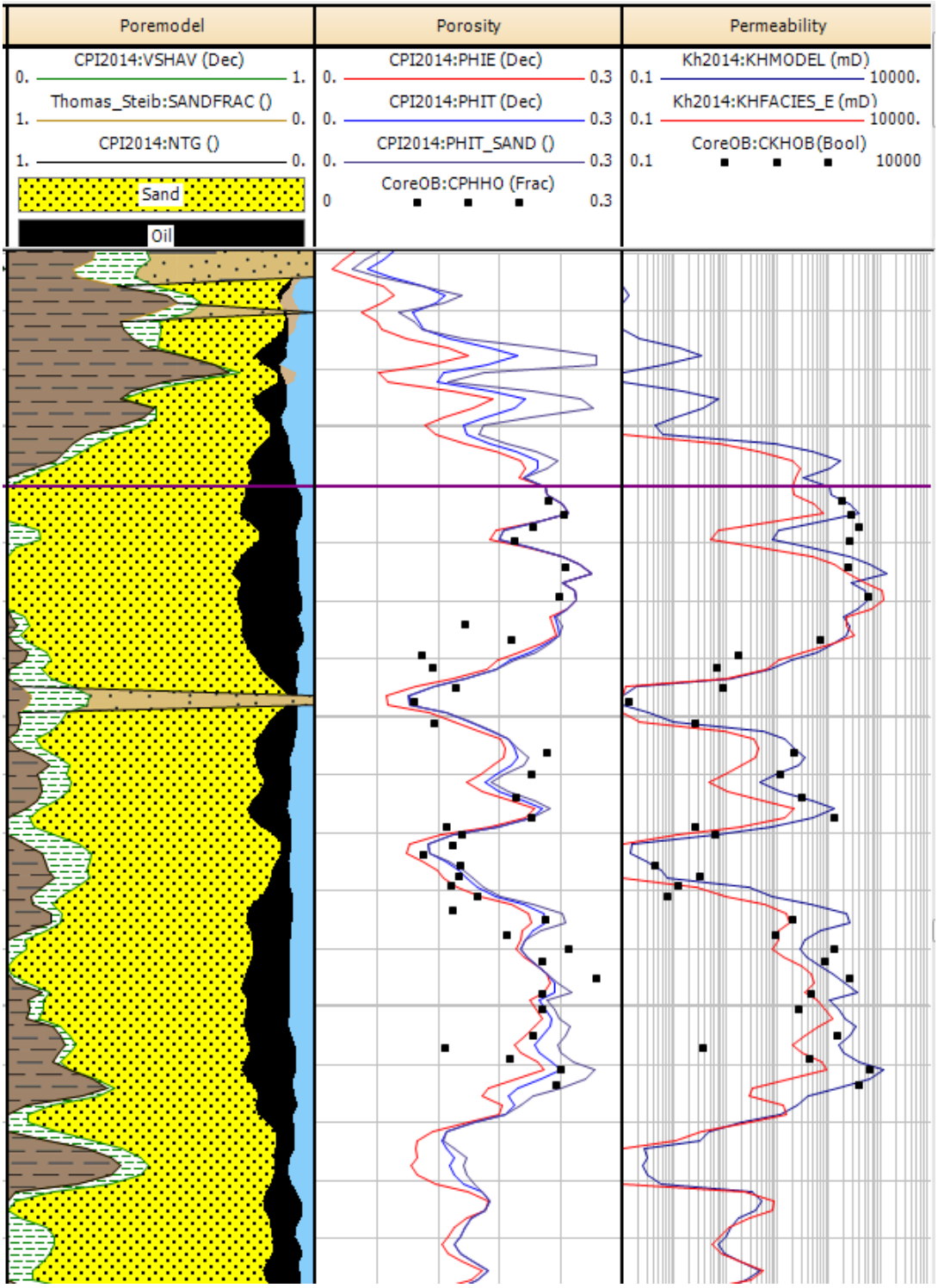

Figure 72: *Log - Core comparison, 16/1-9*

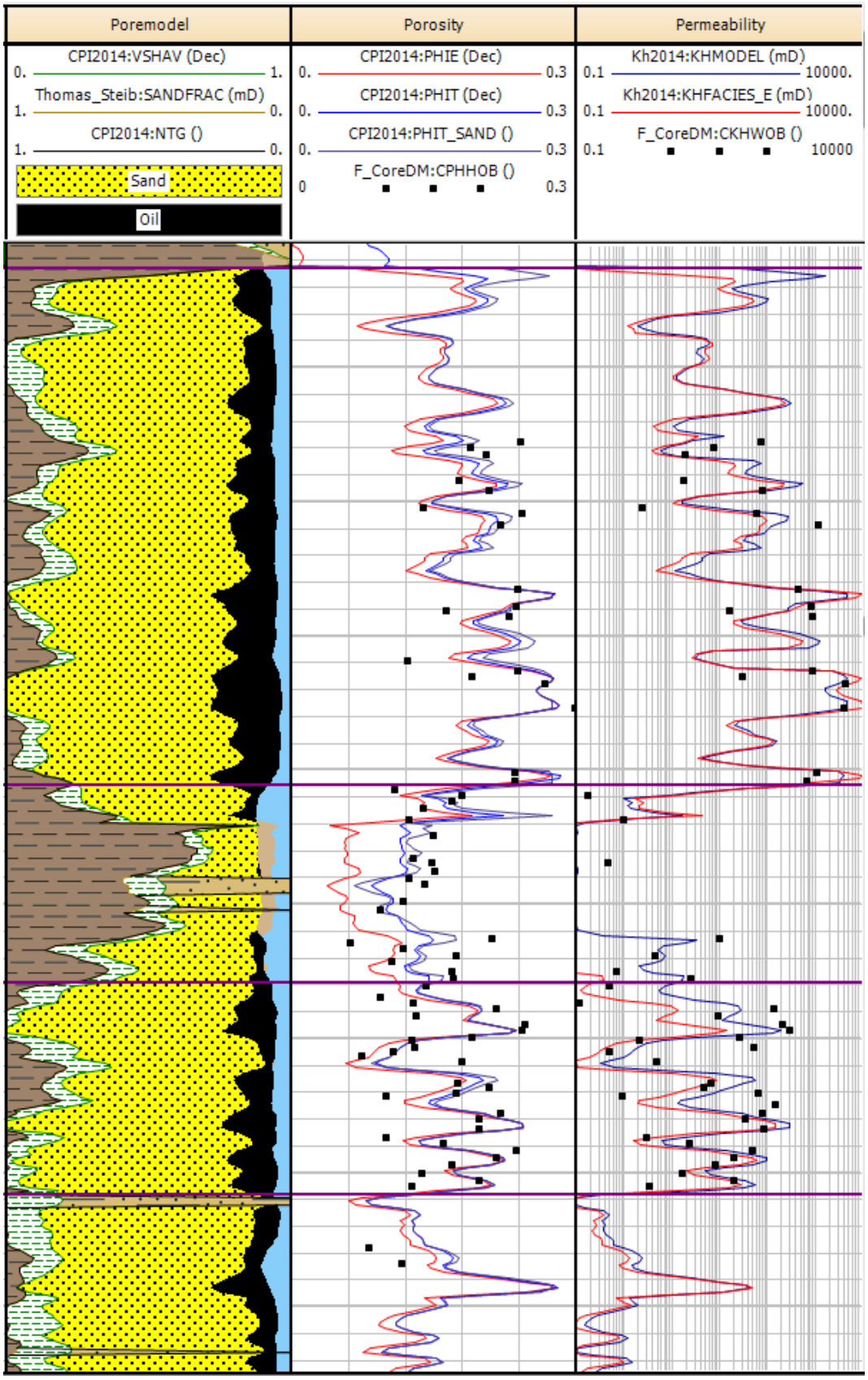

Figure 73: *Log - Core comparison, 16/1-11*

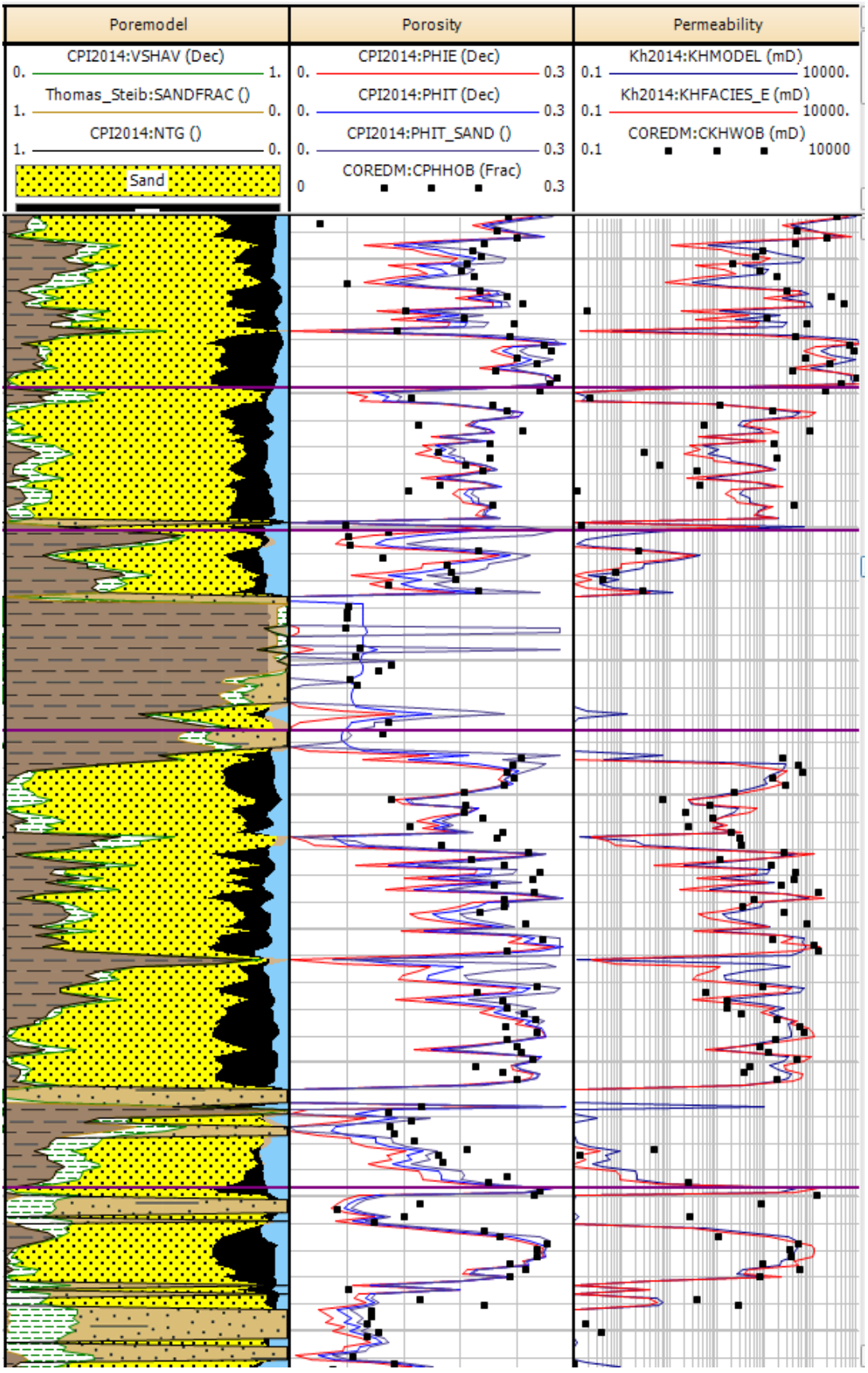

Figure 74: *Log - Core comparison, 16/1-16*